의학박사 학위논문

CST3 와 GDF15 cytokine 의 폐와 신장의 섬유화 치료제로서의 유용성 평가

Validation of CST3 and GDF15 as potential therapeutics for pulmonary and kidney fibrosis

2018 년 8 월

서울대학교 대학원
의과학과 의과학전공 (약리학)
김 영 임

A thesis of the Degree of Doctor of Philosophy

Validation of CST3 and GDF15 as potential therapeutics for pulmonary and kidney fibrosis

CST3 와 GDF15 cytokine 의 폐와 신장의 섬유화 치료제로서의 유용성 평가

August 2018

The Department of Biomedical Sciences
(Pharmacology),
Seoul National University
College of Medicine
Young-Im Kim

Validation of CST3 and GDF15 as potential therapeutics for pulmonary and kidney fibrosis

by
Young-Im Kim

A thesis submitted to the Department of Biomedical science in partial fulfillment of the requirements for the Degree of Doctor of Philosophy in Biomedical science at Seoul National University College of Medicine

August 2018

Approved by Thesis Committee:

Professor _____Chairman
Professor _____Vice chairman
Professor _____
Professor _____
Professor _____

ABSTRACT

Fibrosis is a chronic disease evoked by pathological wound healing process in various organs. Wound healing process is divided into three phases: (1) inflammation, (2) proliferation; and (3) damaged tissue remodeling with scar formation. Throughout the tissue repair process, interaction of epithelial cell and fibroblast gradually regulates mid-and late phase of tissue-damaged microenvironment. These proliferative myofibroblasts are the major production source of extracelluar matrix for normal scar formation. After regeneration in normal tissue, myofibroblasts are eliminated by apoptosis effect, however, un-eliminated myofibroblasts interrupt the regeneration of epithelial layer and stimulate tissue stiffness.

In the present study, I suggest that epithelial derived molecules induce myofibroblast death and block differentiation in cell base experiments, furthermore, the complementation of epithelial derived cytokine, cystatin C (CST3) and GDF15, are novel and effective therapeutic strategy for fibrotic disease in various organs. Normal epithelial cell secretory factors inhibited fibroblast proliferation and differentiation. To identify these cytokines, I used proteome profiler and found out that recombinant CST3 and GDF15 reduce fibroblast growth and differentiation in vitro. In primary fibroblasts isolated from the mouse organs, each cytokine induced apoptotic cell death and reduced collagen production. These anti-fibrotic effects were further augmented by co-administration of both cytokines. To confirm the effect

of recombinant CST3 and GDF15 on fibrotic disease, I used bleomycin induced lung fibrosis model and ureteral obstruction-induced fibrosis model. Furthermore, CST3 and GDF15 expression level diminished in ILD human lung tissues. In detailed mechanism, recombinant CST3 and GDF15 antagonized TGF-β receptor and blocked SMAD2/3 signaling cascade and the N-Myc signaling pathways in fibroblast activation.

These findings suggests cytokine from normal epithelial cells regulate progression of fibrosis by inhibiting fibroblast growth and differentiation. Taken together, this study that CST3 and GDF15 show a new function as fibroblast inhibitor and provide the potential target to prevent fibrosis.

Keywords: Epithelium, Fibroblast, Lung Fibrosis, Renal Fibrosis, cystatin C, growth differentiation factor 15

Student number: 2013-31175

CONTENTS

Abstract i
Contents iii
List of tables and figures iv

General introduction 1
Chapter 1 3
Epithelial cell-derived cytokines CST3 and GDF15 as potential therapeutics for pulmonary fibrosis
Introduction 4
Material and Methods 7
Results 18
Discussion 75
Chapter 2 79
Recombinant peptides CST3 and GDF15 ameliorate renal fibrosis by deactivating fibroblasts
Introduction 80
Material and Methods 83
Results 90
Discussion 122
References 125
Abstract in Korean 135

LIST OF TABLES AND FIGURES

Chapter 1

Figure 1. Lung fibroblast growth is inhibited in the conditioned medium from pulmonary alveolar epithelial cells. 25

Figure 2. Lung fibroblast death is induced by the conditioned medium from pulmonary alveolar epithelial cells. 27

Figure 3. Lung fibroblast differentiation and growth is inhibited in the conditioned medium from pulmonary alveolar epithelial cells. 29

Figure 4. Identification of cytokines secreted from hPAE cells..... 32

Figure 5. CST3 and GDF15 levels in hPAE conditioned media. 34

Figure 6. CST3 and GDF15 are responsible for fibroblast growth inhibition by hPAE CM. 36

Figure 7. CST3 and GDF15 are responsible for fibroblast grwoth inhibition by hPAE CM. 38

Figure 8. CST3 and GDF15 peptides inhibit proliferation in CCD-18Lu cells. 40

Figure 9. CST3 and GDF15 peptides inhibit ECM production in CCD-18Lu cells. 42

Figure 10. CST3 and GDF15 peptides inhibit proliferation and ECM production in PFAF cells. 44

Figure 11. CST3 and GDF15 peptides inhibit proliferation in PFAF cells. 46

LIST OF TABLES AND FIGURES

Figure 12. CST3 and GDF15 peptides inhibit differentiation and ECM production in PFAF cells. 48

Figure 13. CST3 and GDF15 inhibit the TGF-β signaling pathway in CCD-18Lu cells. 50

Figure 14. CST3 and GDF15 inhibit the TGF-β signaling pathway in CCD-18Lu and PFAF cells. 52

Figure 15. CST3 and GDF15 inhibit the TGF-β signaling pathway on SBE-luciferase activity in CCD-18Lu cells. 54

Figure 16. CST3 and GDF15 are down-regulated in human lungs with fibrosis. 55

Figure 17. CST3 and GDF15 are down-regulated in mouse lungs with fibrosis. 57

Figure 18. Expression of CST3 in normal lung tissues from 10 patients with adenocarcinoma. 59

Figure 19. Expression of CST3 in fibrotic lung tissues from 10 patients with interstitial lung disease. 61

Figure 20. Expression of GDF15 in normal lung tissues from 10 patients with adenocarcinoma. 63

Figure 21. Expression of GDF15 in fibrotic lung tissues from 10 patients with interstitial lung disease. 65

LIST OF TABLES AND FIGURES

Figure 22. CST3 and GDF15 protein expression are down-regulated in mouse lung tissue with fibrosis. 67

Figure 23. Recombinant CST3 and GDF15 ameliorate weight loss and mortality rate in bleomycin-treated mice. 69

Figure 24. Recombinant CST3 and GDF15 ameliorate lung fibrosis in bleomycin-treated mice..... 71

Figure 25. Recombinant CST3 and GDF15 reduce myofibroblast activation in bleomycin-treated mice. 73

Chapter 2

Figure 1. Verification of activated renal fibroblasts using immunefluor-escence and FACS..... 94

Figure 2. Verification of activated renal fibroblasts with western blotting and growth rate. 96

Figure 3. CST3 and GDF15 inhibit fibroblast growth..... 98

Figure 4. CST3 and GDF15 inhibit fibroblast growth and differ rentiation. 100

Figure 5. TGF-β receptor signaling pathway is activated in UUO kidney fibrosis. 102

Figure 6. CST3 inhibits the TGF-β/SMAD signaling pathway in UUO kidney fibrosis. 104

Figure 7. CST3 inactivates the TGF-β receptor signaling pathway in sham or UUO kidney fibroblasts..... 106

Figure 8. N-Myc expression is activated in fibrotic kidneys. 108

Figure 9. GDF15 represses N-Myc expression in fibrotic kidneys. 110

Figure 10. GDF15 represses N-Myc expression in activated kidney fibroblast. 112

Figure 11. UUO mouse model..... 114

Figure 12. CST3 and GDF15 inhibit renal fibrosis progression in a UUO mouse model. 116

Figure 13. CST3 and GDF15 inhibit fibrotic phenotype in a UUO mouse model.. 118

Figure 14. CST3 and GDF15 inhibit activation of kidney fibroblast in mouse UUO model..... 120

LIST OF ABBREVIATIONS

ECM : Extracellular matrix

CST3 : Cystatin C

GDF15 : Growth differentiation factor-15

TGF-β : Transforming growth factor beta

hPAE : Human pulmonary alveolar epithelial cell

ILD : Interstitial lung disease

PFAF : Pulmonary fibrosis-associated fibroblasts

TGFβR1 : Transforming growth factor beta receptor 1

SBE : SMAD Binding Element

α-SMA : alpha -smooth muscle actin

IL-1α : Interleukin 1 alpha

PARP : Poly ADP ribose polymerase

CI : combination index

TCA : Trichloroacetic acid

BALF : Bronchoalveolar lavage fluid

IL-6 : Interleukin 6

TNF-α : Tumor necrosis factor-alpha

CKD : Chronic kidney disease

PDGF : Platelet-derived growth factor

FGF-2 : Fibroblast growth factor 2

GFR : Glomerular Filtration Rate

LIST OF ABBREVIATIONS

ALK5 : TGFβ type I receptor kinase

UUO : Unilateral ureter obstruction

ERK : Extracellular-signal-regulated kinase

AKT : Protein kinase B

CCL17 : Chemokine (C-C motif) ligand 17

NDRG : N-Myc downstream regulated genes

GENERAL INTRODUCTION

Wound healing response is universal biological processes in various organs after tissue damage. This dynamic, interactive processes comprised with soluble mediators, blood cells, extracellular matrix, and parenchymal cells. The three phases of wound healing pathway are inflammation, tissue formation, and tissue remodeling. After tissue injury various intracellular and intercellular signaling pathways are activated and regenerate tissue homeostasis. In inflammation stage, disrupted blood vessels extravasated of blood constituents, and blood clots established hemostasis stimulated production of several mediators such as PDGF (platelet-derived growth factor) or TGF-β (Transforming growth factor beta). These mediators recruit inflammatory immune cell to damaged site. During new tissue formation, epidermal cells removed blood clots from damaged layers and undergo mesenchymal phenotype alteration. The growth factors such as, epidermal growth factor, transforming growth factor α, and keratinocyte growth factor stimulate these transformations and finally attract the fibroblast from the edge of the wound. The fibroblasts and myofibroblasts are contribute to the synthesis, deposition, and remodeling of the extracellular matrix in many organs. Myofibroblasts are known as differentiated fibroblasts from mesenchymal cells, such as pericytes and epithelial cells. At the third stage of wound remodeling, the elimination of most of the endothelial cells, macrophages and myofibroblasts is important event for tissue homeostasis.

Fibrosis is the final chronic inflammatory diseases evoked by common

pathological process. The main problem of fibrosis is irreversible and excessive accumulation of fibrous connective tissue with severe or repetitive or wound-healing response, which can lead to permanent scarring, malfunctioning organs and death. Despite the large effort for overcoming the fibrosis, there is no therapeutic target for elimination of myofibroblasts.

In this study, I investigated potential roles of cystatin C (CST3) and GDF15 for regulation of tissue homeostasis and prevention of fibrotic progression in pulmonary fibrosis (Part I) and kidney fibrosis (Part II).

CHAPTER 1

Epithelial cell-derived cytokines CST3 and GDF15 as potential therapeutics for pulmonary fibrosis

INTRODUCTION

Pulmonary fibrosis is a chronic progressive lung disorder associated with excessive extracellular matrix (ECM) deposition and collapse of the lung parenchymal architecture, leading to severe respiratory dysfunction with a median survival of 2–4 years (King, 2011). Anti-inflammatory and immunosuppressive drugs have been tested as therapeutic regimens for pulmonary fibrosis, but none have been sufficiently effective in prolonging the survival period of patients (Friedman, 2013). Based on a consensus that pulmonary fibrosis is attributed to an overgrowth of activated fibroblasts (King, 2001), anti-fibrotic agents have been tried as emerging drugs for treating pulmonary fibrosis. Indeed, nintedanib and pirfenidone were clinically tried and evaluated to delay the progression of fibrosis (Raghu et al., 1999; Richeldi et al., 2014). However, these drugs were reported to provoke serious adverse effects in the clinical trial (Meyer et al., 2017; Hajari et al., 2017; Richeldi et al., 2014).

Basically, the abnormal tissue homeostasis in wound healing response cause fibrosis pathogenesis (Ghosh et al., 2013; Reinke et al., 2012) In most tissues, epithelial-mesenchymal homeostasis must be maintained for normal structures and functions (Imokara et al., 1997). For appropriate recovery of injured epithelium, the wound healing process must complete three steps – inflammation, proliferation, and maturation phases. Finally, outgrown fibroblasts should be eliminated from the repaired tissue for the recovery of epithelial-mesenchymal homeostasis (Gabbiani, 2003). Currently, pulmonary

fibrosis is understood as a disorder of epithelial-mesenchymal homeostasis because the epithelial integrity fail to be repaired during repeated injury–regeneration. Consequently, the wound healing process cannot be halted and the fibroblast stimulation continues (Yanagi et al., 2015). Furthermore, myofibroblasts induce epithelial cell death and disturb the epithelial repair process. In fibrotic tissue, injured epithelial cells and outgrown myofibroblasts activate a positive feedback loop that results in massive fibrosis and alveolar destruction (Golan-Gerstl et al., 2007).

Cystatin C (CST3) is a cytokine ubiquitously expressed in most mammalian cells and also detected in blood and body fluids (Villa et al., 2005). Given that it potently inhibits cysteine proteases like cathepsins, CST3 is expected to stimulate fibrosis by inhibiting the protease-mediated digestion of ECM (Moles et al., 2009; Canbay et al., 2003). In contrast, cathepsins have been also reported to promote liver or lung fibrosis by facilitating TGF-β-driven differentiation of fibroblasts (Zhang et al., 2014; Sokol et al., 2005). To date, the roles of cathepsins and CST3 in organ fibrosis are controversial. On the other hand, growth differentiation factor 15 (GDF15) is a TGF-β family member that is induced immediately after a harmful stress (Liu et al., 2003). GDF15 is believed to be associated with stress responses, but its biological functions have not been clearly identified. Although GDF15 has been shown to promote cancer cell death, whether it controls fibroblast proliferation and activation is unclear (Liu et al., 2003; An et al., 2011; Kadara et al., 2016).

Despite many efforts to understand the pathogenesis of pulmonary fibrosis, little is known about the mechanism of epithelial cell control over fibroblasts

in maintaining epithelial-mesenchymal homeostasis. Identifying fibroblast-controlling cytokines could provide novel peptide drugs for pulmonary fibrosis therapy. In this study, I identified two epithelial cell-derived cytokines CST3 and GDF15 capable of inhibiting proliferation and activation of fibroblasts. Furthermore, I tested the ability of the cytokines to ameliorate bleomycin-induced pulmonary fibrosis in mice.

MATERIALS AND METHODS

Cell culture and conditioned media

CCD-18Lu (normal lung fibroblast), A549 (adenocarcinomic alveolar epithelial cell), and HCT116 (colon cancer cell) were purchased from the American Type Culture Collection (ATCC, Manassas, VA); hPAE (human pulmonary alveolar epithelial cell) was from ScienceCell Research Laboratory (Carlsbad, CA). hPAE cells were cultured in Eagle Alveolar Epithelial Cell Medium supplied by the manufacturer. To prepare conditioned media, various types of cells were seeded in a 100-mm dish at 80% confluency and incubated in cell type-specific media for 24 hr. Next day, the cells were washed with PBS and incubated commonly in Dulbecco's Modified Eagles media without FBS. After 2 or 3 day-incubation (~1×10^7 cells per 100-mm dish), the conditioned medium (5 mL per dish) was centrifuged, filtered, and mixed with an equal volume of a fresh medium.

Human lung tissues

Lung biopsy samples were obtained from 10 patients with ILD and 10 lung cancer patients without ILD. Of 10 ILD patients, 3 lung cancer patients with interstitial pneumonia were included. ILD was finally diagnosed by pathologists in Seoul National University Hospital. Detailed information on tissue donors is summarized in Supplementary table 1. The study protocol was approved by the Institutional Review Board of Seoul National University

Hospital (approval No. 1704-172-849).

Bleomycin-induced pulmonary fibrosis

C57BL/6J mice (male, 11 weeks) were purchased from Central Laboratory Animal Inc., and kept in specific pathogen-free rooms. Mice were anesthetized with a mixture of tiletamine/zolazepam (30 mg/kg) and xylazine (10 mg/kg), and subjected to an intratracheal injection with saline or bleomycin sulfate (2 mg/kg, MBcell, CA) in a total volume of 50 μL. CST3/GDF15 peptides (50 μg/kg each) or PBS were injected intraperitoneally into mice on days 6, 9, 12, 15, 18 after the bleomycin challenge. Recombinant peptides of mature CST3 (aa. 27-146, NM_000099) and mature GDF15 (aa. 195-308, NM_004864) were purchased from Abcam and Sino Biological Inc. (Beijing, China), respectively. On day 21, the lung tissues were removed from mice and divided into two lobes. The left lobes were fixed in 4% paraformaldehyde, and the right lobes were stored in liquid nitrogen. All procedures were approved by the Seoul National University Institutional Animal Care and Use Committees (Approval No. 141006-3).

Mouse lung fibroblast isolation and culture

Normal lung fibroblasts were isolated from the lung tissues of normal mice. To get pulmonary fibrosis-associated fibroblasts (PFAF), mice were subjected to a single challenge of bleomycin via bronchial instillation and the lungs were excised on day 12. Lung tissues were washed and dissected using surgical blades. The minced tissues were digested with 2.4 U/mL dispase and

0.1% collagenase at 37°C for 45 min. The suspension was filtered through 70 μm nylon strainer and centrifuged at 1,000xg for 10 min. The cell pellet was resuspended in DMEM containing 20% FBS and incubated overnight at 37°C. Attached fibroblasts were subcultured in DMEM containing 10% FBS, 100 U/mL penicillin, and 100 g/mL streptomycin.

Cytokine profiling

Cytokine profiling was performed using the proteome profiler Human XL cytokine array kit (# ARY022) provided by R&D Systems. Cells were incubated in serum-free media for 3 days and the conditioned media were prepared as mentioned above. The media (1 mL per membrane) were applied to the nitrocellulose-based array membrane and incubated at 4°C overnight. Array membranes were treated with the detection antibody cocktail (R&D Systems) for 1 hr and further with the streptavidin-HRP solution for 30 min. The immune complexes were visualized using the Chemi-Reagent Mix kit and the arrays were exposed to X-ray films. Based on the mean intensity of reference spots (A1/2, A23/24, and J1/2), the intensity of each dot was normalized.

Masson's trichrome assay and Ashcroft scoring

The paraffin sections (4 μm) of lungs were deparaffinized, rehydrated, and sequentially stained with Weigert's iron hematoxylin and biebrich scarlet-acid fuchsin for 10 min. Finally, the sections were stained with 2.5% aniline blue for 10 min and destained with 1% glacial acetic acid for 3 min.

Photomicrographs were taken from 4 random fields in a tissue section. The severity (0 to 8) of interstitial fibrosis was evaluated based on the Ashcroft fibrosis scoring system (Hübner, 2008).

Lung homogenization

Frozen lung tissues were thawed and homogenized in a PBS solution containing 1% Triton X-100, 1% NP-40, 10 mM EDTA, protease inhibitor (Sigma), and PMSF (Sigma) using a Polytron homogenizer. The homogenates were centrifuged at 13,000xg at 4°C for 30 min, and the supernatants were collected as tissue extracts. Protein concentration was measured with the bicinchoninic acid assay kit (Pierce). For protein separation on SDS/polyacrylamide gels, tissue extracts were boiled for 10 min in a denaturing SDS sample buffer.

Hydroxyproline assay

The frozen right lungs were homogenized in distilled water (100 μl/10 mg tissue). The homogenates were incubated at 95°C for 3 hr and centrifuged at 16,000xg for 10 min. Collagen content in the supernatant was measured using the hydroxyproline colorimetric assay kit provided by BioVision (Milpitas, CA). Hydroxyproline levels were spectrophotometrically determined based on the absorbance at 560 nm.

Cell proliferation assay

Cell proliferation was determined by cell counting. 2×10^5 cells were seeded

in 24-well plates in quadruplicate under standard culture conditions and kept overnight at 37 °C humidified incubator with 5% CO_2. Next day, cells were treated with HaCaT and A549, HCT116 and MCF7 cancer cell conditioned media. After 24 hours, cell proliferation was assessed by counting the detached cells. The live cells were stained by 0.04 % trypan blue and grown for 72 h. Cell counting was performed after 24, 48 and 72 h.

PI staining analysis

For cell cycle analysis, CCD-18Lu cell were plated to 60 mm dish for 40 % confluency. Next day, cell conditioned media were treated to CCD-18Lu for 24 hours, 48 hours and 72 hours. Cells were washed with PBS and were fixed with 70% EtOH for overnight (4 °C). Fixed cells were stained by 10 mg/ml RNase A, and 100 mg/ml propidium iodide (Sigma-Aldrich,St. Louis, MO, USA) in PBS for 30 min at room temperature. Stained cells were analyzed with BD FACS Canto II (BD Biosciences, San Jose, CA) and Cell-Quest software.

BrdU incorporation assay

To investigate cell proliferation state, CCD-18Lu cell were incubated with conditioned media during time courses and treated with 10 μM BrdU for 1 hour. After harvest, cells were fixed, permeabilized, treated with DNase, and stained with FITC-conjugated anti-BrdU (BD biosciences, San Jose, CA). Total DNAs were stained with 7-AAD and activately synthesizing DNA were detected by FITC-BrdU. Each cell fraction were analyzed by FACS as

manufacturer's guide.

Analysis of Apoptotic ratio.

Cell death marker were detected by annexin V and analyzed with fluorescence activated cell sorter flow cytometer. Apoptosis fraction was determined by measuring the membrane redistribution of phosphatidylserine with an annexin V-FITC/PI apoptosis detection kit (BD Pharmingen, San Diego, CA). Approximately,$1x10^5$ cells were collected and washed twice with cold-PBS. Each sample was stained with annexin V-FITC and 50 μg/ml propidium iodide for 20 min at room temperature in the dark. The apoptotic ratio were detected by the BD FACSCanto II (BD Biosciences, San Jose, CA) and CellQuest software.

Protein digestion in conditioned media

Trypsin (T7409) and trypsin inhibitor (T6522) were purchased from Sigma (Sigma-Aldrich, St. Louis, MO, USA). Trypsin were resolved in 1 mM HCl (pH 3.0) and these solution were treated with conditioned media. For trypsin digestion of protein, trypsin 200 μg/ml were treated to conditioned media for 8 hour at 37°C. After digestion, trypsin inhibitor resolved in PBS (400 μg/ml) were treated with digestive conditioned media for 2 hours at 37 °C to neutralize trypsin activity. Cell debris in conditioned media were eliminated by 0.20 μm syringe filter.

Luciferase reporter assay.

Cells were co-transfected with SBE-luciferase and CMV-β-galactosidase

plasmids using Lipofectamine 3000 reagent (Invitrogen). The total concentration (1 μg/100-mm dish) of DNA was adjusted with pcDNA. The SBE-Luc reporter construct includes 9 repeated Smad binding elements (SBEs), which was given by Dr. Kim SG (Seoul National University, Seoul, Korea). After stabilized overnight, transfected cells were seeded on 12-well plate and further cultured for 24 hours. The cells were incubated with a recombinant peptide for 2 hours, treated with TGF-β1 for 24 hours, and lysed to determine luciferase activity. To normalize transfection efficiency, β-galactosidase activity was measured using o-nitrophenyl- β -D-galactopyranoside. Assays were quadruplicated and each experiment was repeated three times.

Immunoblotting

Cells were lysed in a denaturing SDS sample buffer. Proteins in the cell lysates were separated on SDS/10-15% polyacrylamide gels and transferred to Immobilon-P membranes. The membranes were pre-incubated with 5% skim milk for 30 min, incubated overnight with primary antibodies (1:1000 dilution) at 4°C, and incubated with HRP–conjugated secondary antibodies (1:5000) at room temperature for 1 hr. The immune complexes were visualized using the SuperSignal West Femto kit (Thermo Scientific, Waltham, MA). Antibodies against Smad2, p-Smad2, Smad3, and p-Smad3 were purchased from Cell Signaling Tech. (Danvers, MA); TGFβR1 antibody from Santa Cruz Biotech. (Dallas, TX); α-SMA, collagen-1α, and p-TGFβR1 antibodies from Abcam

(Cambridge, MA); CST3 antibody from R&D Systems (Minneapolis, MN); GDF15 antibody from Fisher Scientific (Pittsburgh, PA).

Immunohistochemistry and Immunofluorescence

Paraffin sections (4 μm) of lung tissues were deparaffinized, rehydrated, and autoclaved at 121°C for 10 min in 100 mM citrate buffer (pH 6.0) to retrieve antigens. After treated with 3% hydrogen peroxide for 10 min, the sections were incubated in 10% bovine serum at room temperature for 1 hr to block nonspecific interactions. They were incubated with an antibody against collagen-1α (1:250 dilution; Abcam), α-SMA (1:500; Abcam), CST3 (1:1000; R&D Systems), or GDF15 (1: 10000; Abcam) overnight at 4°C. For immunohistochemistry, the sections were incubated with biotinylated secondary antibodies (1:500) provided by Vector Laboratories (Burlingame, CA). The immune complexes were visualized using the VECTASTAIN ABC Kit (Vector laboratories). For immunofluorescence, the sections were incubated with Alexa Fluor 488-conjugated anti-goat secondary antibody (Thermo Fisher), and counterstained with DAPI (Invitrogen). Fluorescent images were acquired using Olympus fluorescence microscope (DP30BW, Melville, NY). Four high power fields were randomly selected in each section to analyze stained areas or fluorescent intensities using the ImageJ program (NIH, Bethesda, MD).

Quantitative RT-PCR

Total RNAs were extracted from cells using the TRIzol kit (Thermo Fisher Scientific). cDNAs were synthesized from 2 μg of RNAs using M-MLV

reverse transcriptase (Promega, San Luis Obispo, CA). The cDNAs were amplified with SYBR Green (Enzynomics, Daejeon, Korea), and quantified using a 7900HT real-time PCR detection system (Bio-Rad, Hercules, CA). The sequences of PCR primers are informed on Supplementary Method.

siRNA transfection

siRNA corresponding to human GDF15, cystatin C and Intereukin 1α were obtained from IDT (Coralville, IA, USA). The siRNA sequences (5' to 3') are as followings; CST3#1: GCACAAUGACCUUGUCGAAAUCCAC; CST3#2: CCUAUCACCUCUUAUGCACACCUCC; CST3#3: CGCCCGCAAGCAG AUCGUAGCUGGG; GDF15#1: GCUGGGAAGAUUCGAACACCGACCT; GDF1#2: AGACUCCAGAUUCCGAGAGUUGCGG; GDF15#3: CGGA UACUCACGCCAGAAGUGCGGC. The hPAE cells were transfected with the oligonucleotides, using Lipofectamine RNA iMAX Reagent (Invitrogen, Carlsbad, CA, USA) in the indicated concentrations. For transfection, cells at 50% confluence were transfected with 20 nM or 40 nM siRNAs with RNAi-MAX reagent according to the manufacturer's protocols. The medium was changed with fresh growth medium at 1 hour post-transfection and cells were incubated for a further 24 h. Next day, all transfected cells were replaced with fresh serum-free media for a further 48 h. Finally, the supernatants were collected and were filtered by 0.20 μm syringe filter.

Statistical analysis

The statistical analysis was performed using the SPSS (window version

15.0.0) software package. Comparisons between two groups were analyzed by Student's t-test for parametric data or by Mann–Whitney U test for non-parametric data. Survival rates were analyzed by the log-rank test. Significant difference was defined when P was less than 0.05.

Table 1. Baseline characteristics of all patients with ILD or without ILD

	Without ILD patients (n=10)	With ILD patients (n=10)
Age years	64 ± 8.6	59 ± 13.7
Underying disease		
Adenoid cystic carcinoma with usual interstitial pneumonia		1
Adenocarcinoma with usual interstitial pneumonia		
Usual interstitial pneumonia		6
Squamous cell carcinoma with usual interstitial pneumonia		1
Acute exacerbation in usual interstitial pneumonia		1
Adenocarcinoma	8	
Squamous cell carcinoma	2	
Sex		
Male	5	6
Female	5	4
Smoking status		
Never-smoker	6	5
Ex-smoker	4	4
Continuing smoker		1
ILD related tx		
None	10	2
Pd		4
Lung TPL		1
Oxygen therapy		1
Cough suppressant		2

Data are presented as mean ± SEM. n=10

RESULTS

Lung fibroblast growth is inhibited in alveolar epithelial cell-conditioned media

To determine which cells produced fibroblast-inhibiting factors, I incubated lung fibroblast cell lines CCD-18Lu in a mixture (1:1) of a fresh medium and a conditioned medium (CM) collected from various epithelium-derived cells, including human pulmonary alveolar epithelial cells (hPAE) and human lung fibroblast (CCD-18Lu) cell lines. Before collecting conditioned media, I verified that all cells could maintain their viabilities in serum-free DMEM medium (data not shown). The growth of CCD-18Lu cells was significantly attenuated in hPAE CM (Figure 1A). To understand the properties of fibroblast growth arrest, proliferating, dead, apoptotic, or necrotic cells were counted. Given that BrdU-positive cell in the S-phase were regarded as proliferative (Figure 1C), cell proliferation was halted in hPAE CM (Figure 1B). To analyze cell death, trypan blue-stained cells were counted, which indicates that cells undergo death in hPAE CM (Figure 2A). I evaluates the types of cell death by co-staining cells with annexin V and propidium iodide (Figure 2D), and found that hPAE CM provoked either apoptosis or necrosis in CCD-18Lu cells (Figures 2B and 2C). To confirm apoptosis, cleaved caspase 3 and PARP were detected by Western blotting. Both apoptosis markers increased in CCD-18Lu cells incubated with hPAE CM (Figure 3A). I next analyzed the cellular levels of α-smooth muscle actin (α-SMA) and collagen-1α, which are representative markers of active myofibroblasts (Gabbiani, 2003; Oruqaj et al., 2015). Given that both extracellular proteins

were upregulated incubation period-dependently, CCD-18Lu cells were spontaneously activated under fetal bovine serum and CM. However, this fibroblast activation did not occur in hPAE CM (Figure 3B). Based on the results, normal epithelial cells are likely to release some factors against fibroblast growth and activation.

Alveolar epithelial cell-derived CST3 and GDF15 inhibit lung fibroblast growth

To examine whether the fibroblast-inhibiting factors are composed of polypeptides, hPAE CM was heated to denature polypeptides or trypsinized to degrade them. After heating or trypsinizing, hPAE CM almost completely lost its ability to inhibit fibroblast growth (data not shown). These results strongly indicate that the fibroblast-inhibiting factors are polypeptides. To identify peptide-based cytokines in CMs, CCD-18Lu and hPAE CMs were tested with the Human XL Cytokine Array Kit. The red boxes (1~14) indicate cytokines that were more abundant in hPAE CM than in CCD-18Lu. (Figure 4A). Cytokine levels quantified from pixels in the ImageJ program are presented as bar graphs (Figure 4C). The cytokines enriched in hPAE CM are summarized in Figure 4B. After reviewing the literatures on cytokine functions, I determined two candidates as fibroblast-inhibiting cytokines: cystatin C (CST3) has been reported to inhibit fibrosis by antagonizing TGF-β; (Sokol et al., 2004; Kasabova et al., 2014) growth differentiation factor 15 (GDF15) to induce cancer cell death (Liu et al., 2003; Kadara et al., 2006). In immunoblot analyses, CST3 and GDF15 were identified to accumulate over time in hPAE

CM. (Figure 5A). To examine whether the cytokines inhibit fibroblast growth, I prepared CMs from hPAE cells in which each cytokine was knocked-down. To rule out off-target effects of siRNAs, I assessed and confirmed the fibroblast-inhibiting effects of CST3 and GDF15 siRNAs targeting different sites of each mRNA (Figures 5B and 6A). These siRNAs per se remaining in the CMs did not affect the CCD-18Lu growth (data not shown). When both cytokines were knocked-down together, cell proliferation and survival both were additively enhanced (Figures 6B-D, and 7A-B). To confirm the roles of these cytokines in fibroblast inhibition, I incubated CCD-18Lu cells in hPAE CM pretreated with a neutralizing antibody against CST3 or GDF15 for 48 hours. Each antibody rescued fibroblast growth even in hPAE CM (Figure 7C). These results suggest that CST3 and GDF15 are secreted from normal alveolar epithelial cells and are involved in the inhibition of fibroblast growth.

Recombinant CST3 and GDF15 inhibit fibroblast growth and activity in cell culture

To confirm the actions of CST3 and GDF15 against fibroblast growth, CCD-18Lu was treated with recombinant peptides of human CST3 (rCST3) and human GDF15 (rGDF15), and cell numbers were counted 24 hr after the treatment. Both peptides reduced the number of CCD-18Lu cells in a concentration-dependent manner (Figure 8A). Based on the IC50 (half maximal inhibitory concentration) values, rGDF15 and rCST3 seem to have the similar efficacy. In contrast, the peptides failed to inhibit cell growth in hPAE cells (Figure 10C), supporting the fibroblast-specific actions of these

peptides. To test the synergistic effects of rCST3 and rGDF15, I compared the fibroblast-inhibiting effects of 1 ng/mL of each peptide with a combination of half-concentrations (0.5 + 0.5 ng/mL) of the two peptides. The combination showed a greater (>2-fold) effect than the single treatment of each peptide (Figure 8B). Given that the combination index (CI) was less than 1.0 on the compusyn software (CompuSyn Inc.; Paramus, NJ), the combination of CST3 and GDF15 seems to have a synergistic effect on fibroblast inhibition (Chou, 2010). Aside from growth inhibition, both peptides downregulated collagen-1α and α-SMA protein and mRNA levels (Figure 9A and 9B). In addition, I isolated pulmonary fibrosis-associated fibroblasts (PFAF) from mouse lungs with bleomycin-induced fibrosis to observe responses of activated lung fibroblasts. rGDF15 or/and rCST3 diminished PFAF numbers (Figure 10A), promoted cell death (Figures 10B and 11A,C), and reduced proliferation potential (Figure 11B and 11D). rGDF15 or/and rCST3 also downregulated collagen-1α and α-SMA protein and mRNA levels (Figures 12A and 12B). These results encouraged us to investigate whether the peptides are applicable to prevent pulmonary fibrosis.

CST3 and GDF15 inhibit the TGF signaling pathway

Given that fibroblast growth and activation largely depend on the TGF-Smad pathway, I first checked whether CST3 and GDF15 inhibit the signaling pathway. As expected, Smad2/3 in CCD-18Lu were phosphorylated (or activated) in the presence of FBS. Interestingly, the phosphorylation was attenuated by recombinant CST3 or/and GDF15 (Figure 13A). When the TGF

signaling pathway was provoked by TGF-β1, TGF-β receptor and Smad2/3 were inactivated by CST3 or/and GDF15 (Figure 13B). In either CCD-18Lu cells (Figure 13C) or primary mouse lung fibroblasts (Figure 13D), cell growth was stimulated by TGF-β1, which was abolished by the recombinant peptides. ECM production in CCL-18Lu and mouse lung fibroblast was also stimulated by TGF-β1, but inhibited by the recombinant peptides (Figure 14A). Collagen 1α and αSMA expressions in mouse lung fibroblasts were repressed at the transcriptional level by the peptides (Figure 14B). I next evaluated the TGF/Smad-dependent gene expression using the SBE-luciferase reporter, and confirmed the inhibitory actions of CST3 and GDF15 to the TGF-Smad signaling pathway (Figure 15).

CST3 and GDF15 are down-regulated in mouse and human lungs undergoing fibrosis

At the last step of wound repair, the epithelium may function to normalize the ECM microenvironment by pacifying fibroblasts excited during ECM reconstruction. Yet, the epithelium-derived, fibroblast-controlling factors have not been identified. These results prompted us to test the possibility that CST3 and GDF15 are bona fide controller of fibroblasts in the lung. Firstly, I analyzed the expression of CST3 and GDF15 in lung tissues of patients with and without interstitial lung disease (ILD). Masson's trichrome staining verified that the lung tissues from ILD patients were filled with massive ECM but those from lung cancer patients without ILD had normal architecture. CST3 and GDF15 were observed to be highly expressed along the alveolar

wall in non-ILD lungs. Surprisingly, both cytokines were barely present in ILD lungs (Figure 16A, right). All histological data in human lung specimens are shown in Figures 18-21. To quantify the cytokine levels, fluorescence intensities were normalized to cell numbers. The expressions of both cytokines were significantly lower in ILD lungs than in non-ILD lungs (Figure 16B). To confirm the suppression of the cytokines during fibrosis, I adopted an animal model for pulmonary fibrosis. C57/B6 mice were subjected to a single challenge of bleomycin via bronchial instillation, and intraperitoneally injected twice weekly with PBS. On Day 21 after the bleomycin treatment, lung tissues were prepared for histological analyses. Figure 17A shows the experimental schedule and the results from Masson's trichrome staining. The procedure using bleomycin successfully induced excessive deposition of collagen in the interstitium of mouse lungs. As was shown in ILD lungs, both the cytokines were markedly suppressed in fibrotic lungs of mice, which was double-checked by immunofluorescence analysis (Figure 17B, right) and immunoblotting (Figure 22A and 22C). To examine whether these cytokines were released from alveolar epithelium, we measured CST3 and GDF15 in BALF, and found that CST3 and GDF15 levels Ire substantially reduced in fibrotic lungs (Figures 22B and 22D). Accordingly, the suppression of these cytokines in fibrotic lungs provides a rationale to restore the cytokines for treating lung fibrosis.

Recombinant CST3 and GDF15 ameliorate pulmonary fibrosis in vivo

After a bronchial instillation of bleomycin, C57/B6 mice were systemically injected twice weekly with PBS, rCST3 (100 μg/kg), rGDF15 (100 μg/kg), or both peptides (50 μg/kg of each). On the 21st day, lung tissues were excised, as illustrated in Figure 23A. Body weight was measured continuously to monitor apparent health. Mouse weights gradually decreased over the 21 days, but was significantly recovered by combined peptides (Figure 23B). Mouse survival was also improved by the combination (Figure 23C). To evaluate the extent of pulmonary fibrosis, I stained lung specimens with Masson's trichrome and hematoxylin/eosin (Figure 24A). As expected, bleomycin induced an obstruction of the alveolar sacs with thickened inter-alveolar septa and massive collagen in the lung interstitium. Administration of either rCST3 or rGDF15 saved airways spaces and lessened fibrosis in bleomycin-treated lungs, and the combination of these peptides at the half doses was more effective than any single administration (Figure 24A). To quantify the fibrotic changes, I measured fibrotic areas and Ashcroft scores on Masson's trichrome-stained specimens, and biochemically analyzed hydroxyproline levels in lung tissues (Figure 24B, 24C, and 24D). The results of these fibrosis parameters further supported these hypothesis that rCST3 and rGDF15 in combination attenuates bleomycin-induced pulmonary fibrosis. Next, I analyzed α-SMA and collagen-1α levels to evaluate the degree of fibroblast activation. Both markers were densely stained in the lungs treated with bleomycin, but were less obvious in peptide-treated lungs (Figure 25A, 25B). Collectively, recombinant CST3 and GDF15 could be developed as potential biopharmaceuticals for treating pulmonary fibrosis.

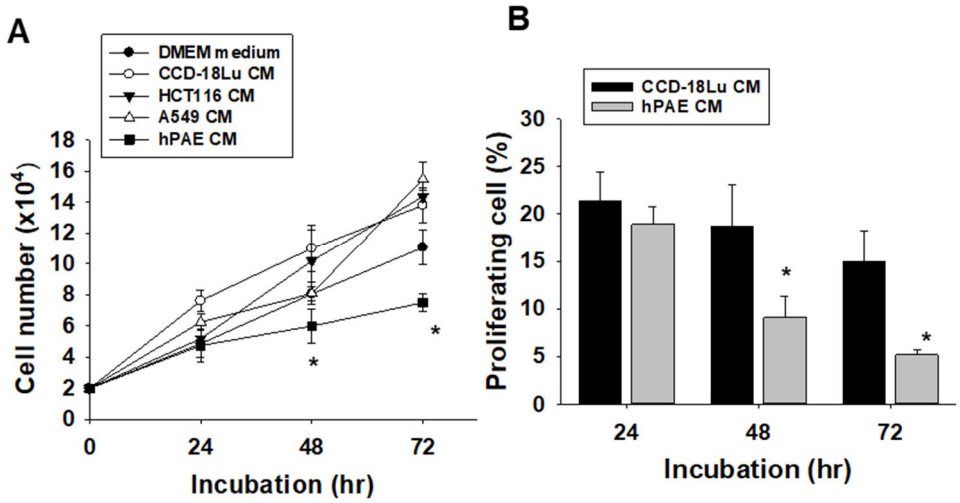
A
DMEM medium
CCD-18Lu CM
HCT116 CM
A549 CM
hPAE CM
Cell number (x10^4)
Incubation (hr)
B
CCD-18Lu CM
hPAE CM
Proliferating cell (%)
Incubation (hr)

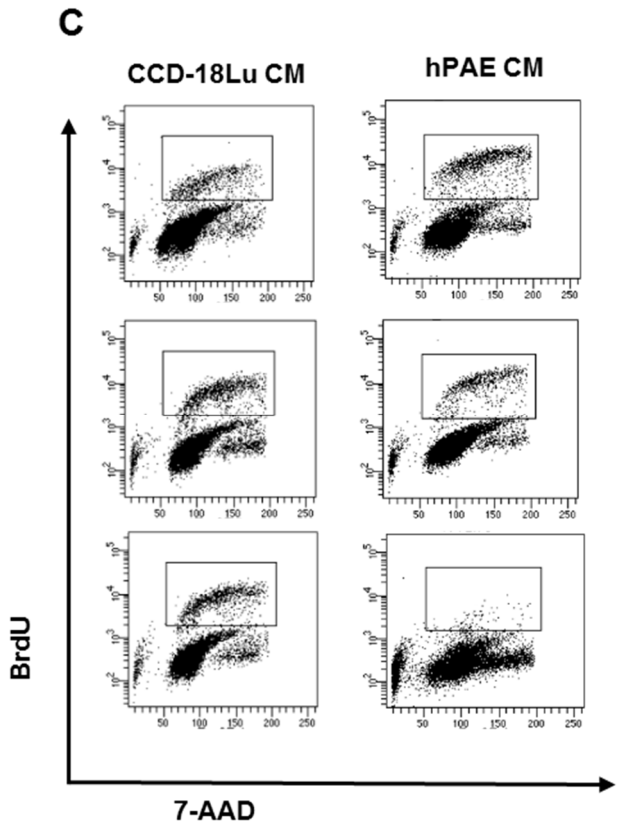
C
CCD-18Lu CM
hPAE CM
BrdU
7-AAD

Figure 1. Lung fibroblast growth is inhibited in the conditioned medium from pulmonary alveolar epithelial cells. (A) CCD-18Lu cells were incubated in conditioned media (CM) collected from the indicated cells. Viable CCD-18Lu cells (unstained with trypan blue) were counted using a hemocytometer. (B) After CCD-18Lu cells were incubated in the indicated CMs for 1-3 days, the population of proliferating cells was determined by counting BrdU-stained cells at the S phase on flow cytometry. (C) CCD-18Lu cells were co-stained with BrdU and 7-AAD, and analyzed by flow cytometry.

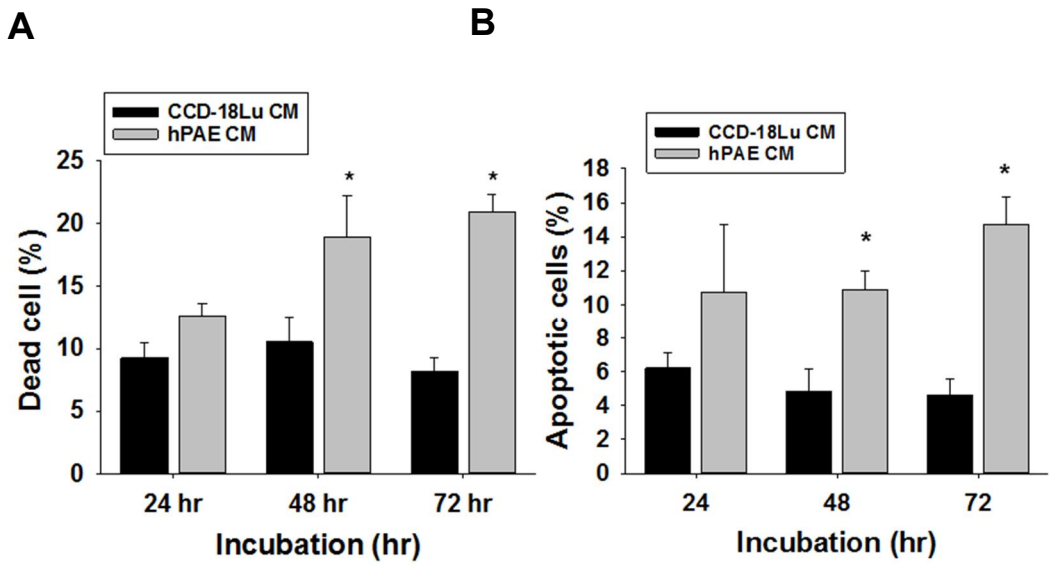
A
B
CCD-18Lu CM
hPAE CM
Dead cell (%)
Apoptotic cells (%)
Incubation (hr)
24 hr
48 hr
72 hr
24
48
72
*

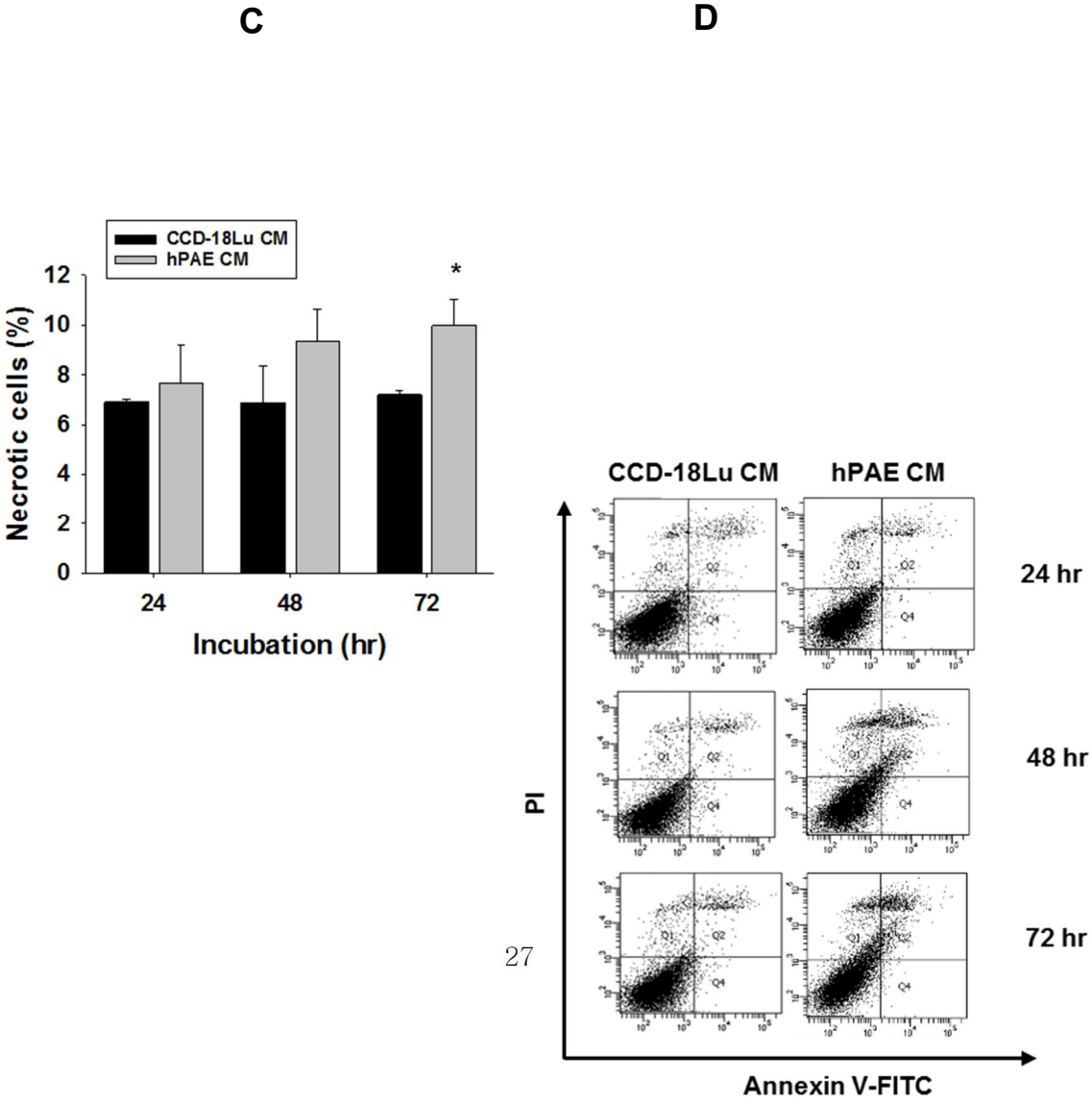
C
D
CCD-18Lu CM
hPAE CM
Necrotic cells (%)
Incubation (hr)
24
48
72
*
CCD-18Lu CM
hPAE CM
24 hr
48 hr
72 hr
PI
Annexin V-FITC
Q1
Q2
Q4

Figure 2. Lung fibroblast death is induced by the conditioned medium from pulmonary alveolar epithelial cells. (A) CCD-18Lu cells were incubated in the indicated CM, and dead cells (stained with trypan blue) were counted using a hemocytometer. (B, C) CCD-18Lu cells were co-stained with annexin V-FITC for apoptosis and propidium iodide for necrosis, and subjected to flow cytometry. Data in all panels are presented as the means and s.d. ($n = 3$). *, $P < 0.05$ versus the CCD-18Lu CM group. (D) CCD-18Lu cells were co-stained with annexin-V and propodium iodine, and analyzed by flow cytometry.

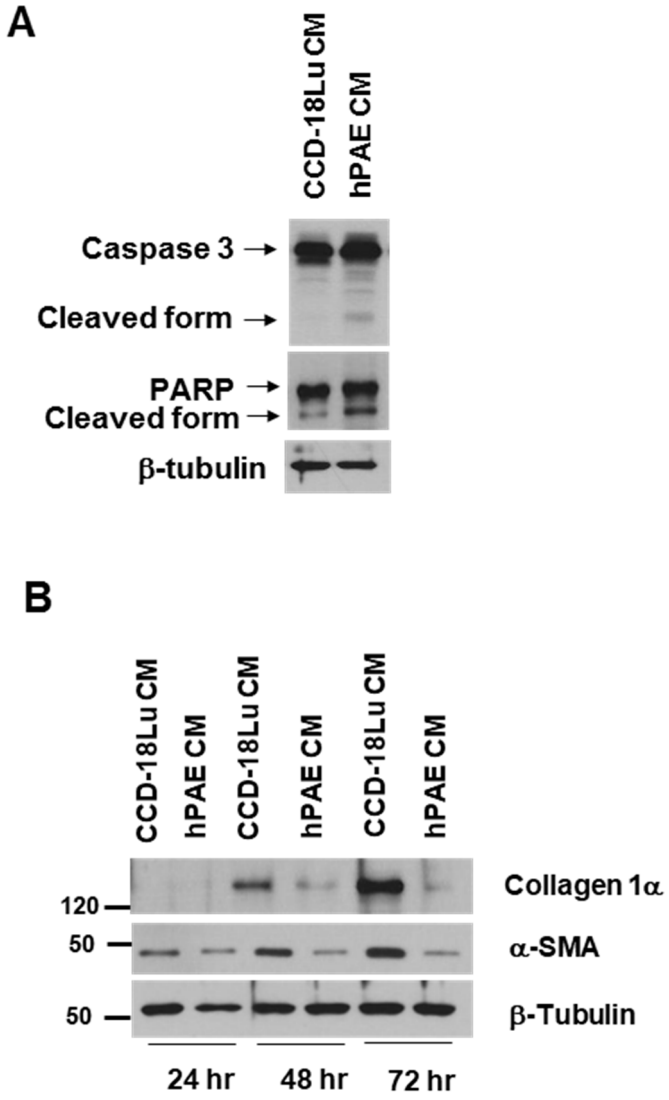
A
CCD-18Lu CM
hPAE CM
Caspase 3
Cleaved form
PARP
Cleaved form
β-tubulin
B
CCD-18Lu CM
hPAE CM
CCD-18Lu CM
hPAE CM
CCD-18Lu CM
hPAE CM
120
50
50
Collagen 1α
α-SMA
β-Tubulin
24 hr
48 hr
72 hr

Figure 3. Lung fibroblast differentiation and growth is inhibited in the conditioned medium from pulmonary alveolar epithelial cells. (A) CCD-18Lu cells were incubated in the indicated CMs for 1-3 days. After floating cells were removed, attached cells were subjected to immunoblotting and Caspase 3 and PARP expression level were determined (B) Collage 1α and α-SMA expression level were determined by western blot.

A

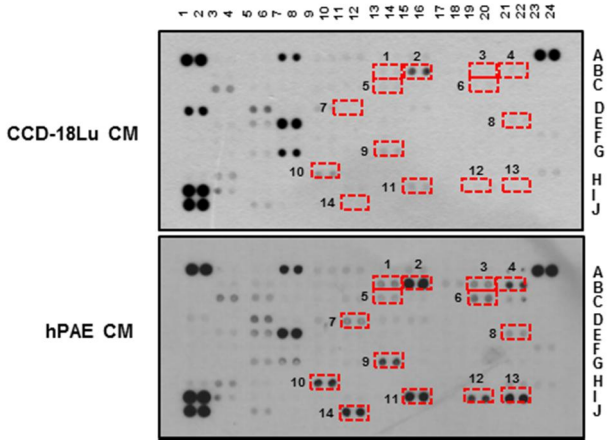

B

	Cytokines	Growth
1	CST3	-
2	DKK1	+
3	EGF	+
4	EMMPRIN	+
5	FGF19	+
6	GDF15	-
7	IGBP2	+
8	IL17A	+
9	MIF	+
10	PTX3	+
11	THBS1	±
12	PLAUR	+
13	VEGF	+
14	VCAM1	+

continued

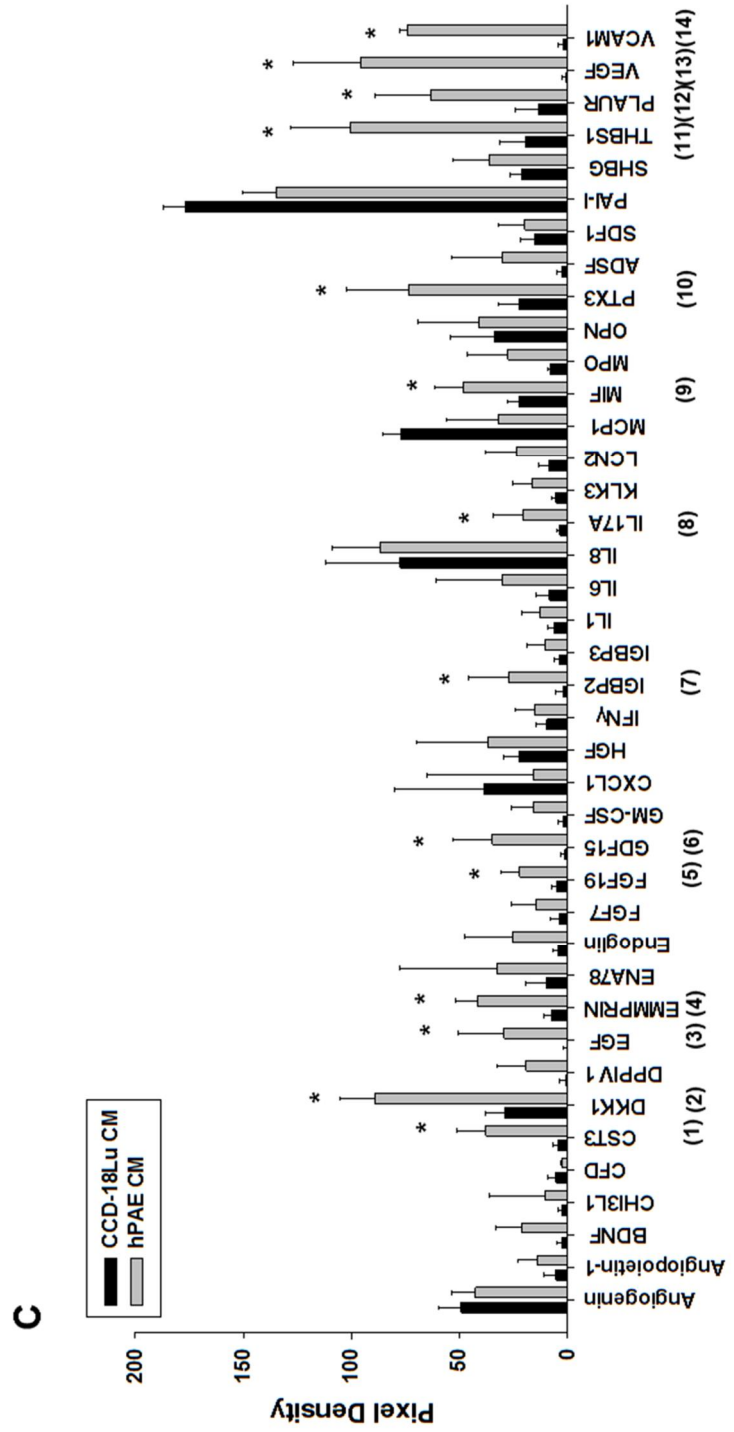
C
CCD-18Lu CM
hPAE CM
Pixel Density
200
150
100
50
0
Angiogenin
Angiopoietin-1
BDNF
CHI3L1
CFD
CST3
DKK1
DPPIV 1
EGF
EMMPRIN
ENA78
Endoglin
FGF7
FGF19
GDF15
GM-CSF
CXCL1
HGF
IFNγ
IGBP2
IGBP3
IL1
IL6
IL8
IL17A
KLK3
LCN2
MCP1
MIF
MPO
OPN
PTX3
ADSF
SDF1
PAI-1
SHBG
THBS1
PLAUR
VEGF
VCAM1
(1) (2)
(3) (4)
(5) (6)
(7)
(8)
(9)
(10)
(11)(12)(13)(14)

Figure 4. Identification of cytokines secreted from hPAE cells. (A) The conditioned media collected from CCD-18Lu and hPAE cells were applied to the proteome profiling arrays and proteins were visualized using ECL. Red boxes indicate the cytokines whose levels are relatively higher in hPAE-conditioned media compared to CCD-18Lu. (B) The intensities of dots in the arrays were quantified using the ImageJ program. The pixel densities are presented as bars (means + s.d., n = 3) and * denotes $P < 0.05$ versus both CCD-18Lu CM. (C) The cytokines enriched in hPAE-conditioned media are listed. In the growth category, -, +, and ± represent negative, positive, and controversial effects on cell growth, respectively.

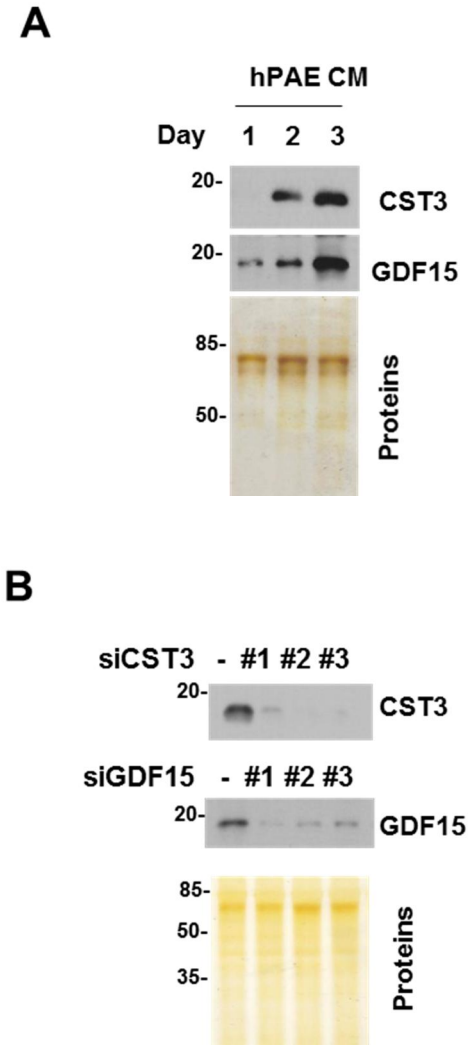
A
hPAE CM
Day 1 2 3
20-
CST3
20-
GDF15
85-
50-
Proteins
B
siCST3 - #1 #2 #3
20-
CST3
siGDF15 - #1 #2 #3
20-
GDF15
85-
50-
35-
Proteins

Figure 5. CST3 and GDF15 levels in hPAE conditioned media. (A) Conditioned media (CMs) were collected from hPAE on the indicated times and proteins were precipitated using TCA. (B) CMs were collected on day 3 from hPAE which had been transfected with the indicated siRNAs. Proteins were precipitated using TCA. Proteins were subjected to immunoblotting and silver staining.

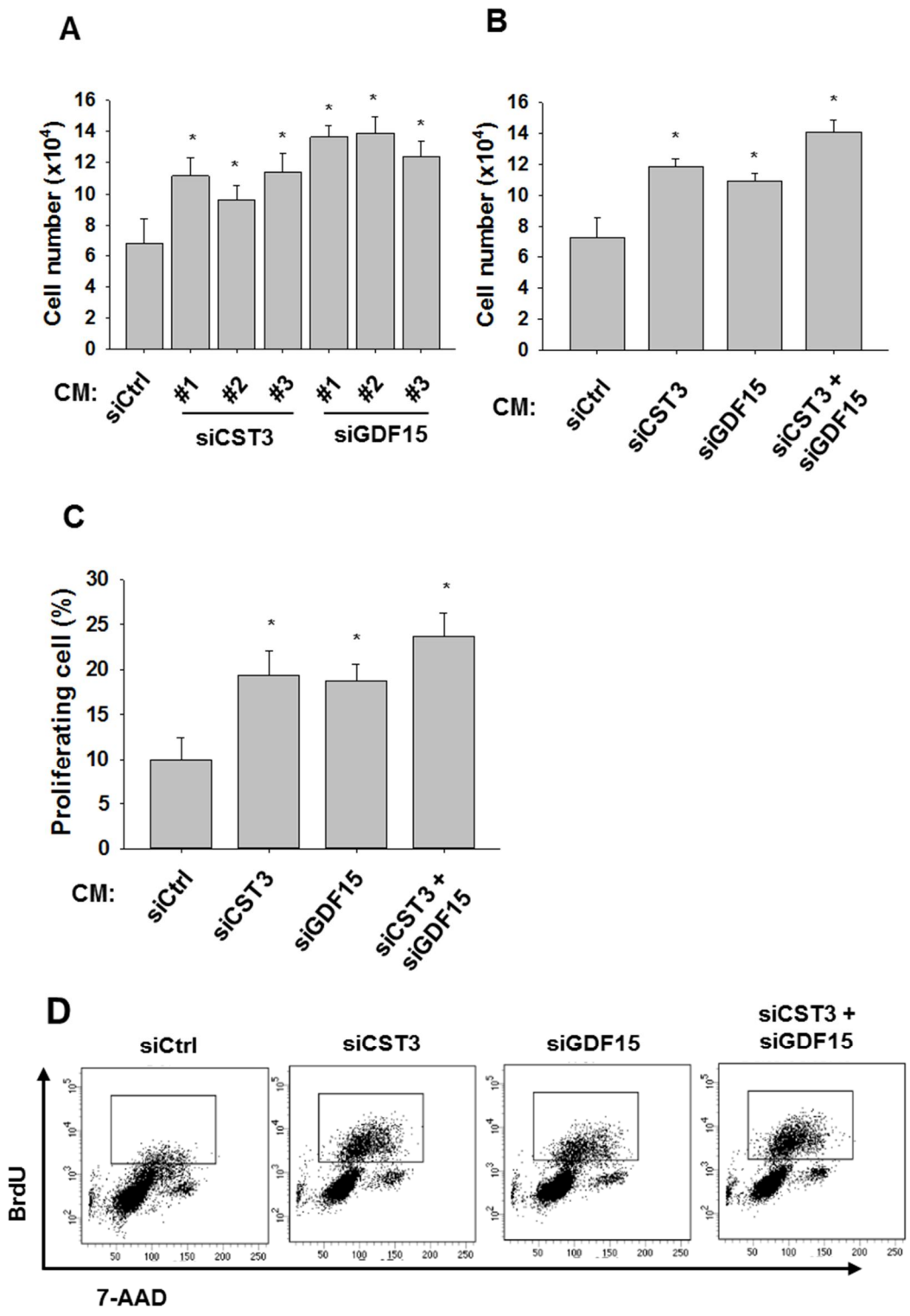
A
Cell number (x10^4)
CM:
siCtrl
#1
#2
#3
#1
#2
#3
siCST3
siGDF15
B
Cell number (x10^4)
CM:
siCtrl
siCST3
siGDF15
siCST3 + siGDF15
C
Proliferating cell (%)
CM:
siCtrl
siCST3
siGDF15
siCST3 + siGDF15
D
siCtrl
siCST3
siGDF15
siCST3 + siGDF15
BrdU
7-AAD

Figure 6. CST3 and GDF15 are responsible for fibroblast growth inhibition by hPAE CM. (A) CCD-18Lu cells were incubated for 48 hr in CM from hPAE cells transfected with the indicated siRNAs (40 nM). Three different siRNAs (#1, #2 and #3) for CST3 or GDF15 were tested. Viable CCD-18Lu cells were counted (right). (B) (C) hPAE cells were transfected with 20 nM siRNA targeting CST3 or GDF15, or with both (20 nM each). After 48 hr, cell growth rate were measured by hematocytometer, and (D) the population of BrdU-stained CCD-18Lu cells at S phase were analyzed by flow cytometry. Each bar in all panels represents the mean + s.d. (n = 3). *, $P < 0.05$ versus the si-Ctrl group or the IgG group.

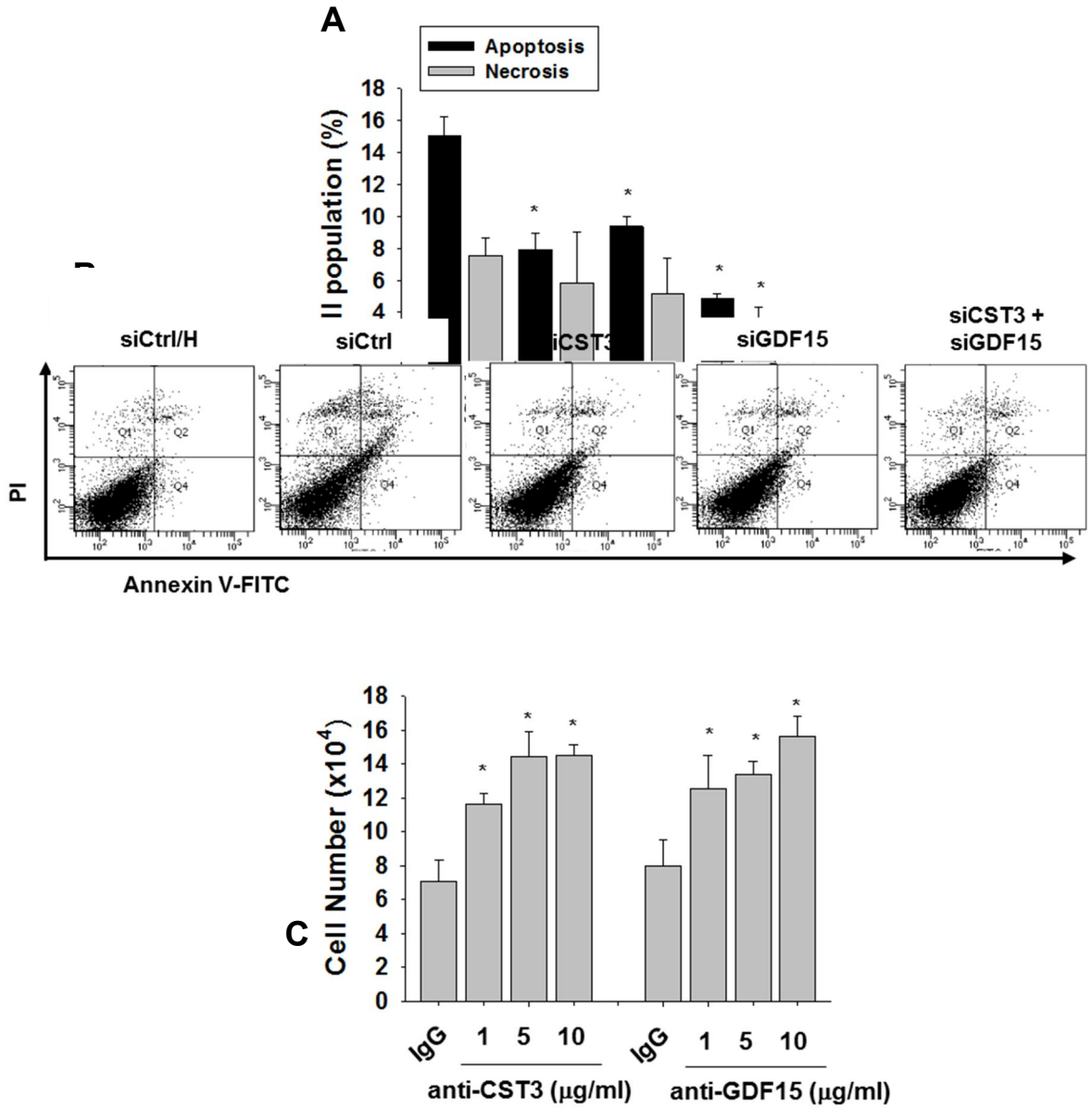

Figure 7. CST3 and GDF15 are responsible for fibroblast grwoth inhibition by hPAE CM. Effects of CST3 and GDF15 knock-down on fibroblast proliferation and death. hPAE cell were transfected with each or both of CST3- and GDF15-targeting siRNAs (20 nM of each). CCD-18Lu cells were incubated for 48 hours in the 72 hour-conditioned media from the

transfected cells. (A) Apoptotic and necrotic CCD-18Lu cells were marked with annexin V-FITC and propidium iodide and subjected to flow cytometry. (B) Cells were co-stained with annexin-V and propodium iodine to analyze apoptosis and necrosis (C) hPAE CM was pre-incubated with non-immunized serum (IgG), anti-CST3, or anti-GDF15 antibody at the indicated doses for 1 hr. CCD-18Lu cells were incubated for 48 hr in the conditioned media, and viable cells were counted. Each bar in all panels represents the mean + s.d. (n = 3). *, $P < 0.05$ versus the si-Ctrl group or the IgG group.

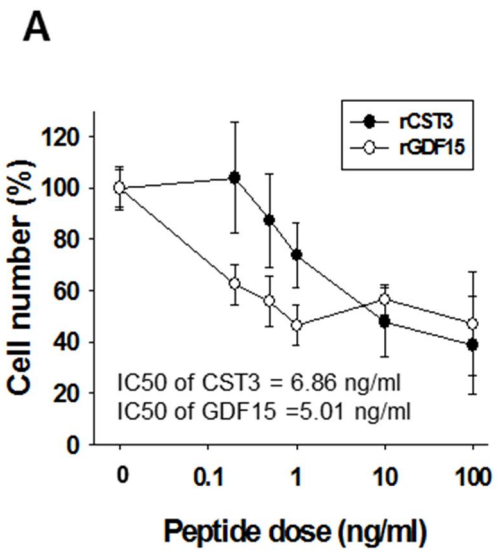

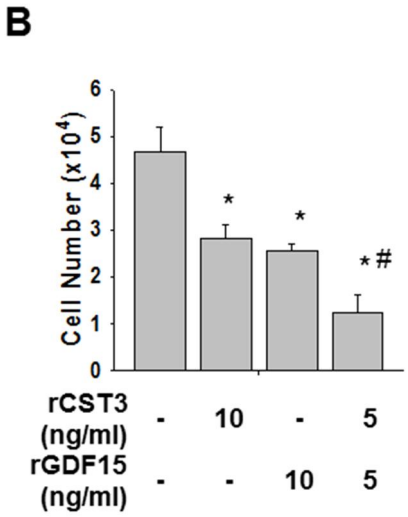

Figure 8. CST3 and GDF15 peptides inhibit proliferation in CCD-18Lu cells. (A) CCD-18Lu cells were treated with a recombinant peptide of CST3 or GDF15 and cultured in 2% serum-containing medium for 24 hr. IC50s are the doses of peptides showing 50% growth

inhibition. (B) CCD-18Lu cells were incubated with one of two peptides (10 ng/mL) or both peptides (5 ng/mL each) for 48 hr.

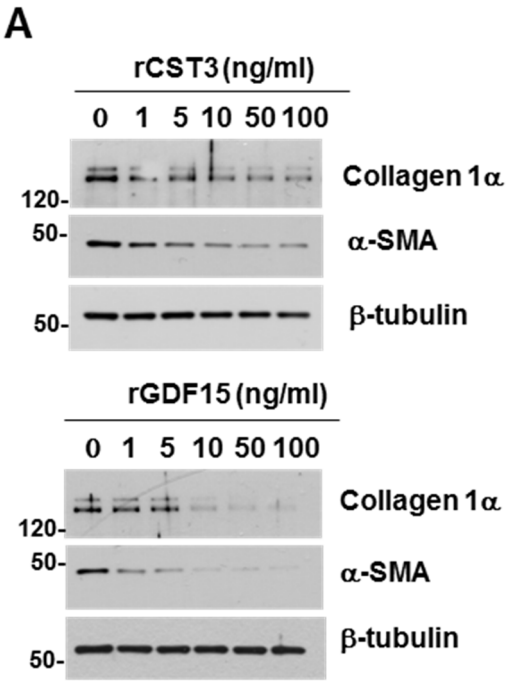

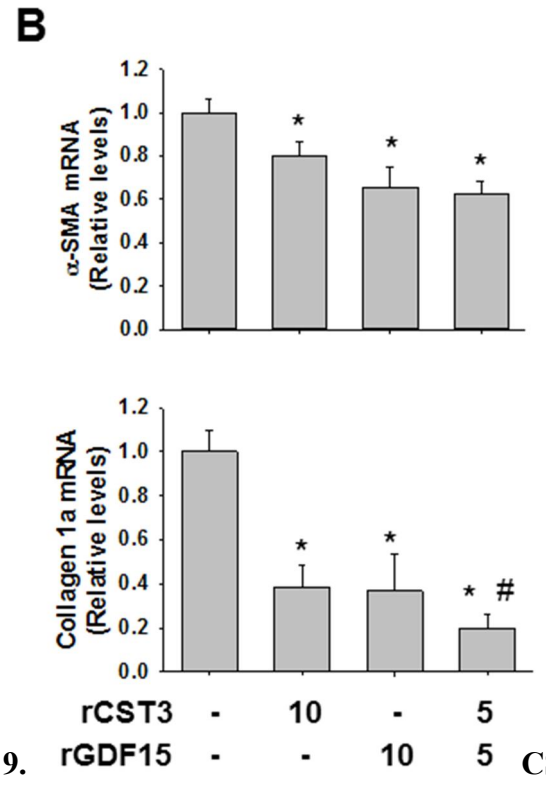

Figure 9. CST3 and GDF15 peptides inhibit ECM production in CCD-18Lu cells. (A) CCD-18Lu cells were incubated with CST3 or GDF15 peptide for 48 hr, and subjected to immunoblotting. (B) CCD-18Lu cells were incubated with

one of two peptides (10 ng/mL) or both peptides (5 ng/mL each) for 24 hr. The mRNA levels were measured by RT-qPCR. All data are presented as the means + s.d. from 3 experiments. *, $P < 0.05$ versus the PBS group; #, $P < 0.05$ versus the CST3 or GDF15 only group.

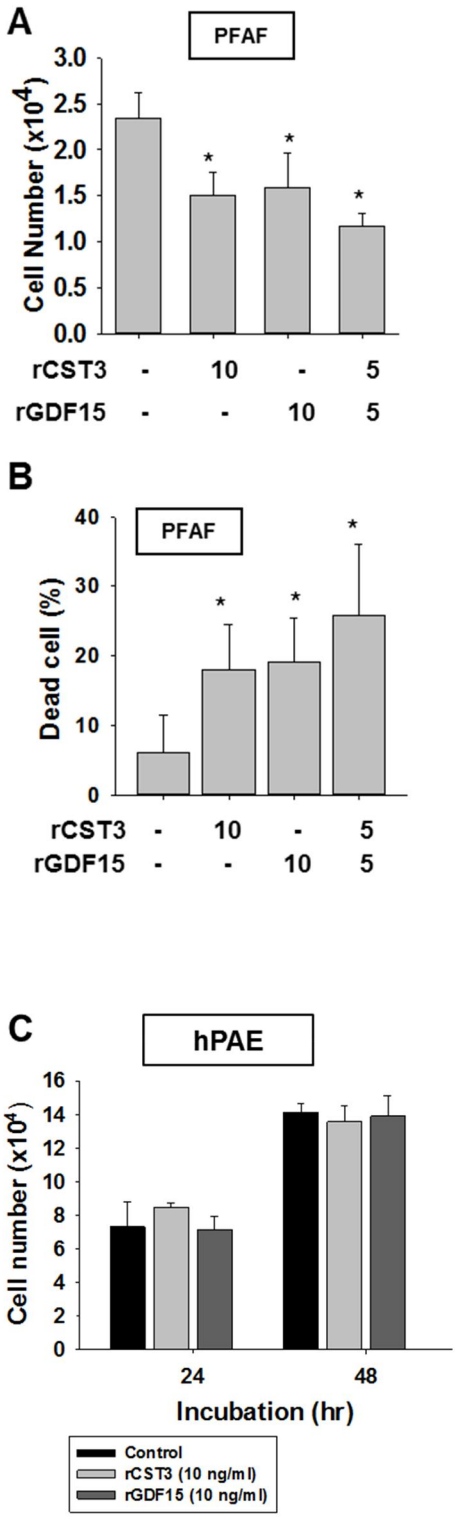
A
PFAF
Cell Number (x10^4)
3.0
2.5
2.0
1.5
1.0
0.5
0.0
rCST3 - 10 - 5
rGDF15 - - 10 5
B
PFAF
Dead cell (%)
40
30
20
10
0
rCST3 - 10 - 5
rGDF15 - - 10 5
C
hPAE
Cell number (x10^4)
16
14
12
10
8
6
4
2
0
24
48
Incubation (hr)
Control
rCST3 (10 ng/ml)
rGDF15 (10 ng/ml)

Figure 10. CST3 and GDF15 peptides inhibit proliferation and ECM production in PFAF cells. (A)(B) Primary lung fibroblasts were isolated from fibrotic tissues of bleomycin-treated mouse lungs, and cultured. The pulmonary fibrosis-associated fibroblasts (PFAFs) were pre-incubated in a 2% FBS-containing medium for 16 hr, and then treated with CST3 or/and GDF15 (5 or 10 ng/mL) for 24 hr. Viable (unstained, e) and dead (stained, f) cells were counted using a hemocytometer. (C) Effects of recombinant peptides on cell growth in hPAE. hPAE cells were treated with a recombinant peptide of CST3 or GDF15 for 24 hours or 48 hours, and the numbers of viable cells were counted using a hemocytometer. Each bar represents the mean and s.d. from four independent experiments**.**

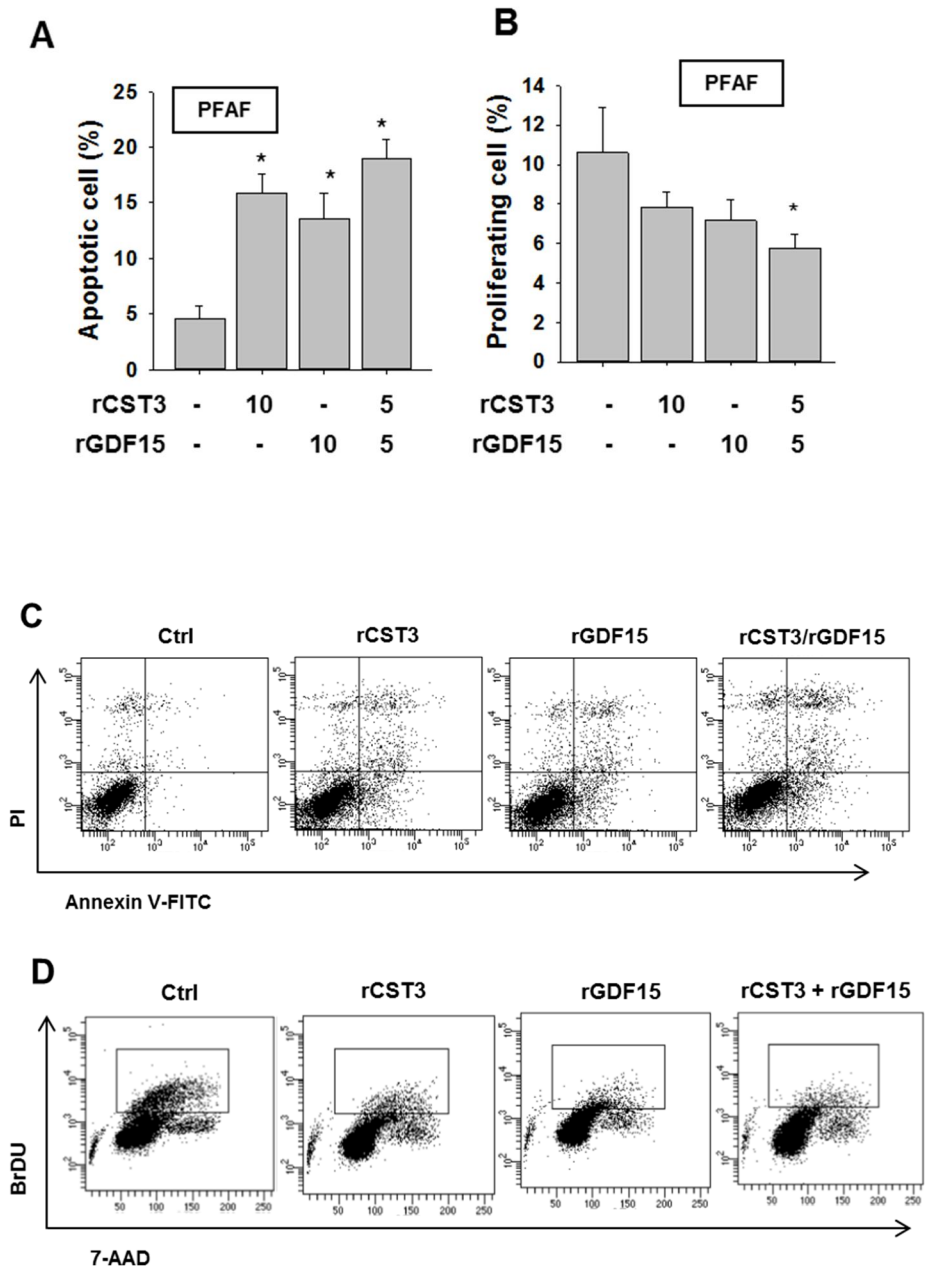
A
PFAF
Apoptotic cell (%)
25
20
15
10
5
0
*
*
*
rCST3 - 10 - 5
rGDF15 - - 10 5
B
PFAF
Proliferating cell (%)
14
12
10
8
6
4
2
0
*
rCST3 - 10 - 5
rGDF15 - - 10 5
C
Ctrl
rCST3
rGDF15
rCST3/rGDF15
PI
Annexin V-FITC
D
Ctrl
rCST3
rGDF15
rCST3 + rGDF15
BrDU
7-AAD

Figure 11. CST3 and GDF15 peptides inhibit proliferation in PFAF cells. (**A**) PFAFs, which had been treated with CST3 or/and GDF15 for 24 hr, were co-stained with annexin V-FITC and propidium iodide (B) or with co-stained with BrdU and 7-AAD, and subjected to flow cytometry. (C) PFAF cells were treated by with a recombinant peptide of CST3 or GDF15 for 24 hours, after that cells were stained by annexin V and PI. (D) Both CST3 or GDF15 treated PFAF cells were stained by BrdU and 7-AAD after 24 hours. All data are presented as the means + s.d. from 3 experiments.*, $P < 0.05$ versus the untreated PFAF group.

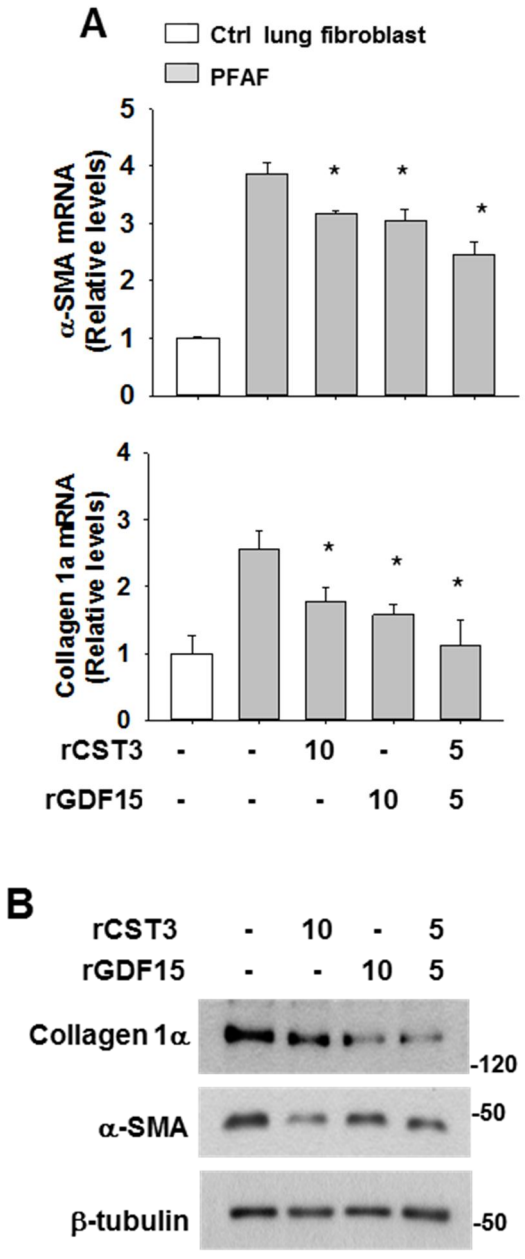
A
Ctrl lung fibroblast
PFAF
α-SMA mRNA (Relative levels)
Collagen 1a mRNA (Relative levels)
rCST3 - - 10 - 5
rGDF15 - - - 10 5
B
rCST3 - 10 - 5
rGDF15 - - 10 5
Collagen 1α
α-SMA
β-tubulin
-120
-50
-50

Figure 12. CST3 and GDF15 peptides inhibit differentiation and ECM production in PFAF cells. (A) Control lung fibroblasts were treated with PBS, and PFAFs were treated with PBS or CST3 or/and GDF15 in 2% FBS-containing media for 24 hr. The mRNA levels were measured by RT-qPCR. (B) PFAFs were treated with CST3 or/and GDF15 for 24 hr, lysed, and subjected to immunoblotting. All data are presented as the means + s.d. from 3 experiments.*, $P < 0.05$ versus the untreated PFAF group.

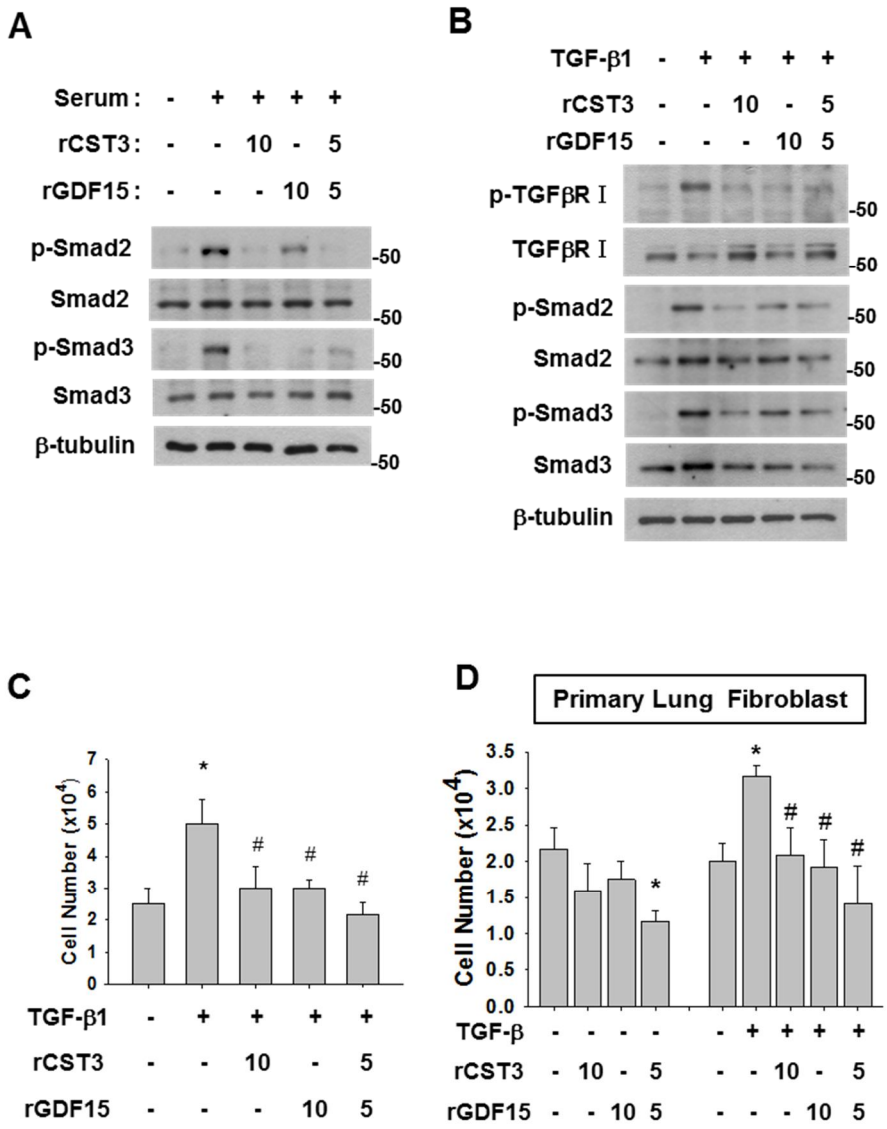
A
Serum : - + + + +
rCST3 : - - 10 - 5
rGDF15 : - - - 10 5
p-Smad2
Smad2
p-Smad3
Smad3
β-tubulin
-50
B
TGF-β1 - + + + +
rCST3 - - 10 - 5
rGDF15 - - - 10 5
p-TGFβR I
TGFβR I
p-Smad2
Smad2
p-Smad3
Smad3
β-tubulin
-50
C
Cell Number (x10^4)
TGF-β1 - + + + +
rCST3 - - 10 - 5
rGDF15 - - - 10 5
D
Primary Lung Fibroblast
Cell Number (x10^4)
TGF-β - - - - - + + + +
rCST3 - 10 - 5 - - 10 - 5
rGDF15 - - 10 5 - - - 10 5

Figure 13. CST3 and GDF15 inhibit the TGF-β signaling pathway in CCD-18Lu cells. (A)(B) CCD-18Lu cells, which had been pre-incubated in serum-free media for 16 hr, were treated with a recombinant peptide (10 ng/mL) of CST3 or GDF15 in the presence of 5 % FBS (a) or 5 ng/mL TGF-β1 (b) for 1 hr, and subjected to immunoblotting. (C) CCD-18Lu cells were pre-incubated in a serum-free medium for 16 hr, and then treated with TGF-β1 and CST3 or/and GDF15 for 24 hr. CCD-18Lu cells were counted using a hemocytometer. (D) Primary lung fibroblasts, which had been isolated from normal mouse lung, were pre-incubated in a serum-free medium for 16 hr, and then treated with TGF-β1 and CST3 or/and GDF15 for 24 hr. CCD-18Lu cells were counted using a hemocytometer. All data are presented as the means + s.d. from 3 experiments. *, $P < 0.05$ versus the untreated group; #, $P < 0.05$ versus the TGF-β1 only group.

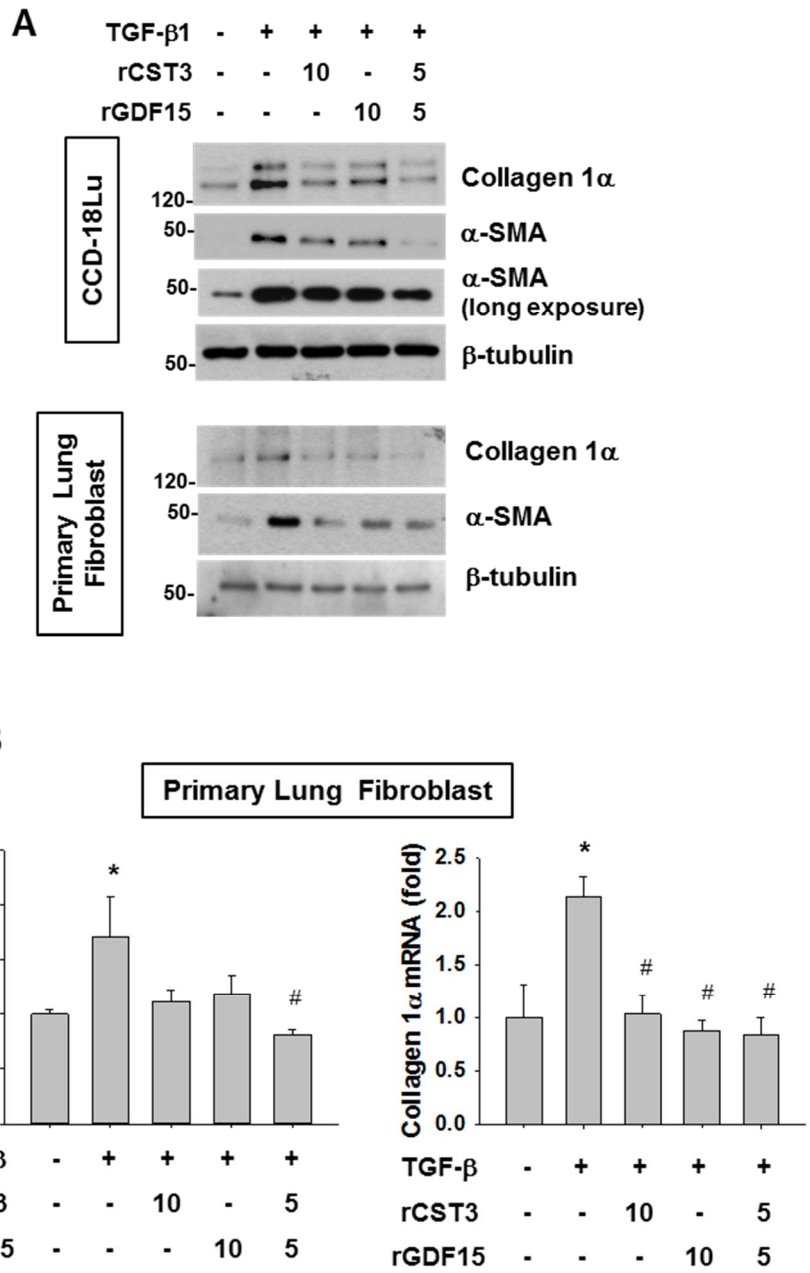

Figure 14. CST3 and GDF15 inhibit the TGF-β signaling pathway in CCD-18Lu and PFAF cells. (A) CCD-18Lu cells or primary lung fibroblasts were treated with TGF-β1 and CST3 or/and GDF15 for 24 hr, and subjected

to immunoblotting. (B) Primary lung fibroblasts were treated with TGF-β1 and CST3 or/and GDF15 for 24 hr. The mRNA levels were measured by RT-qPCR. All data are presented as the means + s.d. from 3 experiments. *, $P < 0.05$ versus the untreated group; #, $P < 0.05$ versus the TGF-β1 only group.

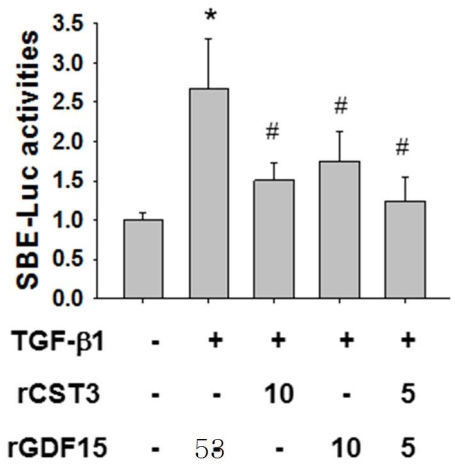

Figure 15. CST3 and GDF15 inhibit the TGF-β signaling pathway on SBE-luciferase activity in CCD-18Lu. CCD-18Lu cells, which had been co-transfected with SBE-Luc and β-galactosidase plasmids, were treated with TGF-β1 and CST3 or/and GDF15 for 24 hr. The luciferase activity was divided by β-galactosidase activity to normalize transfection efficiency. All data are presented as the means + s.d. from 3 experiments. *, $P < 0.05$ versus the untreated group; #, $P < 0.05$ versus the TGF-β1 only group.

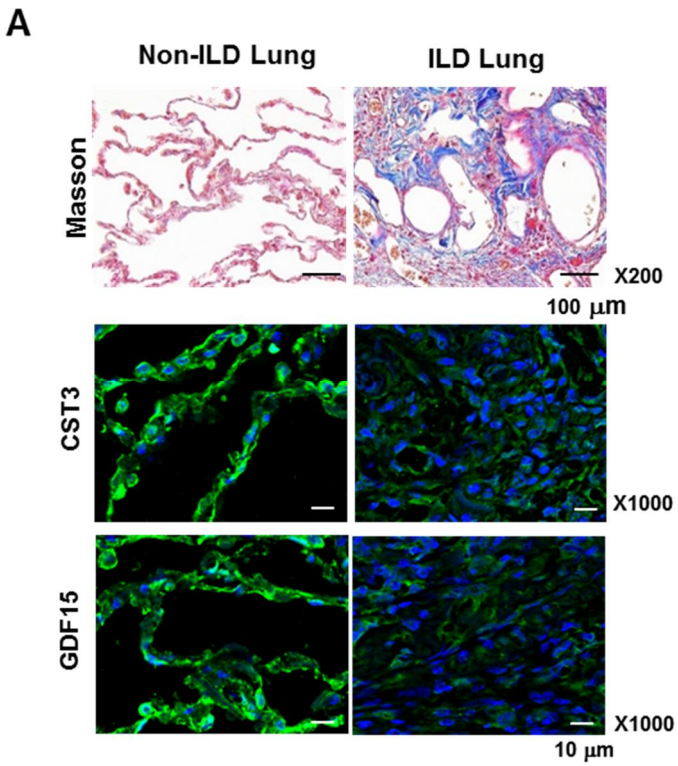

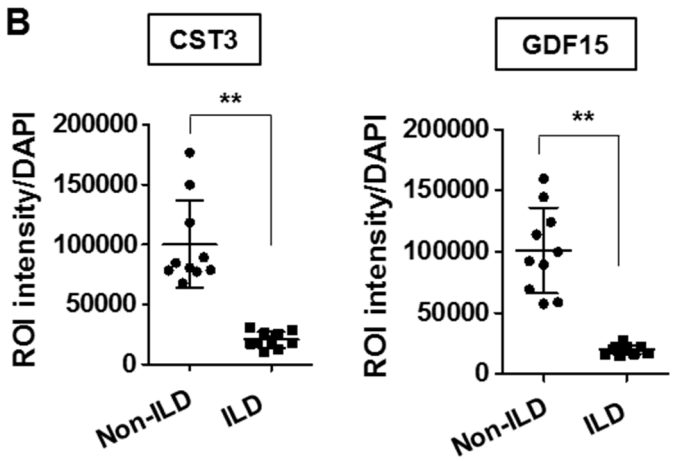

Figure 16. CST3 and GDF15 are down-regulated in human lungs with fibrosis. (A) Tissue specimens of non-ILD (n=10) and ILD (n=10) human lungs were subjected to Masson trichrome staining (top) and immunofluorescence staining with anti-CST3 or anti-GDF15 antibodies (middle). The immune complexes and DAPI-stained nuclei were visualized under a fluorescence microscope. A scale bar is 200 μm. (B) Total

fluorescence intensity was quantified using ImageJ and divided by the number of nuclei. Data are plotted as dots (bottom). A scale bar is 200 μm (top). Total fluorescence intensity was quantified using ImageJ and divided by the number of nuclei (bottom).

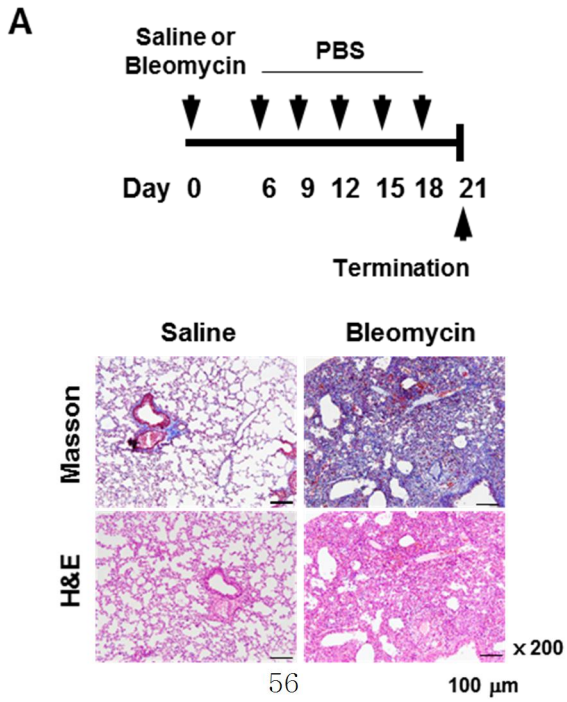

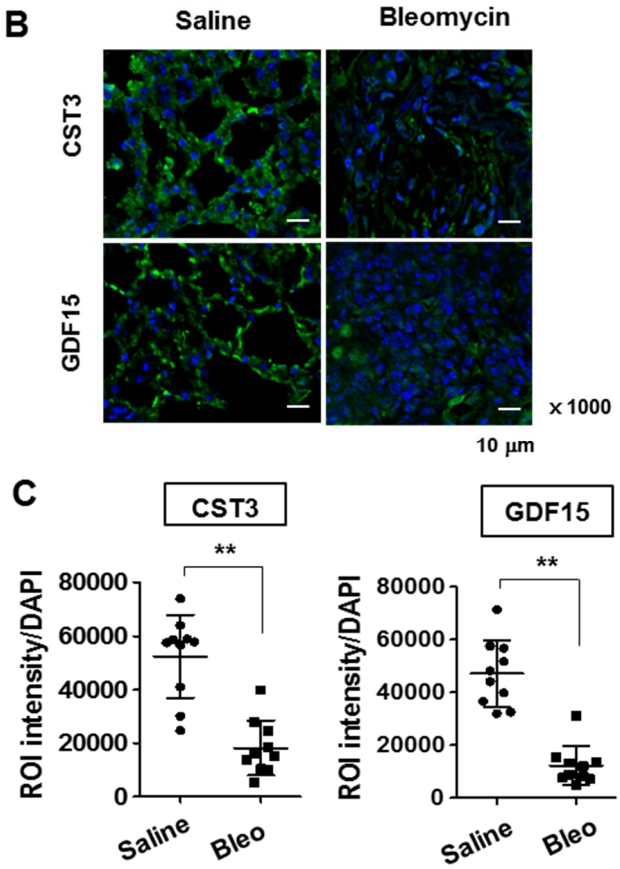

Figure 17. CST3 and GDF15 are down-regulated in mouse lungs with fibrosis. (A) Experimental schedule for bleomycin-induced pulmonary fibrosis (top). (B) Saline- or bleomycin-treated lung sections were stained with Masson trichrome and H&E (bottom). (C) Tissue specimens of saline- or bleomycin-treated mouse lungs (10 in each group) were subjected to immunofluorescence staining with anti-CST3 or anti-GDF15 antibodies. A scale bar is 200 μm (top). Total fluorescence intensity was quantified using ImageJ and divided by the number of nuclei (bottom).

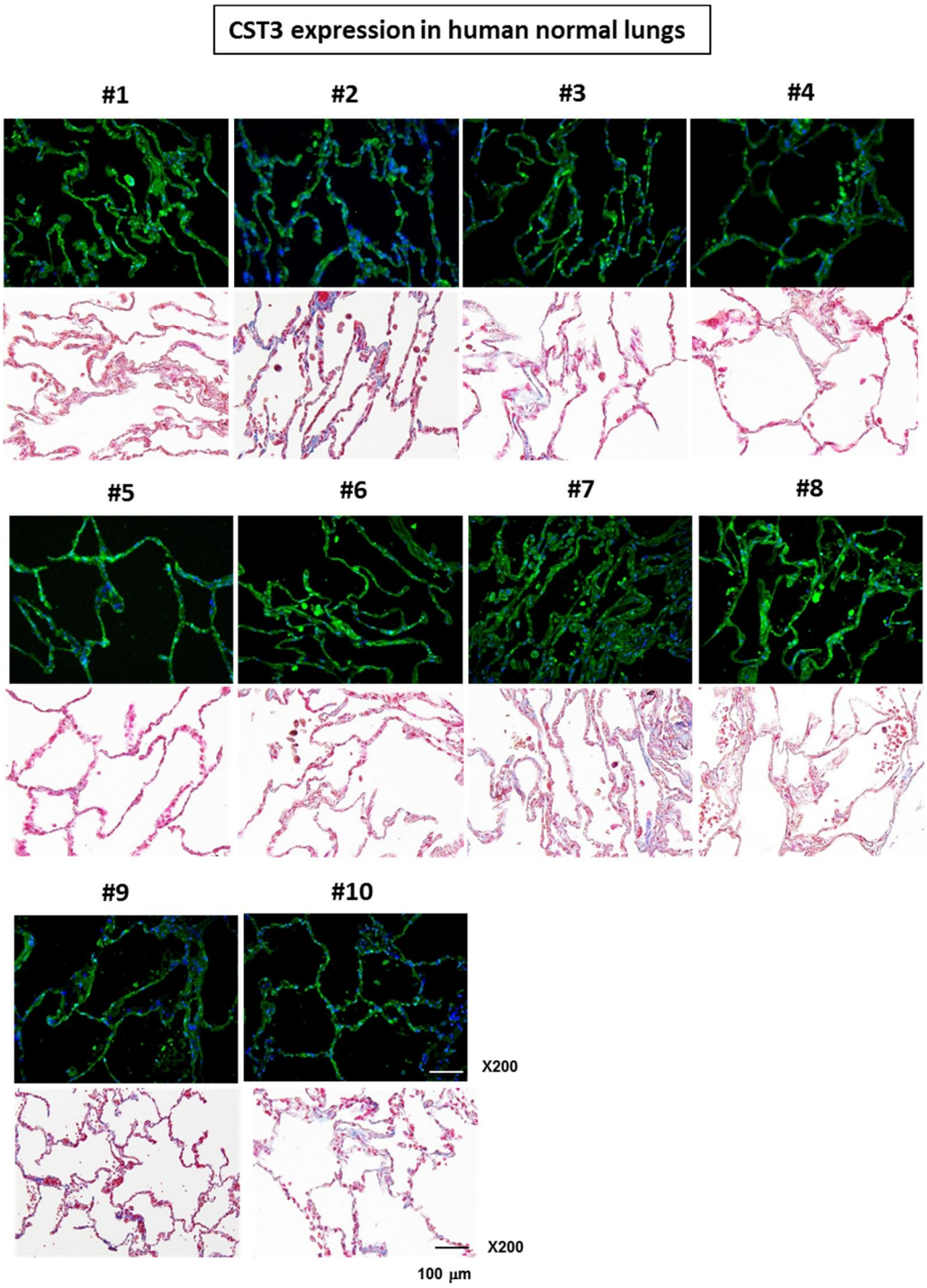
CST3 expression in human normal lungs
#1
#2
#3
#4
#5
#6
#7
#8
#9
#10
X200
X200
100 μm

Figure 18. Expression of CST3 in normal lung tissues from 10 patients with adenocarcinoma. Lung tissue specimens were subjected to immunofluorescence analysis using anti-CST3 antibody or stained with Masson's trichrome.

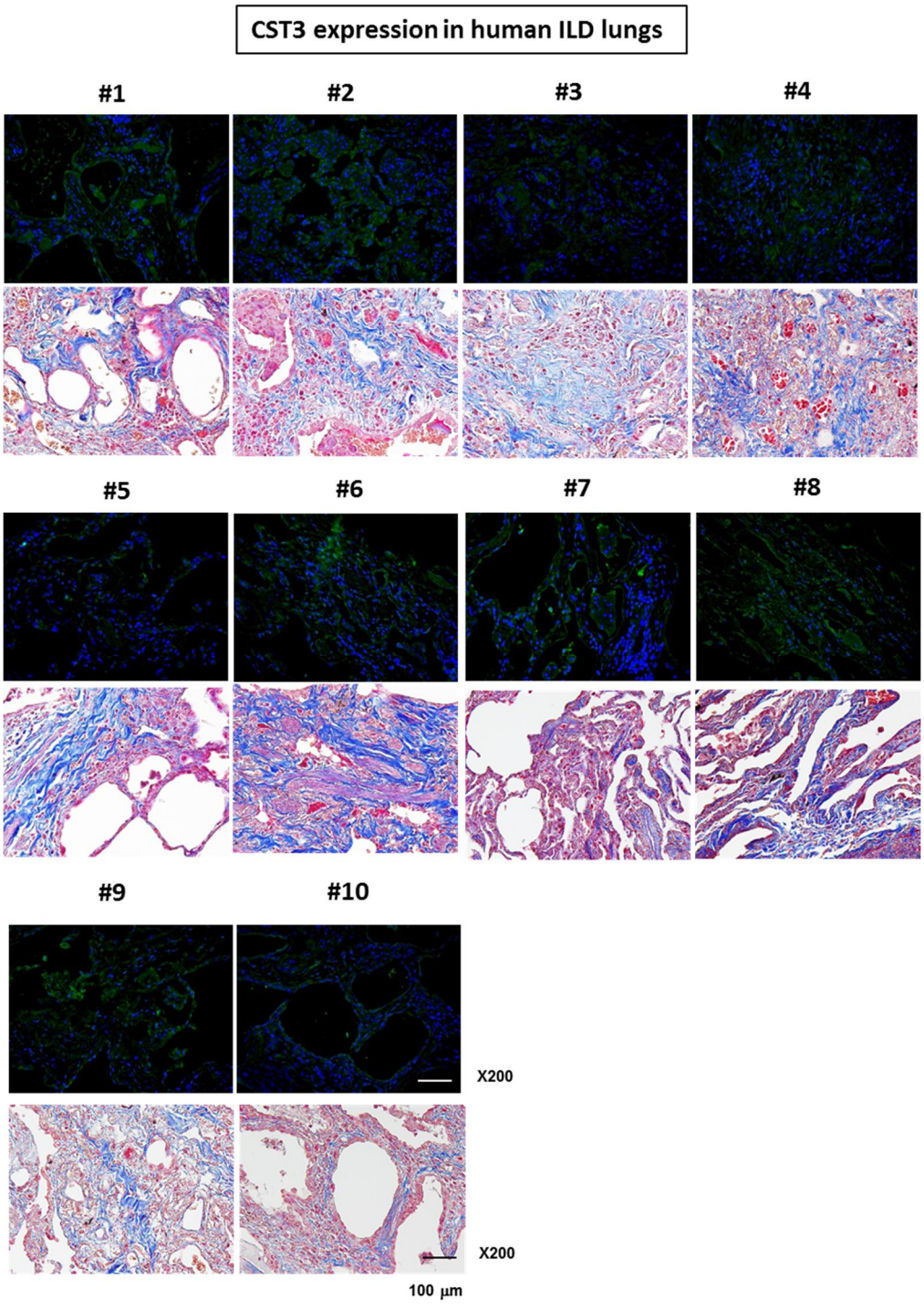
CST3 expression in human ILD lungs
#1
#2
#3
#4
#5
#6
#7
#8
#9
#10
X200
X200
100 μm

Figure 19. Expression of CST3 in fibrotic lung tissues from 10 patients with interstitial lung disease. Lung tissue specimens were subjected to immunofluorescence analysis using anti-CST3 antibody or stained with Masson's trichrome

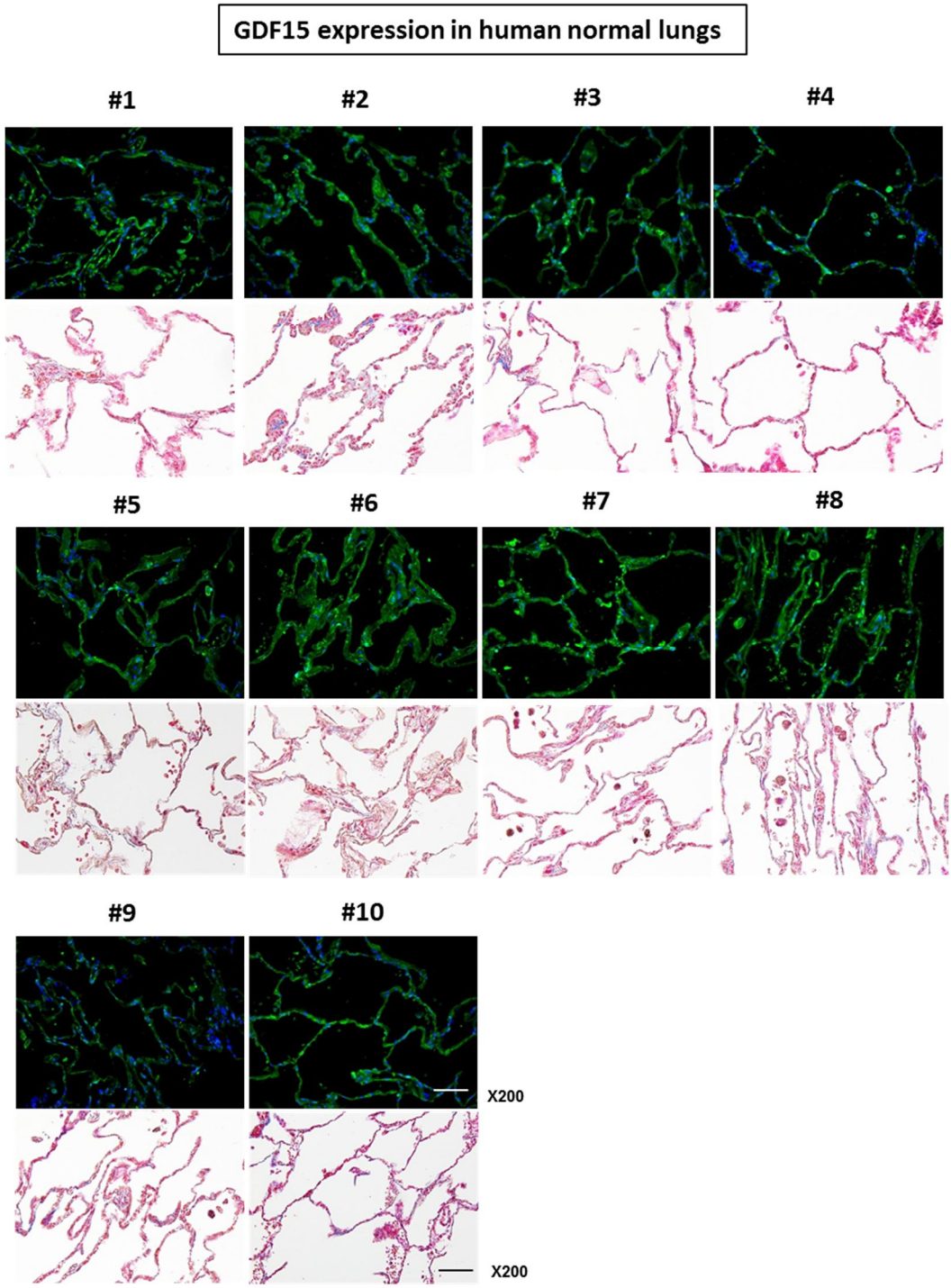
GDF15 expression in human normal lungs
#1
#2
#3
#4
#5
#6
#7
#8
#9
#10
X200
X200

Figure 20. Expression of GDF15 in normal lung tissues from 10 patients with adenocarcinoma. Lung tissue specimens were subjected to immunofluorescence analysis using anti-GDF15 antibody or stained with Masson's trichrome.

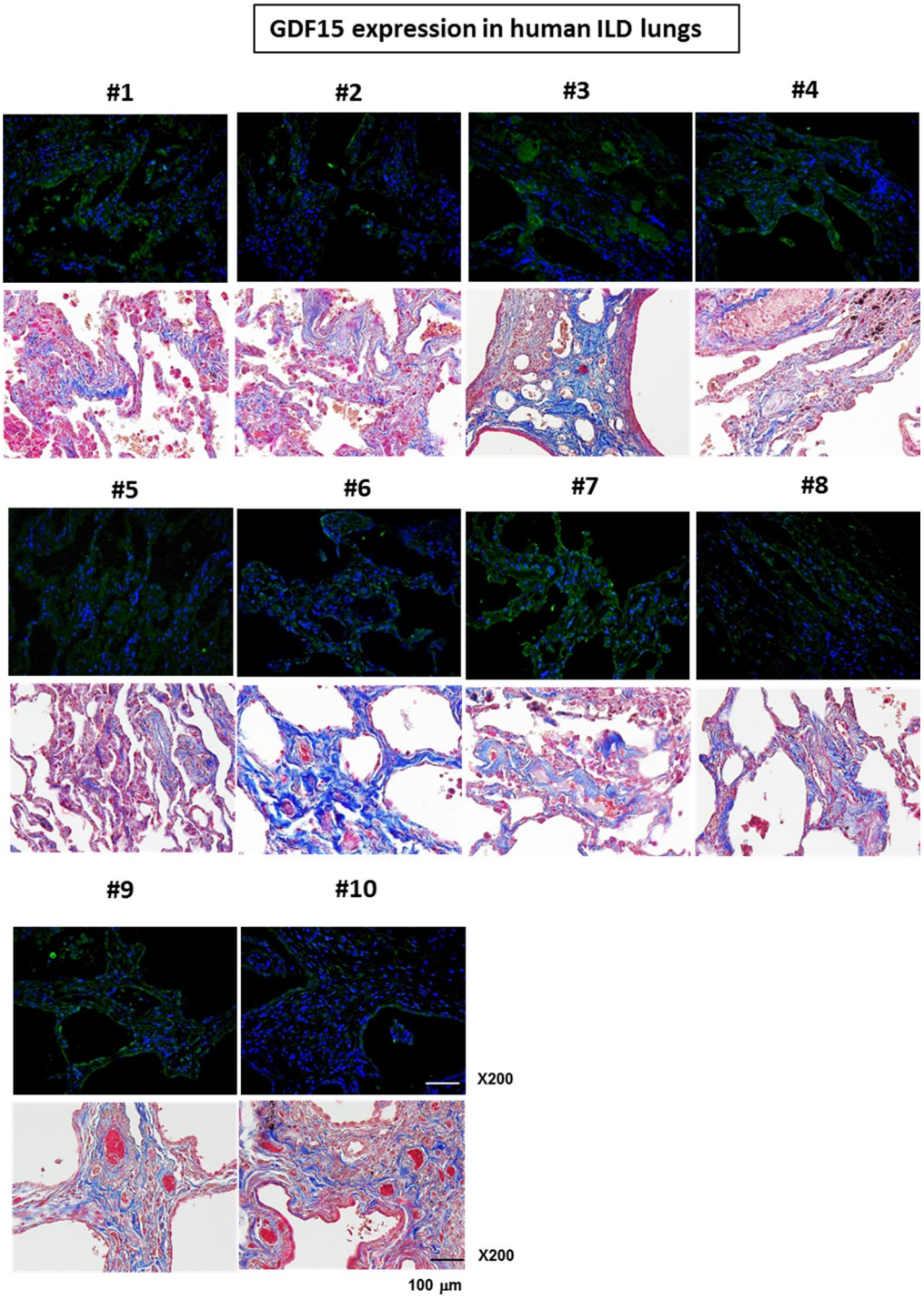
GDF15 expression in human ILD lungs
#1
#2
#3
#4
#5
#6
#7
#8
#9
#10
X200
X200
100 μm

Figure 21. Expression of GDF15 in fibrotic lung tissues from 10 patients with interstitial lung disease. Lung tissue specimens were subjected to immunofluorescence analysis using anti-GDF15 antibody or stained with Masson's trichrome.

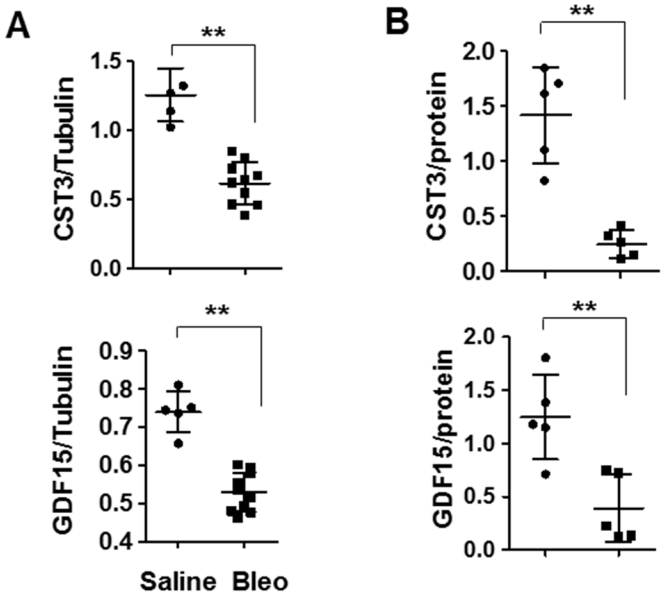
A
B
**
CST3/Tubulin
CST3/protein
GDF15/Tubulin
GDF15/protein
Saline
Bleo

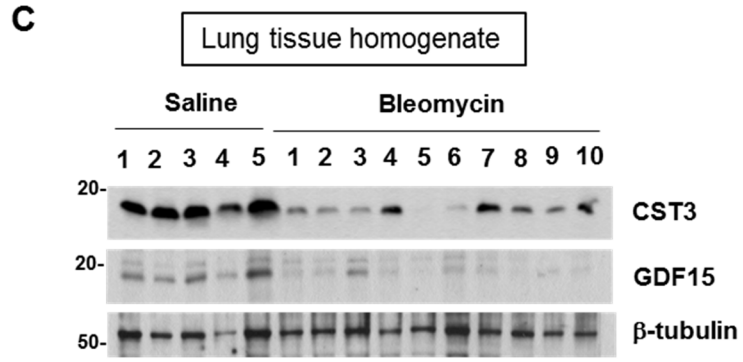
C
Lung tissue homogenate
Saline
Bleomycin
1 2 3 4 5 1 2 3 4 5 6 7 8 9 10
20-
20-
50-
CST3
GDF15
β-tubulin

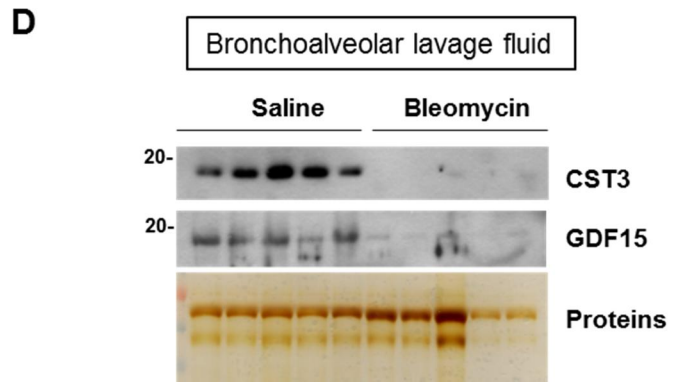
D
Bronchoalveolar lavage fluid
Saline
Bleomycin
20-
20-
CST3
GDF15
Proteins

Figure 22. CST3 and GDF15 protein expression are down-regulated in mouse lung tissue with fibrosis. (A) CST3 and GDF15 proteins were immunoblotted in mouse lung homogenates (top), and their levels versus β-tubulins were quantified using ImageJ (bottom). The means and s.d. in dot plots are presented by long and short horizontal bars and ** denotes $P < 0.01$. (B) The expression level of CST3 and GDF15 proteins in BALF were detected by western blotting and their levels were normalized by total protein using ImageJ. The means and s.d. in dot plots are presented by long and short horizontal bars and ** denotes $P < 0.01$. CST3 and GDF15 levels in lung tissues and BALFs. (C) Western blot analysis of CST3 and GDF15 proteins from saline administrated mouse lung homogenate (saline) and bleomycin administrated for 21 days mouse lung homogenate using antibodies to the indicated proteins. (D) Bronchoalveolar lavage fluid were collected from saline or bleomicin treated mouse for 21 days, and protein in BALF were precipitated by TCA. CST3 and GDF15 cytokine level in BALF were detected by western blotting.

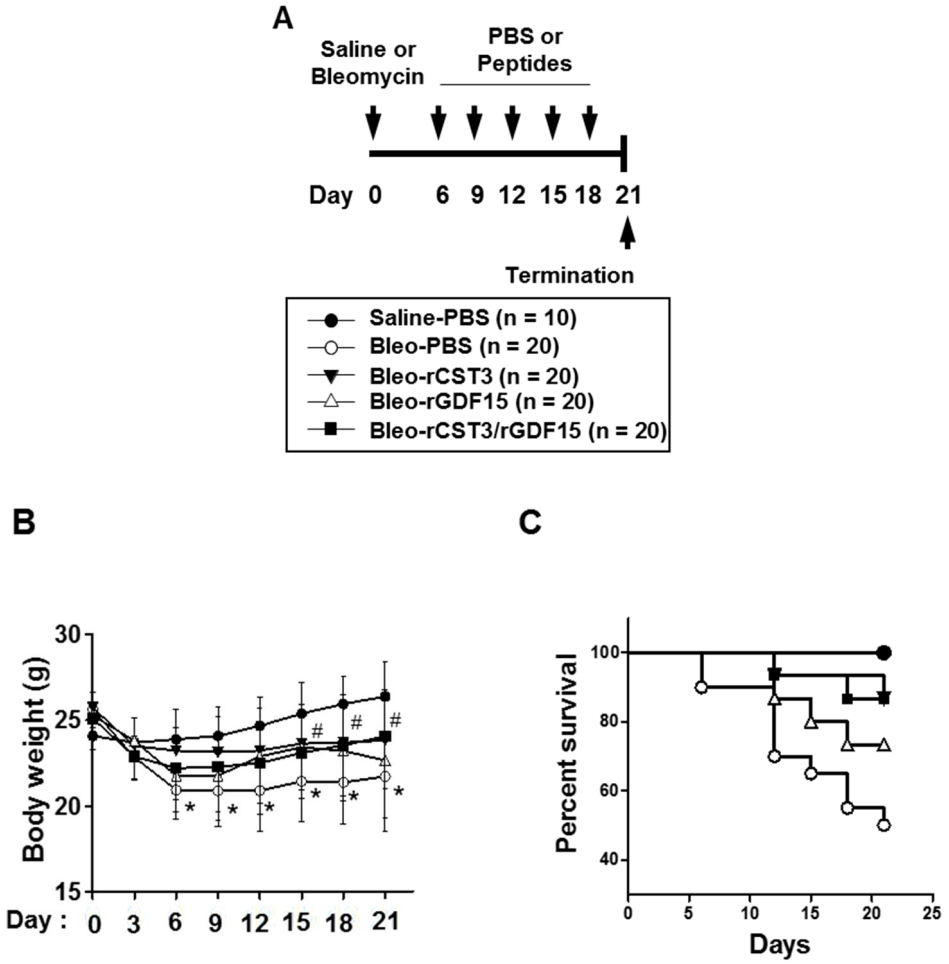
A
Saline or Bleomycin
PBS or Peptides
Day 0 6 9 12 15 18 21
Termination
Saline-PBS (n = 10)
Bleo-PBS (n = 20)
Bleo-rCST3 (n = 20)
Bleo-rGDF15 (n = 20)
Bleo-rCST3/rGDF15 (n = 20)
B
Body weight (g)
30
25
20
15
Day : 0 3 6 9 12 15 18 21
C
Percent survival
100
80
60
40
0 5 10 15 20 25
Days

Figure 23. Recombinant CST3 and GDF15 ameliorate weight loss and mortality rate in bleomycin-treated mice. (A) Experimental schedule for pulmonary fibrosis and peptide injection and the numbers of mice used. (B) Mouse body weights (means and s.d.). (C) Kaplan-Meier survival curves. Survival rates in Bleo-rCST3 and Bleo-rCST3/rGDF15 groups were higher significantly (log-rank test) than in Bleo-PBS group.

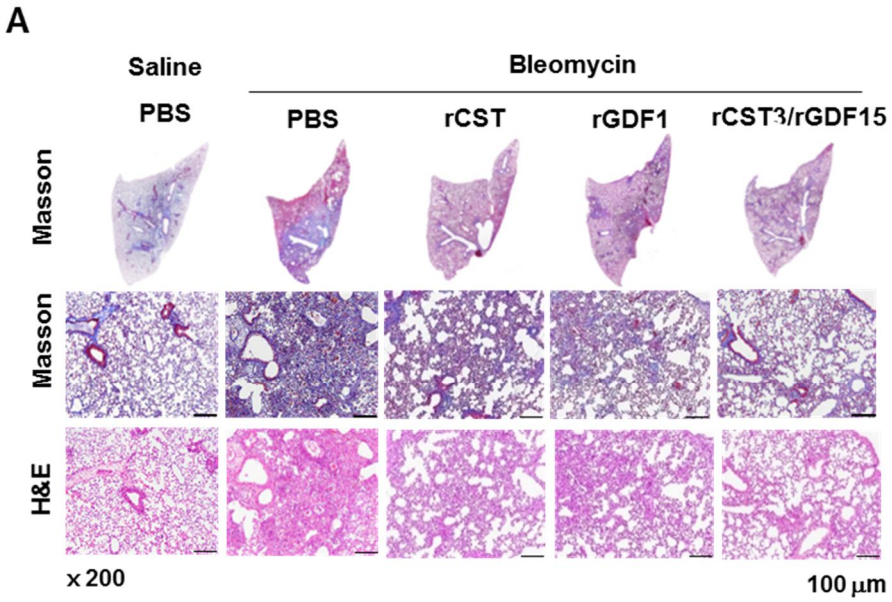
A
Saline
Bleomycin
PBS
PBS
rCST
rGDF1
rCST3/rGDF15
Masson
Masson
H&E
x 200
100 μm

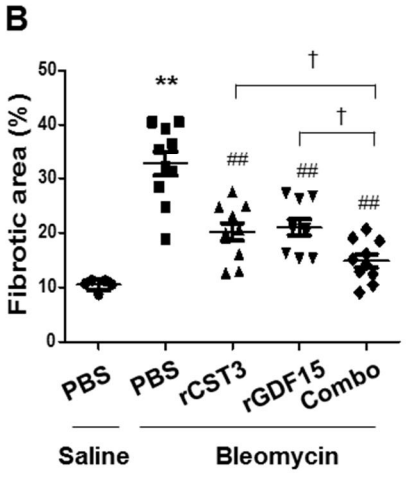
B
Fibrotic area (%)
50
40
30
20
10
0
**
†
†
##
##
##
PBS
PBS
rCST3
rGDF15
Combo
Saline
Bleomycin

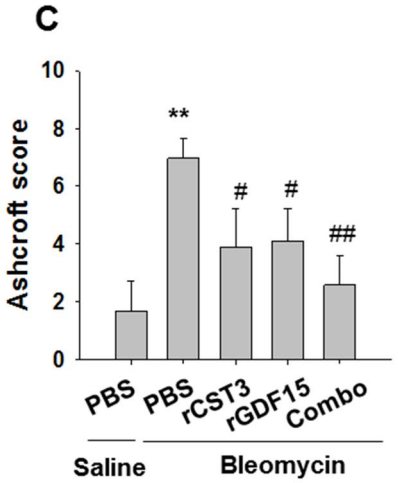
C
Ashcroft score
10
8
6
4
2
0
**
#
#
##
PBS
PBS
rCST3
rGDF15
Combo
Saline
Bleomycin

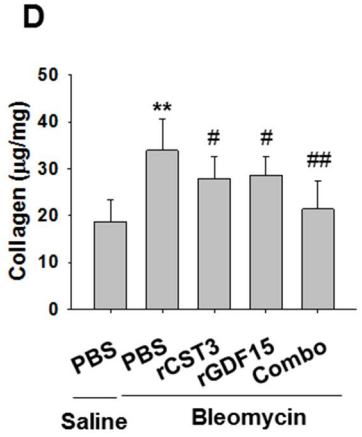
D
Collagen (μg/mg)
50
40
30
20
10
0
**
#
#
##
PBS
PBS
rCST3
rGDF15
Combo
Saline
Bleomycin

Figure 24. Recombinant CST3 and GDF15 ameliorate lung fibrosis in bleomycin-treated mice. (A) Saline- or bleomycin-treated lungs and tissue sections were stained with Masson trichrome or H&E. (B) Masson trichrome staining was quantified using ImageJ. Long and short horizontal bars represent the means and s.d.. (C) Ashcroft scores were analyzed in Masson trichrome-stained sections. (D) Hydroxyproline contents in lung homogenates were quantified spectrophotometrically and collagen expression were determined by lung weight. Each point or bar in all panels represents the mean + s.d.. * and **denote $P < 0.05$ and $P < 0.01$ versus the control group, respectively; # and ##, $P < 0.05$ and $P < 0.01$ versus the Bleo-PBS group; †, $P < 0.05$ between the indicated groups.

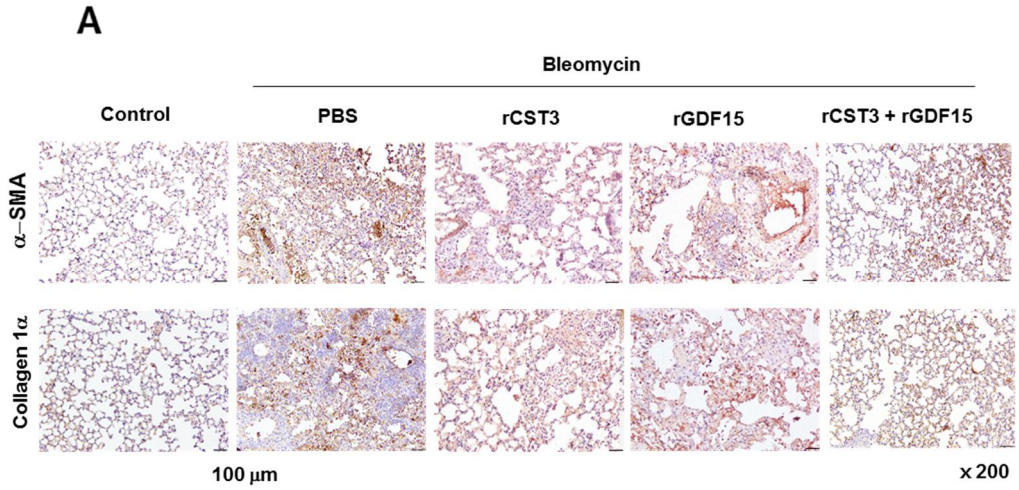
A
Bleomycin
Control
PBS
rCST3
rGDF15
rCST3 + rGDF15
α-SMA
Collagen 1α
100 μm
x 200

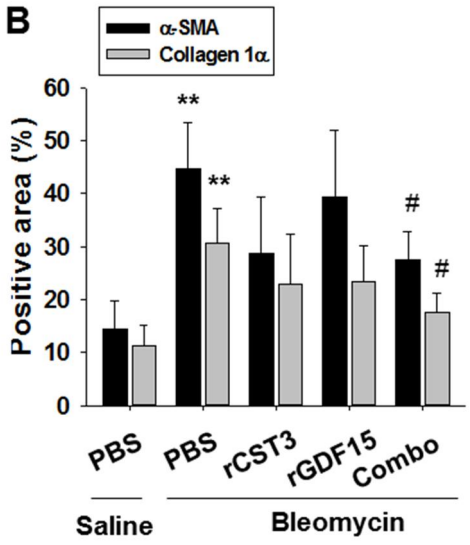
B
α-SMA
Collagen 1α
Positive area (%)
60
50
40
30
20
10
0
**
**
#
#
PBS
PBS
rCST3
rGDF15
Combo
Saline
Bleomycin

Figure 25. Recombinant CST3 and GDF15 reduce myofibroblast activation in bleomycin-treated mice. (A) α-SMA and collagen-1α in lung tissues were immunohistochemically stained. (B) α-SMA and collagen-1α in lung tissues were immunohistochemically stained, and quantified using ImageJ. Each point or bar in all panels represents the mean + s.d.. * and **denote $P < 0.05$ and $P < 0.01$ versus the control group, respectively; # and ##, $P < 0.05$ and $P < 0.01$ versus the Bleo-PBS group; †, $P < 0.05$ between the indicated groups.

DISCUSSION

Under the assumption that inflammation provokes fibrosis, anti-inflammatory medications have been tested as pulmonary fibrosis therapeutics, which include corticosteroids, azathioprine, chlorambucil, cyclophosphamide, cyclosporine, and interferons (Richeldi et al., 2003). However, these therapeutics failed to reduce the mortality rate of pulmonary fibrosis in clinical trials and induced side effects (Douglas et al., 1998; Raghu et al., 1991). More recently, agents with diverse pharmacological actions, including antioxidation and anticoagulation, have been tested clinically, but have not led to sufficient improvements (King et al., 2009; Kubo et al., 2005). The poor outcomes of anti-inflammatory therapies caused the change in the assumption of pulmonary fibrosis pathogenesis. Pulmonary fibrosis is now believed to result from aberrant wound repair accompanying the hyperactivation of interstitial fibroblasts and disorganization of the alveolar epithelium (Meuten et al., 2012). Based on this concept, fibroblast-targeting therapies are becoming a popular focus of research as a new strategy to treat pulmonary fibrosis. For instance, pirfenidone, tyrosine-kinase inhibitors, TGF-β inhibitors, and connective tissue growth factor inhibitors have been evaluated in phase II and III clinical trials (Roth et al., 2009; Taniguchi et al., 2010).

Fibroblast-targeting pulmonary fibrosis therapies can be mainly classified as small molecules or monoclonal antibodies. Since signaling pathways

stimulating fibroblasts have been considered as the primary targets, investigations might focus on chemical inhibitors or antibodies that can block fibroblast-activating pathways (Richeldi et al., 2011; Yamaguchi et al., 2012). However, I here shifted the anti-fibrosis strategy to reinforcing fibroblast-suppressive signaling pathways. According to the epithelial-mesenchymal homeostasis theory, the pulmonary epithelium has the intrinsic ability to suppress active fibroblasts after wound repair completion. This inspired these research for new pulmonary fibrosis therapies. I discovered two fibroblast-inhibiting cytokines, CST3 and GDF15, from normal epithelial cells and demonstrated their therapeutic effects in a bleomycin-induced pulmonary fibrosis mouse model.

Bleomycin-induced pulmonary fibrosis is common in animal models to test potential pulmonary fibrosis therapeutics. Bleomycin acutely simulates pulmonary inflammation, followed by chronic progression of pulmonary fibrosis. As molecular signatures of fibrosis, pro-inflammatory cytokines, such as IL-1, IL-6, and TNF-α, increase at the early phase in lung tissues treated with bleomycin (Moeller et al., 2008). Later, pro-fibrotic markers, such as fibronectin, procollagen-1, and TGF-β, gradually increase in the tissues and their levels peak around 2 weeks after bleomycin treatment (Sunaga et al., 2013; Chaudhary et al., 2006). Actually, therapy during the acute inflammatory phase may not be practical in hospitals, as pulmonary fibrosis can be diagnosed after onset of respiratory symptoms and detection of radiological evidence. Therefore, therapy might be started during the fibrotic phase. Considering the practical period of therapy, I started to inject the

recombinant peptides 6 days after the bleomycin treatment. These preliminary experiment indicated that the lung tissues partially underwent fibrosis on day 6, which helped us to determine the schedule for injecting peptides. Even though pulmonary fibrosis had already started, the peptides were sufficiently effective as to halt the disease progression (Figure 7). Therefore, cytokine therapy is expected to be effective in patients who are already diagnosed with pulmonary fibrosis.

Given that cathepsins can digest extracellular matrix proteins, cathepsins is expected to reduce fibrotic burden. However, the fibrosis-promoting effects of cathepsins have been shown in several literatures. For instance, cathepsin B stimulates hepatic stellate cells to promote fibrogenesis(Moles et al., 2009) and inhibiting cathepsin B suppresses collagen deposition in mouse livers(Canbay et al., 2003). Cathepsin B also stimulates fibrogenesis by facilitating TGF-β-driven differentiation of lung fibroblasts (Zhang et al., 2014; Sokol et al., 2005). Therefore, it is reasonable that CST3 ameliorates lung fibrosis by inhibiting cathepsins. Independent of cathepsin inhibition, CST3 is known to block fibrogenesis by directly antagonizing the TGF-β pathway. It physically binds to the TGF-β receptor, inhibiting TGF-β from interacting with its receptor (Zhang et al., 2014; Sokol et al., 2004). These results showing that CST3 attenuates the TGF signaling in CCD-18Lu support the latter mechanism of CST3. However, I cannot rule out the possibility that CST3 prevents fibrogenesis in bleomycin-treated lungs of mice via the dual effects of CST3 against lung fibroblasts.

The biological roles of GDF15 have been investigated restrictively in cancer cells. GDF15 is known to induce apoptosis in colorectal, prostate, and lung cancer cells (Liu et al., 2003; An et al., 2011; Kadara et el., 2006). Since the GDF15 gene harbors the p53 response element in the promoter region (Tsui et al., 2015). GDF15 is also expected to induce fibroblast death under harmful conditions like hypoxia and inflammation. However, GDF15 was unexpectedly found to inhibit fibroblast growth and activation through the inhibition of the TGF-Smad pathway. In contrast to these results, a recent report demonstrated that GDF15 stimulated proliferation of NIH 3T3 fibroblasts (Ishige et al., 2016). Although GDF15 was used at a 25-fold higher concentration than TGF-β, its effect on fibroblast growth was much less than that of TGF-β. This suggests that GDF15 acts as a partial agonist to the TGF-β receptor. In general, weak agonists can stimulate receptors in the absence of full agonists, but function to inactivate receptor signaling in the presence of full agonists because it competes with the agonist for binding to receptors (Seifert et al., 2001). Considering the TGF-β-enriched environment in fibrotic lungs (Seifert et al., 2001). GDF15 could act as an inhibitor of fibrogenesis. However, the precise role of GDF15 in lung fibroblast growth and activation remains to be investigated.

In conclusion, cytokines CST3 and GDF15 are secreted from normal epithelial cells and inhibit growth and activation of lung fibroblasts. These cytokines are severely deregulated in mouse and human lungs undergoing fibrosis, and systemic administration of them preserves the air way architecture by lessening collagen deposition in the interstitium of bleomycin-

treated mouse lung. CST3 and GDF15 appear to be bona fide regulators that prevent excessive proliferation and activation of fibroblasts in injured lungs.

CHAPTER 2

Recombinant peptides CST3 and GDF15 ameliorate renal fibrosis by deactivating fibroblasts

INTRODUCTION

Chronic kidney disease (CKD), which includes all degrees of failure in renal function, evokes public health problem in worldwide (Go et al., 2004; Synder et al., 2009). Renal fibrosis is a representative pathogenesis in progressive CKD (Liu, 2011). Renal fibrosis is defined as glomerulosclerosis, tubule-interstitial fibrosis, inflammatory infiltration, and parenchymal loss with tubular atrophy, capillary loss, and podocyte depletion (Liu, 2006). Renal fibrosis is defined as glomerulosclerosis, tubule-interstitial fibrosis, inflammatory infiltration, and parenchymal loss with tubular atrophy, capillary loss, and podocyte depletion (Duffield, 2014).

Renal fibrosis is initially involved in abnormal angiogenesis, capillary obliteration, and stimulation of pericytes and perivascular cells, followed by further stimulation of kidney resident cells through pro-inflammatory cytokines. Next, mesangial cells, fibroblasts, and tubular epithelial cells produce and deposit a large amount of extracellular matrix components in the interstitial space (Liu, 2006; Eddy, 2000), which eventually cause chronic renal failure. Of diverse resident and infiltrating cells, activated fibroblast mainly contributes to extracelluar matrix (ECM) deposition in the kidney. In

wound healing process, fibroblast is activated through various injury signals such as TGF-β1, PDGF, and FGF-2, which is also escalated under inflammatory microenvironmental factors such as hypoxia, hyperglycemia, immune cell infiltration, and altered ECM composition (Strutz et al., 2006) Therefore, the clearance of activated fibroblasts is considered as a reasonable strategy for preventing or delaying the progression of renal fibrosis.

To overcome renal fibrosis, many drugs have been tested in clinical trials. Immunosuppressive agents, including corticosteroids and cyclosporine A, are considered as conventional therapeutics to delay the fibrogenic process. However, the long-term usage of such agents is not recommended because of serious metabolic disorders and kidney injury. Some inhibitors of angiotensin-converting enzyme or antagonists of angiotensin II receptor have been also suggested as useful regimens to preserve the glomerular function in renal fibrosis, but these agents also evoke severe side effects such as hypotension, decreased GFR and hyperkalaemia (Breyer et al., 2016). Recently, new anti-fibrotic strategies to specifically target fibroblasts have been developed, which include antibodies neutralizing PDGFs and TGF-β, ALK5 receptor kinase inhibitors, Ras inhibitors, or a fibroblast inactivator pirfenidone (Zeisberg et al., 2010). Despite of the advances of treatment strategy of renal fibrosis, translation to clinical trials has not shown successful result.

Eventually, unsolved fibroblast activation were mainly caused ECM matrix in wound sites and malfunction of tubule-interstitial kidney. The clearance of activated fibroblasts is strategy for experimental antifibrotic therapy. At the terminal stage of wound healing, fibroblast growth and activation naturally

subside, which is reorganized by repaired epithelium. There is a growing consensus of opinion on the anti-fibrotic roles of the epithelium-derived cytokines. Accordingly, I tried to search for anti-fibrotic cytokines in epithelial cell conditioned media. In pervious research, I suggested that loss of normal epithelium by injury should be stimulate abnormal fibroblast proliferation and differentiation in pathologic wound repair system. In various ways, I confirmed and identified these fibroblast inhibitor are peptides named Cystatin C (CST3) and growth differentiation factor (GDF15). These research proved that normal alveolar epithelial cells secreted suppressor of lung fibroblast activation and these secretory molecules shown an effect to regulation of lung fibroblast growth and differentiation in vitro and ameliated the fibrosis progression in bleomycin induced mouse model in vivo. From this background, I identified inhibitor of active fibroblast, CST3 and GDF15, from normal epithelial conditioned media. And, CST3 and GDF15 effectively delayed disease progression and prevent fibroblast differentiation. In the present study, I identified and characterized Cystatin C (CST3) and Growth differentiation factor 15 (GDF15) as the inhibitors of activated renal fibroblasts. I also verified the effects of the cytokines against renal fibrosis in mice subjected to unilateral ureter obstruction (UUO).

MATERIALS AND METHODS

Unilateral Ureter Obstruction (UUO)

Ten week-old c57BL/B6 mice were purchased from Central Laboratory Animal Inc. (Seoul, Korea). The left ureter was tied off at two points for UUO or not for Sham operation (Zhang et al., 2010; Gu et al., 2017). CST3/GDF15 peptides (50 μg/kg each) or PBS were injected intraperitoneally into mice every other day after the surgery. Recombinant peptides of active CST3 (aa. 27-146, NM_000099) and GDF15 (aa. 195-308, NM_004864) were purchased from Abcam (Cambridge, MA) and Sino Biological Inc. (Beijing, China), respectively. On day 10, left (ipsilateral) and right (contralateral) kidneys were prepared for histological and biochemical analyses. All procedures were approved by the Seoul National University Institutional Animal Care and Use Committees (Approval No. SNU-161025-1). All efforts were made to minimize animal suffering and to reduce the number of animals used.

Isolation of primary mouse kidney fibroblasts

Mouse kidneys were excised on day 7 after Sham or UUO surgery. Kidneys were incised longitudinally and renal cortexes were cut out. Minced cortexes

were digested with 0.1% collagenase and 2.4 U/ml of dispase at 37°C for 45 min, and filtered through a 70 μm nylon strainer. After centrifugation at 1700xg for 5 min, cell pellets were suspended in DMEM with 20% FBS, and cultured overnight at 37°C in a 5% CO_2 incubator. Blood cells and non-adhere nt cells were washed out with PBS and attached fibroblasts were further incubated in DMEM with 20% FBS for 3 days.

Cell culture

Primary kidney fibroblasts were cultured with DMEM with 10% FBS (WelGENE, Daegu, Korea). WT 9-7 (human kidney epithelial cell line) was purchased from the American Type Culture Collection (ATCC, Manassas, VA) and cultured in DMEM with 10% FBS.

siRNA transfection

Cells were plated at 50% confluency and trasfected using the Lipofectamine RNAi-MAX reagent (Invitrogen, Carlsbad, CA). Opti-MEM medium and *Mycn* siRNAs (#1, #2 and #3) were purchased from Idt (Coralville, IA). *Mycn* siRNAs (40 nM) were transfected into UUO kidney fibroblasts. After stabilized for 24 h, cells were prepared for cell growth rate analysis and Western blotting experiments. The sequences of siRNAs are summarized in Supplemental table 2.

Reporter assay

Luciferase-based reporter assays were carried out to analyze the SMAD activity in kidney fibroblasts. Cells were co-transfected with the pGL-SBE4-luciferase and CMV-galactosidase plasmids. After stabilized for 24 h, transfected cells were incubated with or without 5 ng/mL of TGF-β1 for 4 h and lysed for luciferase and galactosidase assays. The luciferase activities were divided by the glactosidase activities to normalize transfection efficiencies.

Masson's trichrome assay and Ashcroft scoring

The paraffin sections of kidneys were deparaffinized, rehydrated, and sequentially stained with Weigert's iron hematoxylin and biebrich scarlet-acid fuchsin (Sigma-Aldrich, St. Louis, MO) for 10 min. The sections were stained with 2.5% aniline blue for 10 min, followd by destaining with 1% glacial acetic acid. Microscopic images were captured at 4 fields in each section. The severity (0 to 8) of fibrosis was evaluated based on the Ashcroft fibrosis scoring system.

Sirius red staining

Kidney tissue sections were hydrated with distilled water and stained with Picro-Sirius red solution (Abcam, Cambridge, MA) at room temperature for 1 hr. The sections were rinsed twice with 0.5% acetic acid, and dehydrated twice in absolute alcohol.

Immunohistochemistry of kidney tissues

Paraffin sections of kidney tissues were deparaffinized, rehydrated, and autoclaved for 10 min in 100 mM citrate buffer (pH 6.0). After treated with 3% H_2O_2 for 10 min, the sections were incubated in 10% bovine serum for 1 h. They were incubated with an antibody against collagen-1α (1:250 dilution; Abcam) or α-SMA (1:500; Abcam) overnight at 4°C. The immune complexes were visualized using Polink-2 HRP plus rabbit DAB detection system (Golden Bridge International, Inc., WA). Four high power fields were randomly selected in each section to analyze stained areas or fluorescent intensities using the ImageJ program.

Hydroxyproline assay

Hydroxyproline levels in kidney tissues were determined using the BioVision Kit (Mountain View, CA). Frozen kidney tissues (10 mg) were homogenized in 100 μL of deionized water. The homogenates were mixed with 100 μL of 12 N HCl and hydrolyzed at 120°C for 3 h, vortexed, centrifuged at 10000 x g for 15 min, and dired in a vaccum evaporator. Samples were resolved in 100 μL of Chloramine T reagent for 5 min, and mixed with 100 μL of DMAB reagent at 60°C for 90 min. Optical density was measeured at 560 nm.

Annexin V assay.

Kidney fibroblasts were spun down and stained with FITC-conjugated annexin V (BD Pharmingen, San Jose, CA) and Propidium Iodide (Sigma Aldrich). Stained cells were analyzed using a BD LSRII flow cytometer (BD Biosciences, San Diego, CA). Data files were exported and analyzed with FACSDiva software (BD Biosciences).

Immunoblotting

Cells were lysed in a denaturing SDS sample buffer, and proteins were separated on SDS polyacrylamide (10% or 15%) gels and transferred to Immobilon-P membranes. The membranes were incubated with a primary antibody overnightat 4°C and sequentially with HRP–conjugated anit-goat or rabbit IgG antibody (1:5000) for 1 h. The immune complexes were visualized using the ECL Plus or SuperSignal West Femto kit (Thermo Scientific, MA, USA). Anti-collagen-1α and anti-α-SMA antibodies were purcahsed from Abcam; anti-SMAD, anti-ERK, and anti-AKT antibody series from Cell Signaling (Beverly, MA); anti-tubulin and anti-E-cadherin from Santa Cruz (Dallas, TX). Relative intensities were normalized by the ratio between phosphorylated and total protein amounts using imagej.

Quiantitative RT-PCR

Total RNAs were extracted from mouse skidney fibroblasts using Trizol reagent (Life Technology, Carlsbad, CA). cDNAs were synthesized from 2 μg

of total RNAs using the M-MLV Reverse Transcriptase kit (Promega, Madison, WI). Real-time PCR was performed using the standard SYBR Green reagent (Enzynomics, Daejeon, Korea) and specific mRNAs were quantified by 7900HT real-time PCR detection system (BioRad, Hercules, CA). In all experiments, mRNA levels were normalized to GAPDH mRNA levels. Each sample was determined in triplicate, and at least 3 independent samples were analyzed for each experimental condition. The sequences of primers are summarized in Supplemental table 2.

Statistical analyses

The statistical analysis was performed using the SPSS (Window version 15.0.0) software package. Comparisons between two groups were analyzed by Student's t-test and those of three or more groups by one-way ANOVA and Post-hoc Tukey test. Significant difference was defined when P was less than 0.05.

Table 2. Nucleotide sequence of RNA and oligo primers for qRT-PCR

Purpose	**Target**	**Sequence (5′ →3′)**
siRNAs	siMycn#1	GUUGCUAAAGAAGAUCGAACACGCT
	siMycn#2	GGAAGUUUUGAGUAGAUAUUACUTT
	siMycn#3	GAUACCUUGAGCGACUCAGAUGATG
Purpose	**Target**	**Forward (5′ →3′)**
RT-qPCR	α-SMA	CCCTTGAGAAGAGTTACGAG
	Col1A1	TACAAAACCACCAAGACCTC

Numbers in parentheses indicate the nucleotide isoformation which the 5′ end of the sense strand of the siRNA matches the target sequence Mycn(NM_008709) and qRT-PCR matches the target sequence for a-SMA (NM_001141945) and Col1A1(NM_000088).

RESULTS

CST3 and GDF15 inhibit survival and collagen production of kidney fibroblasts

To test the cytokine effects on renal fibrosis-associated fibroblasts, primary renal fibroblasts were isolated from the kidneys subjected to Sham or UUO operation (Grimwood et al., 2009). To verify activated fibroblast phenotype of isolated cells, I checked two representative markers for myofibroblast, α-SMA and collagen-1α, and an epithelial marker E-cadherin. Immunofluorescence analyses showed that isolated fibroblasts highly expressed both myofibroblast markers but not E-cadherin compared to a kidney epithelial cell line WT9-7 (Figure 1A). The differential expressions of markers were confirmed by flow cytometry (Figure 1B). The mesenchymal markers for fibroblasts were also checked by Western blotting (Figure 2A). It was also observed that renal fibrosis-associated fibroblasts (UUO KF) grew more actively than normal kidney fibroblasts (Ctrl KF) (Figure 2B). All of these findings verify that the primary cells isolated from UUO kidneys have the properties of myofibroblasts. To test the anti-fibrotic activities of recombinant CST3 and GDF15 peptides, UUO KF cells were treated with each peptide or the half-and-half of two peptides 24 h. An MTT-based

viability assay showed that UUO KF viability was reduced by each peptide and further declined by the combination (Figure 3A). In contrast, ctrl kidney fibroblast viability was seldom affected by the peptides. To know the type of cell death, cells were subjected to FACS analysis with annexin V (for apoptosis) and PI (for necrosis) staining without permeabilization of cell membranes (Figure 3D). CST3 or /and GDF15 forcefully induced apoptosis, but did not necrosis (Figure 3B and 3C). The peptide-induced apoptosis was confirmed by immunoblotting cleaved forms of PARP and caspase-3 (Figure 4A). In addition to apoptosis, myofibroblast markers (collagen-1α and α-SMA) in UUOKF were repressed by peptide alone or the combination in either transcriptional or translational level (Figure 4B and 4C).

CST3 inactivates fibroblasts by antagonizing the TGF-β-SMAD signaling pathway

SMAD2/3 have been reported to be highly activated in fibrotic kidneys from CKD patients and animal models (Meng et al., 2013) To understand how CST3 and GDF15 inactivate fibroblasts, I measured the levels of phosphorylated SMAD2/3 in Sham and UUO kidney tissues, and found that SMADs are activated in mouse kidneys undergoing fibrosis (Figure 5A and 5B). In the fibrotic kidneys, CST3 and the combination of CST3 and GDF15 inhibited the activation of SMADs, but GDF15 alone did not (Figure 6A and 6B). In primary renal fibroblasts, TGF-β1 activated its receptor and SMAD2/3, and this was attenuated by CST3 but not by GDF15 (Figure 7A). In a SBE-luciferase reporter assay reflecting SMAD activity, CST3 was also confirmed

to repress SMAD function (Figure 7B). Therefore, CST3 seem to inhibit fibroblast activation by antagonizing the TGF-β-SMAD signaling pathway.

GDF15 inhibits the N-Myc induction in activated kidney fibroblasts.

To understand how GDF15 controls fibroblast growth, I checked the expression of robust oncogenic proteins C-Myc and N-Myc (Bretones et al., 2015; Shen et al.,2017) As a result, I observed that N-Myc, rather than C-Myc, was highly induced in UUO kidney tissues (Figure 8A and 8B). Interestingly, such an induction of N-Myc was markedly diminished in kidneys from mice treated with GDF15 (Figure 9A and 9B). In isolated fibroblasts, the N-Myc expression in UUO kidney fibroblasts was substantially downregulated by administering GDF15 into culture dishes (Figure 10A). Given that fibroblast growth was significantly attenuated by N-Myc knock-down (Figure 10B), the GDF15-induced growth arrest is regarded to be attributed to the N-Myc downregulation.

Recombinant CST3 and GDF15 ameliorate kidney fibrosis *in vivo*

After UUO surgery, C57/B6 mice were intraperitoneal injected twice weekly with PBS, rCST3 (100 μg/kg), rGDF15 (100 μg/kg), or both peptides (50 μg/kg of each). On the 10st day, kidney tissues were excised, as illustrated in Supplementary figure 11A. Body weight was measured continuously to monitor apparent health. Mouse body weights were not significantly altered in all groups during this period (Figure 11B). To evaluate renal fibrosis and fibroblast activation, I stained kidney tissues with Masson's trichrome and

Sirius red as fibrosis markers(Figure 12), and also immunostained α-SMA and collagen 1 as fibroblast activation markers (Figure 14A). Compared with control kidneys, all the markers were more stained in UUO kidneys of PBS-treated mice, verifying that renal fibrosis was induced by UUO. When UUO mice were injected with recombinant CST3 or GDF15, the fibrotic burden and fibroblast activation were significantly reduced in the kidneys (Figure 13A and 13B). The combination of both peptides at the half doses also attenuated the fibrosis effectively. To accurately quantify the content of collagen, the hydroxyproline level was measured in tissue homogenates. This assay showed that the combination treatment of half-dose peptides has a better efficacy in reducing fibrotic burden than treatment of single peptide (Figure 13C). The inhibitory effects of the peptides were confirmed by Western blotting of tissue homogenates (Figure. 14C).

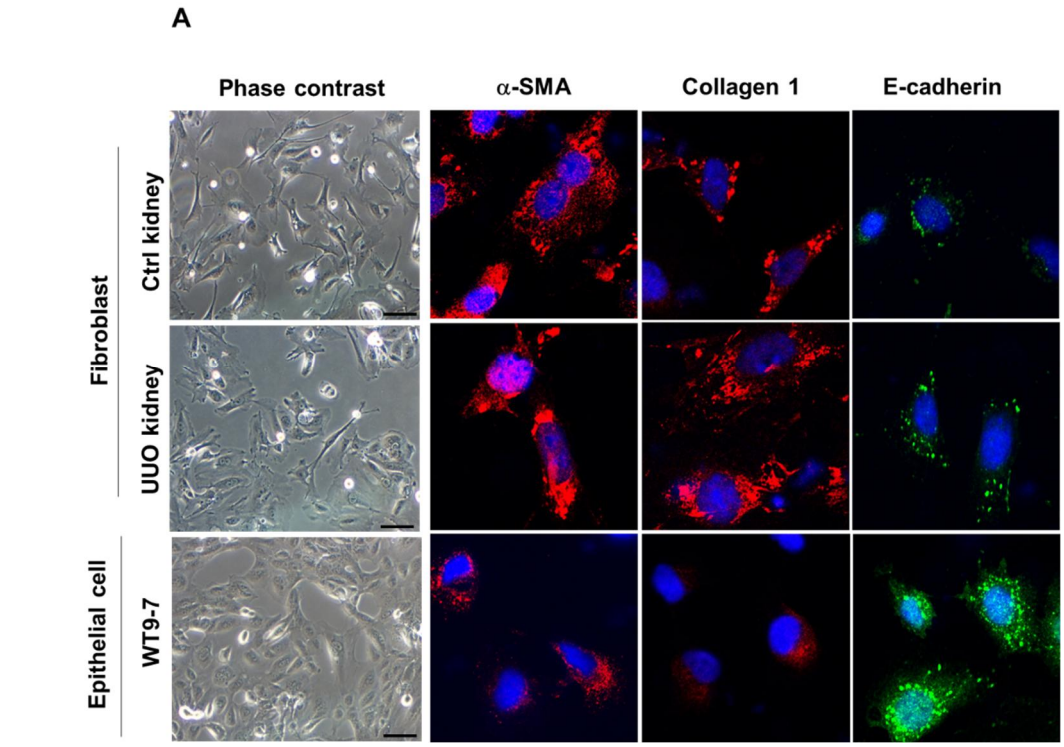
A
Phase contrast
α-SMA
Collagen 1
E-cadherin
Fibroblast
Ctrl kidney
UUO kidney
Epithelial cell
WT9-7

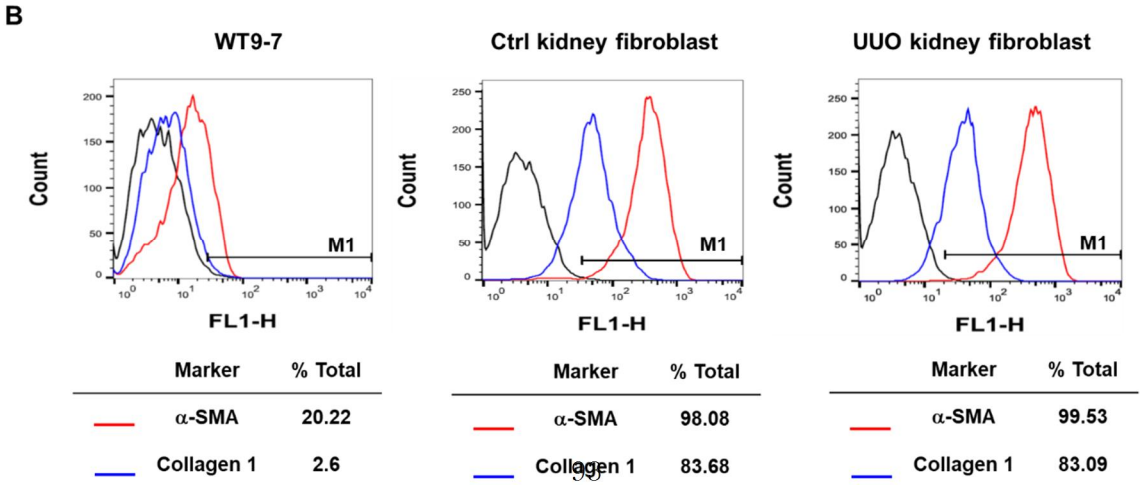
B
WT9-7
Ctrl kidney fibroblast
UUO kidney fibroblast
Count
FL1-H
M1
Marker
% Total
α-SMA
20.22
Collagen 1
2.6
α-SMA
98.08
Collagen 1
83.68
α-SMA
99.53
Collagen 1
83.09

Figure 1. Verification of activated renal fibroblasts using immunofluores - cence and FACS. (A) Kidney fibroblasts were fixed with 3.7 % PFA and permeabilized by triton X-100. Blocking solution and antibody solution contain 3% BSA in Tween-PBS. The cells were labeled with an antibody against collagen-1a (1:250 dilution; Abcam), a-SMA (1:500; Abcam), or E-cadherin (1:500; cell signaling) overnight at 4°C. Cells were incubated with Alexa Fluor 488-conjugated anti-rabbit IgG antibody (Thermo Fisher), and counterstained with DAPI (Invitrogen). Fluorescent images were captured under Olympus fluorescence microscope (DP30BW, Melville, NY). (B) Fibroblasts were fixed with 2% PFA, permeabilazed by 0.1% Triton X-100, blocked with 0.5% BSA/2% FBS. Cells were incubated with primary antibodies against collagen-1a (1:1000 dilution; Abcam) and a-SMA (1:1000; Abcam) on ice for 30 min, and incubated with a fluorescent dye-conjugated secondary antibody for 30 min.

A

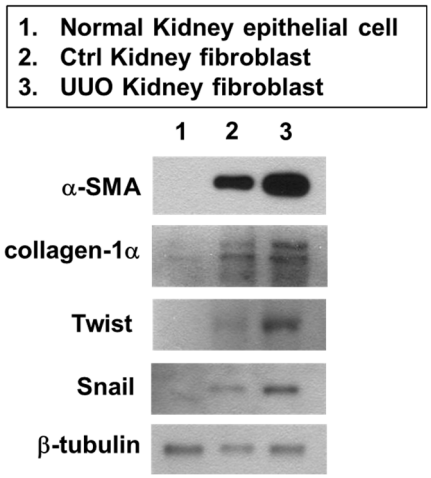
1. Normal Kidney epithelial cell
2. Ctrl Kidney fibroblast
3. UUO Kidney fibroblast
1 2 3
α-SMA
collagen-1α
Twist
Snail
β-tubulin

B

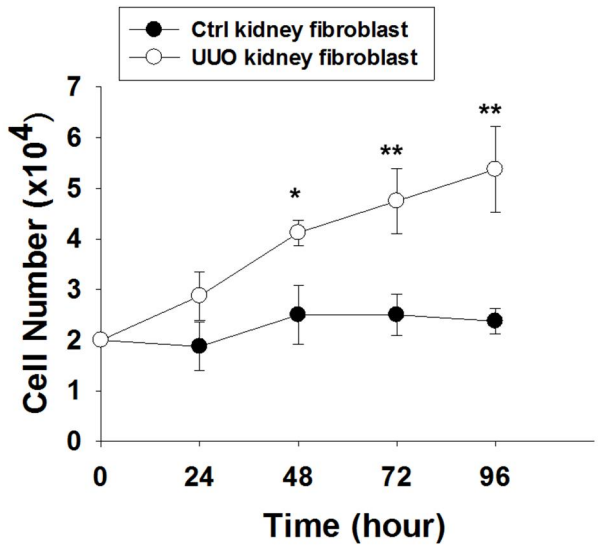
Ctrl kidney fibroblast
UUO kidney fibroblast
Cell Number (x10^4)
0
1
2
3
4
5
6
7
*
**
**
0
24
48
72
96
Time (hour)

Figure 2. Verification of activated renal fibroblasts with western blotting and growth rate. (A) Four representative markers for activated fibroblast were determined by Western blotting. (B) Ctrl and UUO fibroblast growth rate were measured by counting viable cells unstained with trypan blue. * $P < 0.05$ versus the Ctrl kidney fibroblast.

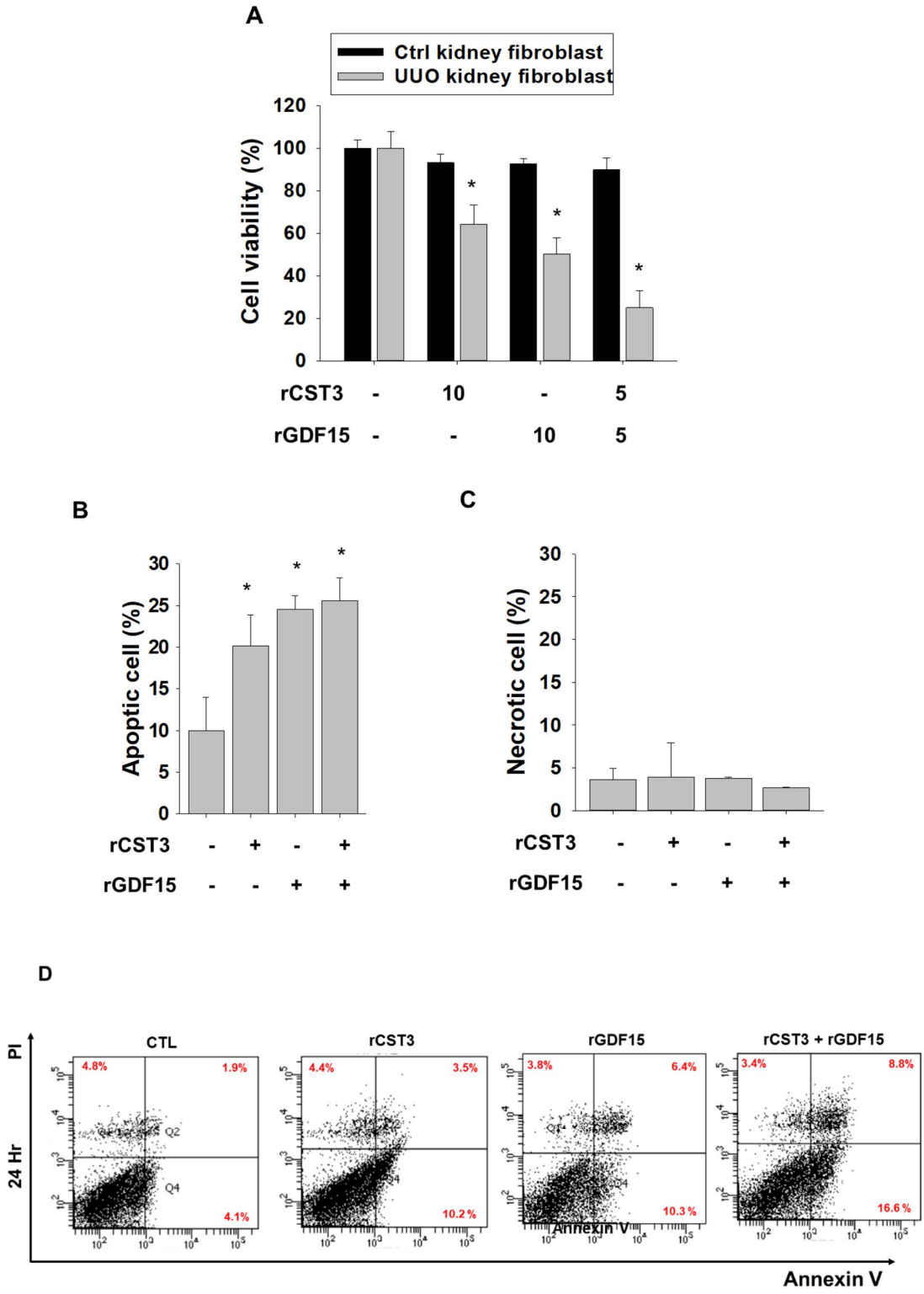
A
Ctrl kidney fibroblast
UUO kidney fibroblast
Cell viability (%)
120
100
80
60
40
20
0
*
*
*
rCST3 - 10 - 5
rGDF15 - - 10 5
B
Apoptic cell (%)
30
25
20
15
10
5
0
*
*
*
rCST3 - + - +
rGDF15 - - + +
C
Necrotic cell (%)
30
25
20
15
10
5
0
rCST3 - + - +
rGDF15 - - + +
D
PI
24 Hr
CTL
rCST3
rGDF15
rCST3 + rGDF15
4.8%
1.9%
Q2
Q4
4.1%
4.4%
3.5%
10.2 %
3.8%
6.4%
10.3 %
3.4%
8.8%
16.6 %
Annexin V
Annexin V

Figure 3. CST3 and GDF15 inhibit fibroblast growth. (A) Control and UUO kidney fibroblasts were cultured in 2% FBS-containing media and treated with CST3 (10 ng/mL), GDF15 (10 ng/mL), or both (5 ng/mL each) for 24 h. Cell viability was checked using MTT. (B) To analyze apoptosis and (C) necrosis, UUO kidney fibroblasts were co-stained with annexin V-FITC and propidium iodide, and subjected to flow cytometry. The population of apoptotic cells was assessed by annexin V staining. (D) After co-stained with Annexin V and PI, UUO kidney fibroblasts were subjected to flow cytometry. t single or combination treatment of rCST3 and rGDF15 stimulated cell death in. (B) The population of necrotic UUO kidney fibroblasts stained with PI. Bars represent the mean + s.d. (n = 3) by one-way ANOVA, followed by post hoc..

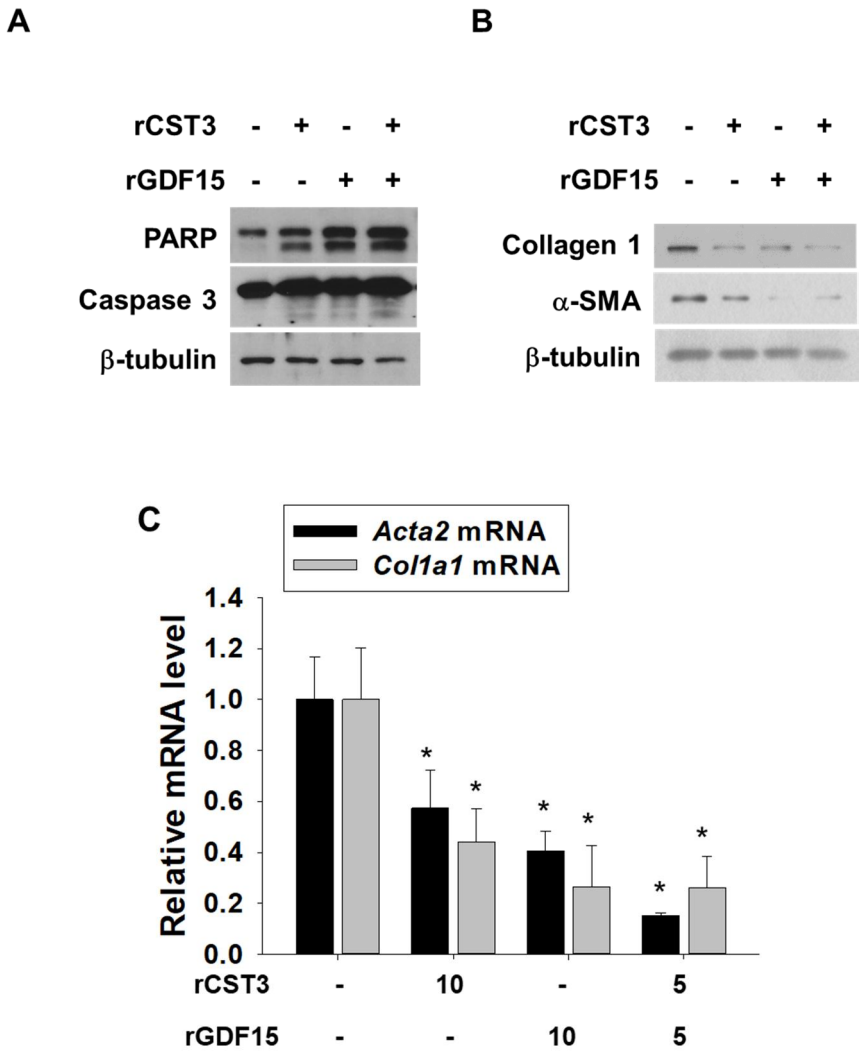
A
rCST3 - + - +
rGDF15 - - + +
PARP
Caspase 3
β-tubulin
B
rCST3 - + - +
rGDF15 - - + +
Collagen 1
α-SMA
β-tubulin
C
Acta2 mRNA
Col1a1 mRNA
Relative mRNA level
1.4
1.2
1.0
0.8
0.6
0.4
0.2
0.0
rCST3 - 10 - 5
rGDF15 - - 10 5

Figure 4. CST3 and GDF15 inhibit fibroblast growth and differentiation. (A) The cleavage of PARP and caspase-3 was determined as apoptosis markers by Western blotting. (B) Collagen 1 and a-SMA levels were immunoblotted as markers for fibroblast activation. (C) *Acta2* and *Col1a1* mRNA levels were measured in UUO kidney fibroblasts which had been treated with peptides, using quantitative RT-PCR. (C) Bar graphs in all panels are presented Data are presented as the mean ± s.d. (n = 3). *P<0.05 by one-way ANOVA, followed by post hoc.

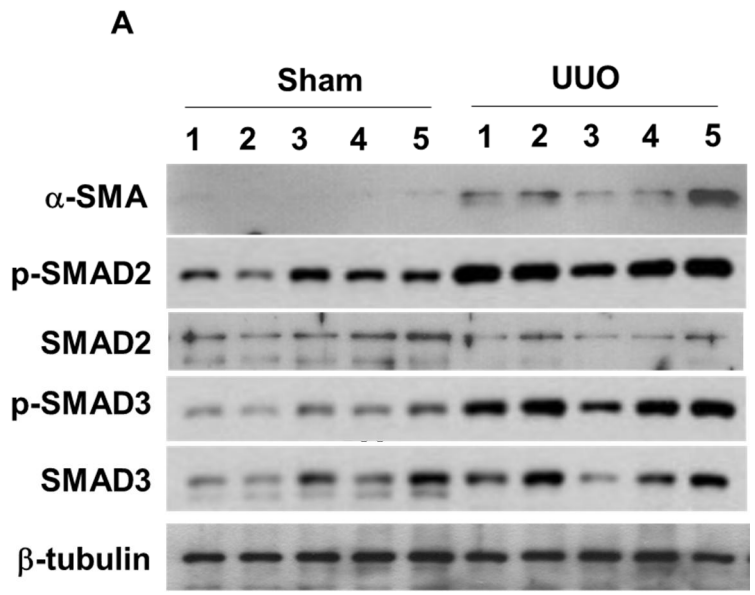

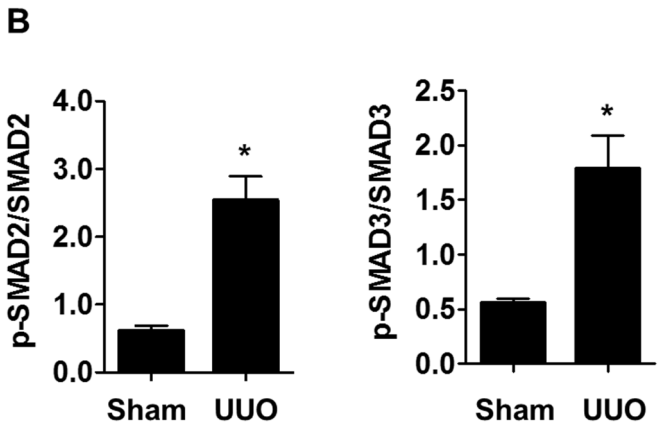

Figure 5. TGF-β receptor signaling pathway is activated in UUO kidney

fibrosis. (A) p-SMAD2 and p-SMAD3 levels were immunoblotted (Ctrl kidney; n=5, UUO kidney; n=5). (B) In the Sham (n = 5) and UUO (n = 5) kidney tissues, activation of SMAD2 and SMAD3 was accessed by immunoblotting their phosphorylated forms. * $P < 0.05$ versus the Sham group. Each bar represents the mean + s.d. (n = 5). The relative levels of phosphorylated forms versus total forms are presented as bar graphs. # $P < 0.05$ versus the untreated group. Each bar represents the mean + s.d. (n = 5).

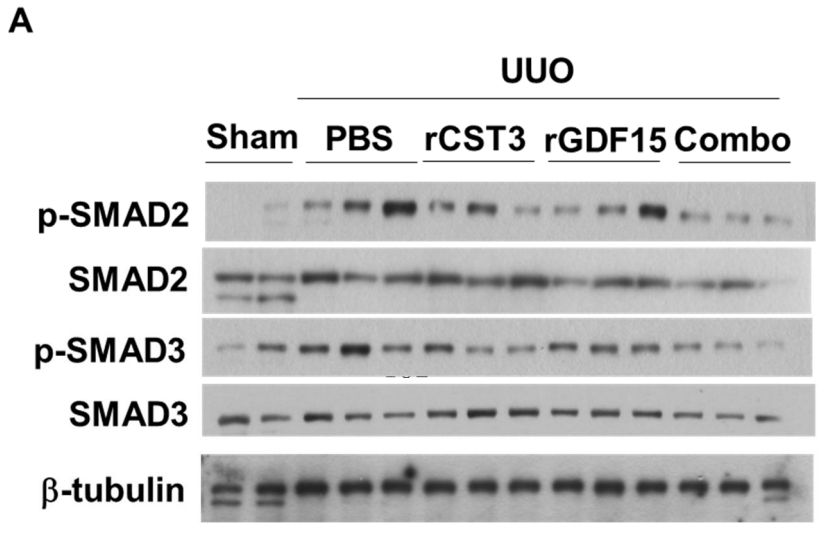

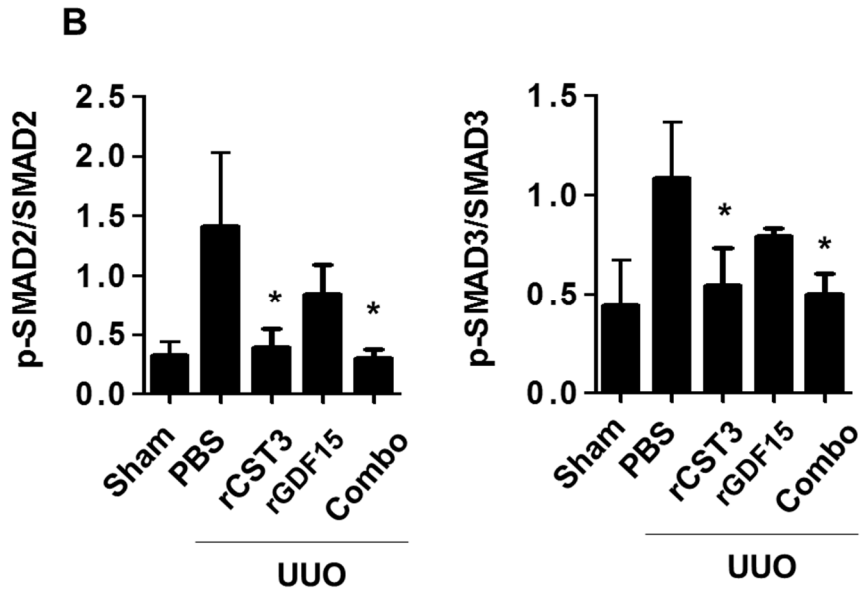

Figure 6. CST3 inhibits the TGF-β/SMAD signaling pathway in UUO kidney fibrosis. (A) After UUO operation, CST3 or/and GDF15 were administrated into mice. Kidney tissues were lysed and immunoblotted. (B) UUO mice were treated

with CST3, GDF15 or both every other day for 10 days. Kidney tissues were excised and prepared to immunoblot p-SMAD2 and p-SMAD3. The relative levels of phosphorylated forms versus total forms are presented as bar graphs. *P<0.05 by one-way ANOVA, followed by post hoc. Each bar represents the mean + s.d. (n = 3

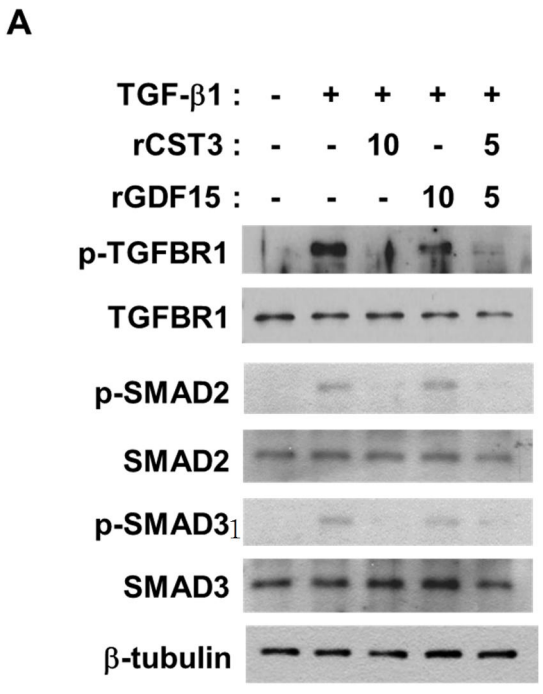

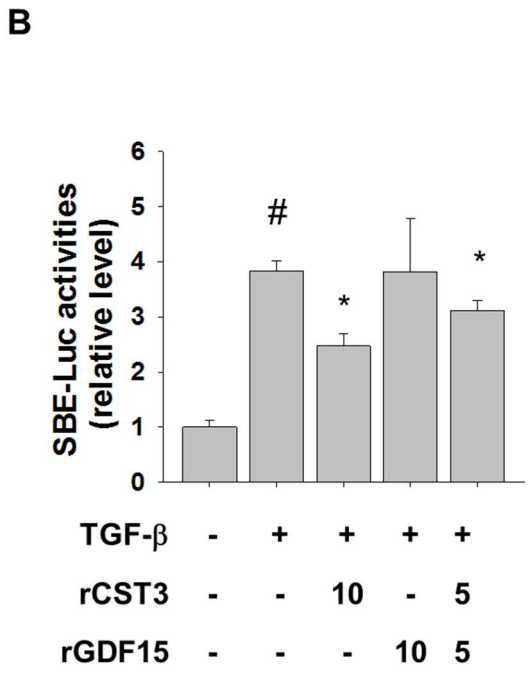

Figure 7. **CST3 inactivates the TGF-β receptor signaling pathway in sham or UUO kidney fibroblasts.** (A) Control kidney fibroblasts were pre-incubated with CST3, GDF15, or both for 4 h. After treated with TGF-β1

(5ng/ml) for 1 hr, fibroblasts were subjected to Western blotting of p-TGFBR1 (TGF-β receptor 1), p-SMAD2, and p-SMAD3. (B) Control kidney fibroblasts, which had been co-transfected with the SBE-Luc reporter and β-galactosidase plasmids, were treated with TGF-β1 and CST3 or/and GDF15 for 24 h. The luciferase activity was measured by luminometry, which was normalized to the β-galactosidase activity. # $P < 0.05$ versus the untreated group; *$P<0.05$ by one-way ANOVA, followed by post hoc. Each bar represents the mean + s.d. from 3 experiments.

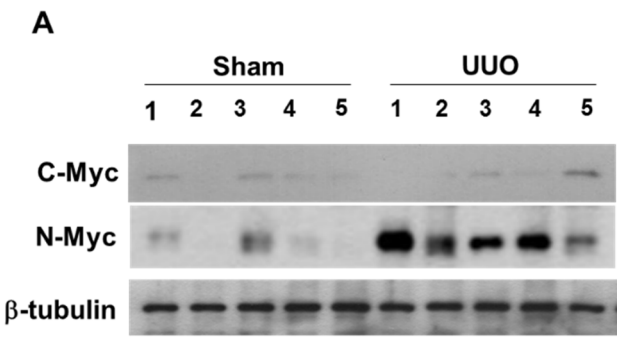

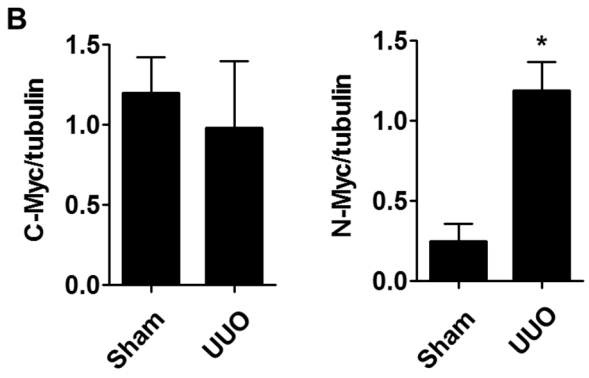

Figure 8. N-Myc expression is activated in fibrotic kidneys. (A) Sham or UUO kidneys were lysed and immunoblotted to analyze C-Myc and N-Myc

levels (top). (B) Intensities of blots were quantified using ImageJ and presented as bar graphs (means + s.d., n = 5). * $P < 0.05$ versus the Sham group.

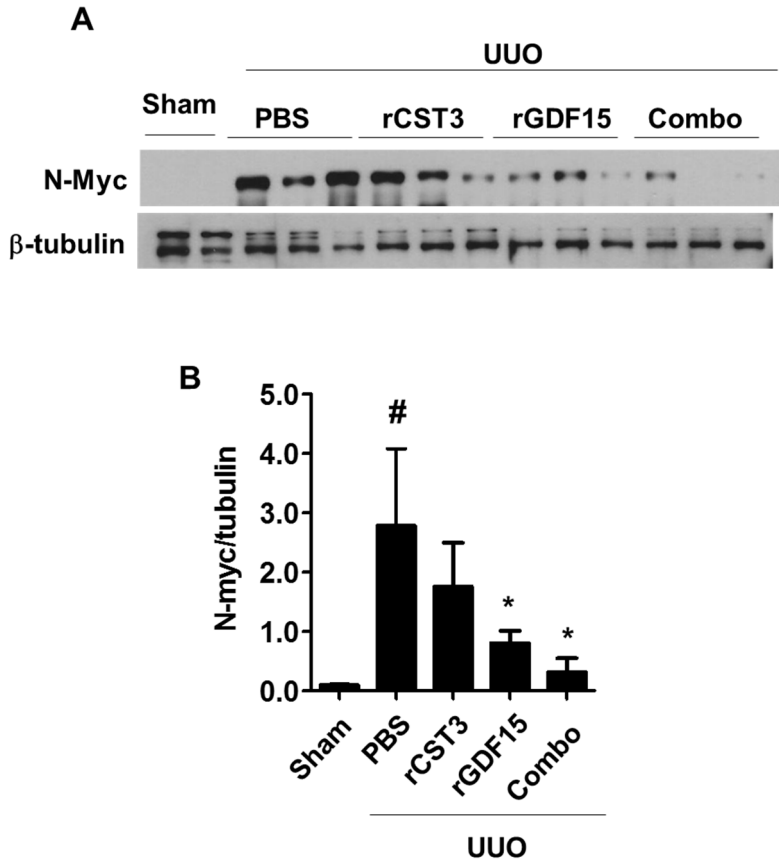

Figure 9. GDF15 represses N-Myc expression in fibrotic kidneys. (A)

UUO mice were treated with CST3, GDF15 or both every other day for 10 days. Kidney tissues were excised and prepared to immunoblot N-Myc. (B) Data are presented as the means + s.d. of 3 samples per each group. *, # $P<0.05$ by one-way ANOVA, followed by post hoc.

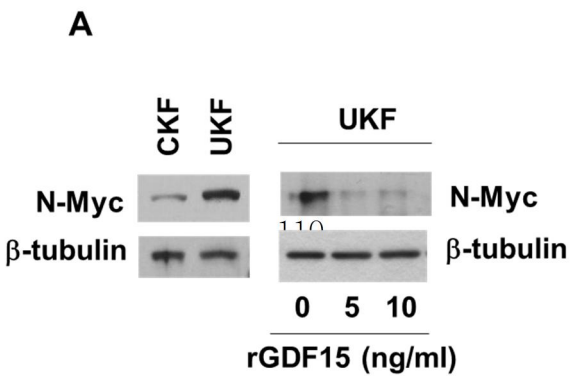

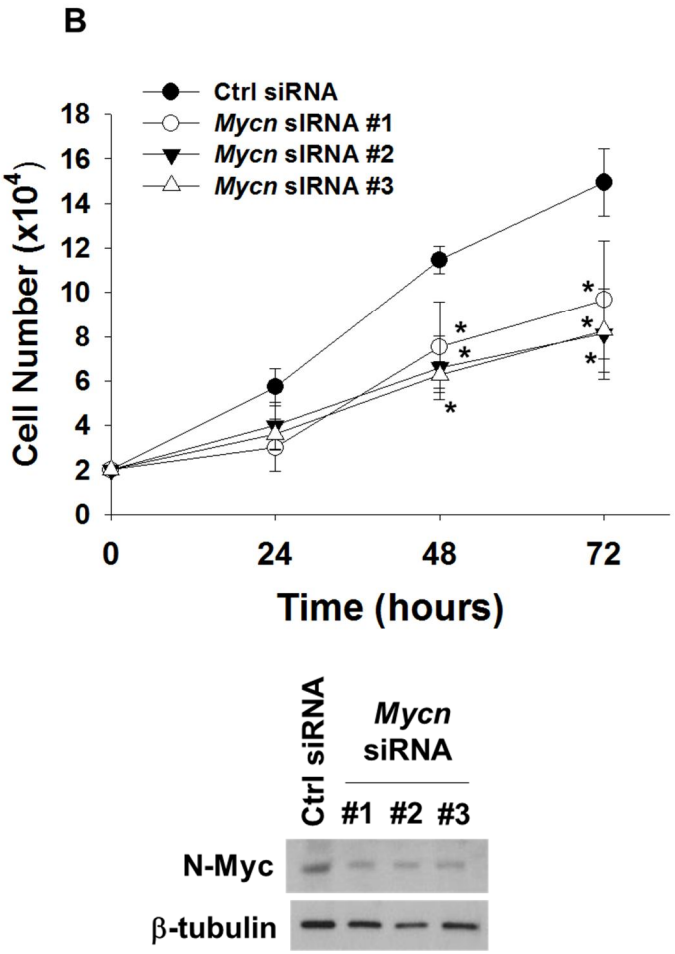

Figure 10. GDF15 represses N-Myc expression in activated kidney fibroblast. (A) N-Myc levels were determined in control (CKF) and UUO (UKF) kidney fibroblasts. UKF was incubated with recombinant

GDF15 (5 or 10 ng/mL) for 4 h and subjected to immunoblotting. (B) After transfection with *Mycn* siRNA, viable UKF cells was counted at the indicated times. Data are presented as the means + s.d. from 3 experiments. *, $P < 0.05$ versus the control siRNA

\

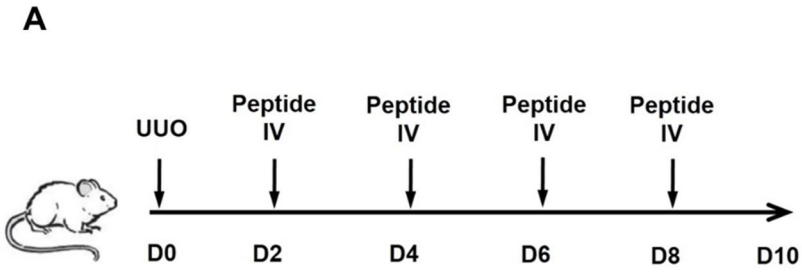

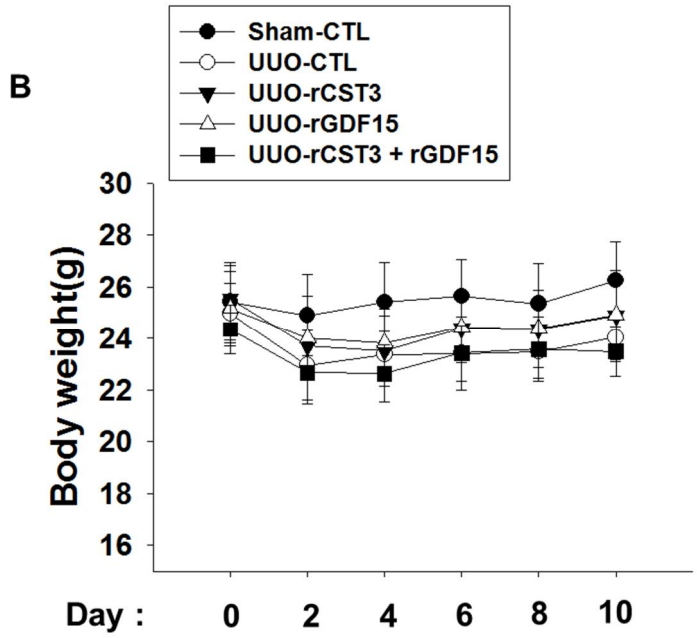

Figure 11. UUO mouse model. (A) Schematic schedule of the induction of kidney fibrosis with UUO surgery and peptide administration. C57BL/6 mice received rCST3 or rGDF15 by intraperitoneal instillations (indicated by

arrows) of only PBS vehicle: rCST3 alone or rGDF15 or rCST3 and rGDF15 combination, after UUO surgery. (B) Mouse body weights were measured indicated time points (means and s.d.).

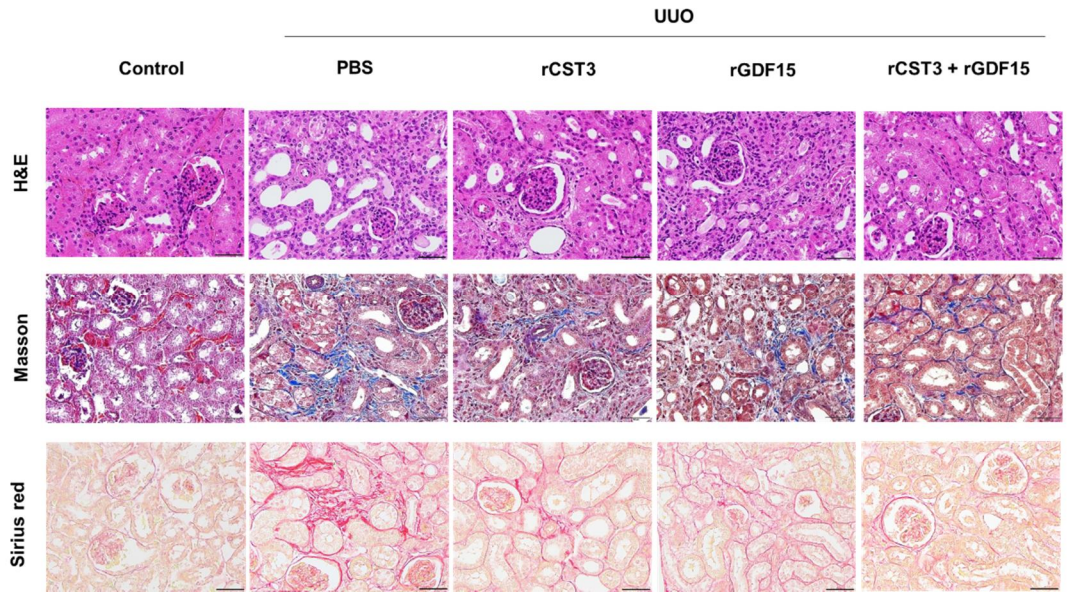

Figure 12. CST3 and GDF15 inhibit renal fibrosis progression in a UUO mouse model. UUO-perfomed (fibrotic) but not excuted (Sham) kidney and

peptide administrated kidney after UUO surgery were stained by Sirius red dye, Masson trichrome dye.

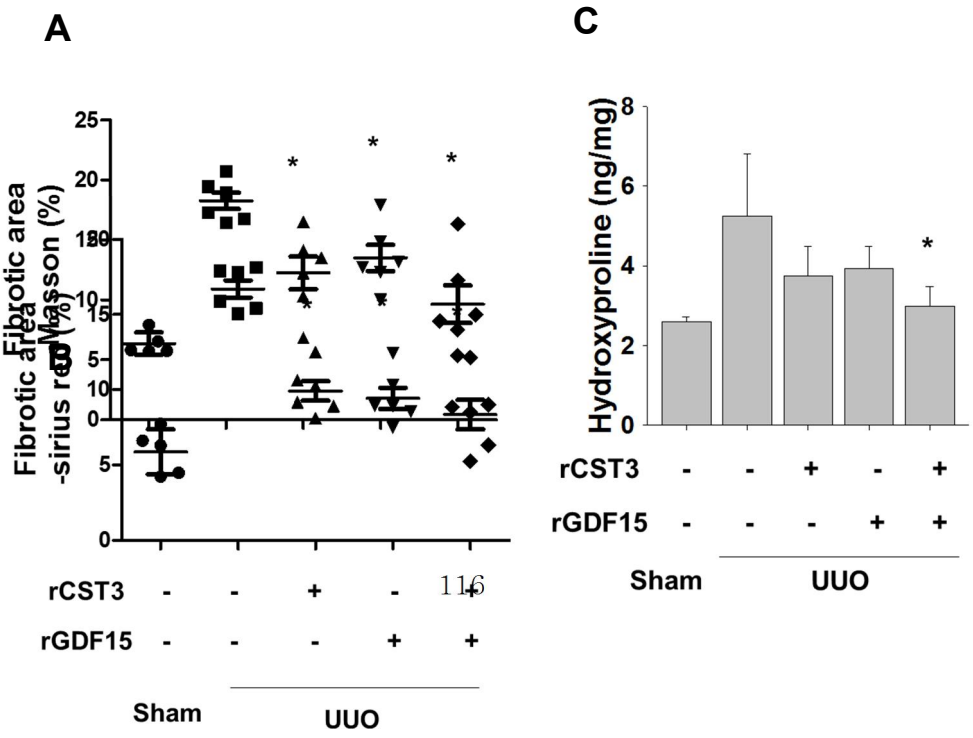

Figure 13. CST3 and GDF15 inhibit fibrotic phenotype in a UUO mouse model. (A)(B) To evaluate fibrotic burden, PBS or recombinant peptide-treated UUP kidneys were stained with Masson trichrome or Sirius red. The areas of fibrotic zones were calculated using imageJ and presented as dot graphs. Long and short horizontal bars represent the mean ± s.d. *P<0.05 by one-way ANOVA, followed by post hoc. (C) Collagen contents in kidneys were determined by hydroxyproline assay. Each bar represents the means + s.d. from 6 experiments. *P<0.05 by one-way ANOVA, followed by post hoc.

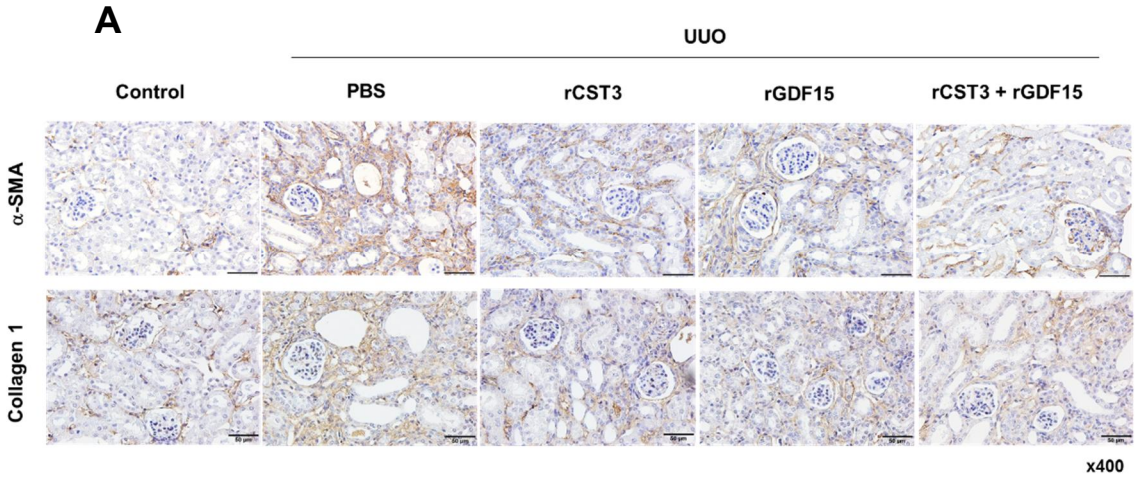
A
UUO
Control
PBS
rCST3
rGDF15
rCST3 + rGDF15
α-SMA
Collagen 1
x400

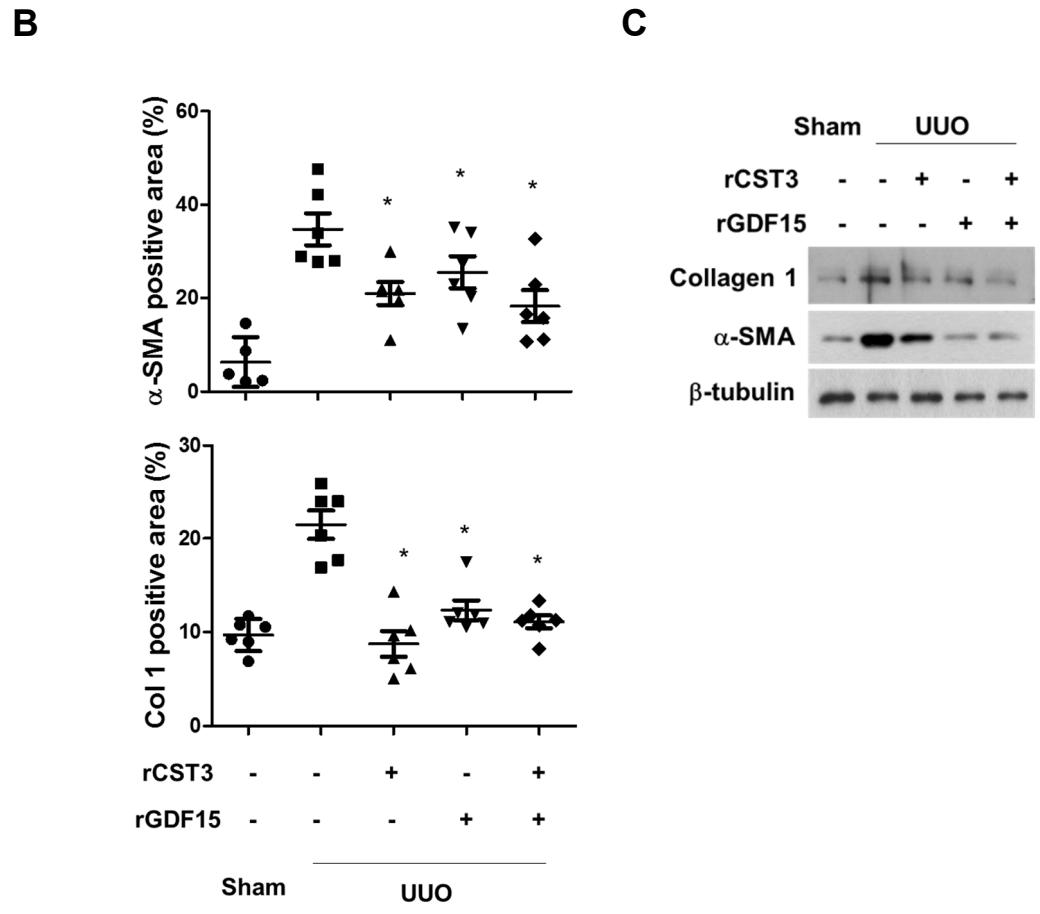

Figure 14. CST3 and GDF15 inhibit activation of kidney fibroblast in mouse UUO model. (A) The kidneys were subjected to immunohistochemistry using antibodies against collagen 1 and α-SMA. (B) The areas of immunostained zones were calculated using imageJ and presented as dot graphs. Long and short horizontal bars represent the mean ± s.d. *P<0.05 by one-way ANOVA, followed by post hoc. (C) Collagen and α-SMA contents in kidneys were determined by Western blotting. Representative images of 3 independent experiments are presented.

DISCUSSION

Chronic kidney disease (CKD) is diagnosed as irreversibly injured kidney function structure and its final destination is renal fibrosis. Renal fibrosis known as unsuccessful wound-healing process of kidney tissue damaged by chronic, sustained injury, and is characterised by glomerulosclerosis, tubular atrophy, and interstitial fibrosis (Webster et al., 2017) CKD incidence and

prevalence of end stage kidney substantially increases the risks of death, cardiovascular disease, and become a global problem (Go et al.,2004). To overcome burden of CKD in global health many therapeutic study has suggested from experiment to clinical trials. Corticosteroids have been used to treat young children with idiopathic steroid-resistant nephrotic syndrome (SRNS) (Yorgin et al., 2001). Cyclosporine is the only treatment that has been verified to be efficacious with controlled, prospective trial (Cattran et al., 1998), however, this therapy were shown significant side effect of nephrotoxicity. Anecdotal were known as anti-inflammatory drugs for renal fibrosis, have not yet been tested in larger clinical trial (Schnape, 2005). Inhibition of angiotensin-converting enzyme (ACE) or blockade of the angiotensin II receptor were used as treatment to diabetic nephropathy, however, clinical trial result were not clear effectiency to treat renal fibrosis (Rossing et al., 2003). Antifibrotic treatments were analyzed potential treatment targets, however only few of molecules are were also tested in clinical studies. Fresolimumab is neutralizing antibody to TGF-β and tested a phase 1 trial (Trachtman et al.,2011), but the following phase 2 study failed to show significant renoprotective effects in steroid resistant focal segmental glomerulosclerosis patients. Pirfenidone, a small synthetic molecule, reduced renal fibrosis in preclinical models by blocking the TGF-β promotor (Cho et al., 2010; Klinkhammer et al., 2016). Although a few anti-fibrotic agents like Fresolimumab and Pirfenidone were tested in clinical studies, the outcomes of these trials were evaluated to be unsatisfactory in terms of renal failure treatment (Trachtman et al., 2011; Sharma et al., 2011). Therefore, new agents

should be developed to preserve renal function in patients with renal fibrosis-associated CKD. In this study, I propose that recombinant CST3 and GDF15 be potential biopharmaceuticals for treating renal fibrosis.

UUO is e irreversible kidney fibrosis model that is used as the study of both renal inflammation and fibrosis (Hesketh et al., 2014). UUO rapidly induced disease progression events in the obstructed kidney, leading reduced renal blood flow and glomerular filtration rate within 24 hour (Vaughan et al., 2004). Next, interstitial inflammatory infiltration (macrophages) and tubular cell death were occurred within several days. Severely hydronephrotic kidney with marked loss of renal parenchyma were completed in 1–2 weeks after Completion UUO in rat or mouse (Chevalier et al., 2009). Therefore, I started to administration recombinant peptides 2 days after the UUO surgery,

CST3, which belongs to the cystatin superfamily, is known to inhibit cysteine proteases including cathepsin B. Considering the roles of cysteine proteases in ECM digestion, CST3 is expected to deposit ECM. However, CST3 also functions to antagonize TGF-β receptor (Sokol et al., 2004) and by doing so demotes ECM production from kidney fibroblasts (Akagi et al., 1996; Schnaper et al., 2003). Besides ECM production, TGF-β robustly stimulates fibroblasts to proliferate and differentiate into myofibroblasts, which can be blocked by CST3. These results also support such a role of CST3 in kidney fibroblasts. Taken together, CST3 is regarded as a promising bio-material for renal fibrosis therapy.

GDF15 is a secretory protein belonging to the TGF-β superfamily. Although its biological function is still controversial, GDF15 has been

reported to induce growth arrest and apoptosis in many cancer cell lines (Kadara et al., 2006; Albertoni et al., 2002). Such an anticancer action of GDF15 has been known to be attributed to induction of N-Myc downstream regulated genes (NDRGs) (Tsui et al., 2015). Given that the oncogene N-Myc is the transcriptional repressor for NDRGs, I were encouraged to check the possibility that GDF15 halts myofibroblast growth by inhibiting N-Myc. Consequently, N-Myc was found in this study to be induced in fibrotic kidneys and to be repressed by GDF15.

In summary, I found that CST3 and GDF15 are secreted from epithelial cells and inhibit proliferation and activation of fibroblasts. Based on these findings, I tested and verified the anti-fibrotic effect of each recombinant peptide or the combination of both peptides at the half dose in cell culture and in a UUO mouse model. Recombinant CST3 and GDF15 peptides may be potential candidates as therapeutics for delaying the progression of renal fibrosis.

REFERENCE

1. King TE, Jr., Pardo A, Selman M. Idiopathic pulmonary fibrosis. Lancet. 2011;378(9807):1949-61.
2. Friedman SL, Sheppard D, Duffield JS, Violette S. Therapy for fibrotic diseases: nearing the starting line. Sci Transl Med. 2013;5(167):167sr1.

3. King TE, Jr., Schwarz MI, Brown K, Tooze JA, Colby TV, Waldron JA, Jr., et al. Idiopathic pulmonary fibrosis: relationship between histopathologic features and mortality. Am J Respir Crit Care Med. 2001;164(6):1025-32.
4. Raghu G, Johnson WC, Lockhart D, Mageto Y. Treatment of idiopathic pulmonary fibrosis with a new antifibrotic agent, pirfenidone: results of a prospective, open-label Phase II study. Am J Respir Crit Care Med. 1999;159:1061-9.
5. Richeldi L, du Bois RM, Raghu G, Azuma A, Brown KK, Costabel U, et al. Efficacy and safety of nintedanib in idiopathic pulmonary fibrosis. N Engl J Med. 2014;370(22):2071-82.
6. Meyer KC, Decker CA. Role of pirfenidone in the management of pulmonary fibrosis. Ther Clin Risk Manag. 2017;13:427-37.
7. Hajari Case A, Johnson P. Clinical use of nintedanib in patients with idiopathic pulmonary fibrosis. BMJ Open Respir Res. 2017;4(1):e000192.
8. Ghosh AK, Quaggin SE, Vaughan DE. Molecular basis of organ fibrosis: potential therapeutic approaches. Exp Biol Med (Maywood). 2013;238(5):461-81.
9. Reinke JM, Sorg H. Wound repair and regeneration. Eur Surg Res. 2012;49(1):35-43.
10. Imokawa S, Sato A, Hayakawa H, Kotani M, Urano T, Takada A. Tissue factor expression and fibrin deposition in the lungs of patients with idiopathic pulmonary fibrosis and systemic sclerosis. Am J Resp Crit Care. 1997;156(2):631-6.

11. Gabbiani G. The myofibroblast in wound healing and fibrocontractive diseases. The Journal of pathology. 2003;200(4):500-3.
12. Yanagi S, Tsubouchi H, Miura A, Matsumoto N, Nakazato M. Breakdown of Epithelial Barrier Integrity and Overdrive Activation of Alveolar Epithelial Cells in the Pathogenesis of Acute Respiratory Distress Syndrome and Lung Fibrosis. BioMed research international. 2015;2015:573210.
13. Golan-Gerstl R, Wallach-Dayan SB, Amir G, Breuer R. Epithelial cell apoptosis by fas ligand-positive myofibroblasts in lung fibrosis. American journal of respiratory cell and molecular biology. 2007;36(3):270-5.
14. Villa P, Jimenez M, Soriano MC, Manzanares J, Casasnovas P. Serum cystatin C concentration as a marker of acute renal dysfunction in critically ill patients. Crit Care. 2005;9(2):R139-R43.
15. Moles A, Tarrats N, Fernandez-Checa JC, Mari M. Cathepsins B and D drive hepatic stellate cell proliferation and promote their fibrogenic potential. Hepatology. 2009;49(4):1297-307.
16. Canbay A, Guicciardi ME, Higuchi H, Feldstein A, Bronk SF, Rydzewski R, et al. Cathepsin B inactivation attenuates hepatic injury and fibrosis during cholestasis. The Journal of clinical investigation. 2003;112(2):152-9.
17. Zhang L, Fu X-H, Yu Y, Shui R-H, Li C, Zeng H-Y, et al. Treatment with CA-074Me, a Cathepsin B inhibitor, reduces lung interstitial inflammation and fibrosis in a rat model of polymyositis. Laboratory Investigation. 2014;95(1):65-77.

18. Sokol JP, Neil JR, Schiemann BJ, Schiemann WP. The use of cystatin C to inhibit epithelial-mesenchymal transition and morphological transformation stimulated by transforming growth factor-beta. Breast cancer research : BCR. 2005;7(5):R844-53.
19. Liu T, Bauskin AR, Zaunders J, Brown DA, Pankhurst S, Russell PJ, et al. Macrophage inhibitory cytokine 1 reduces cell adhesion and induces apoptosis in prostate cancer cells. Cancer research. 2003;63(16):5034-40.
20. Kadara H, Schroeder CP, Lotan D, Pisano C, Lotan R. Induction of GDF-15/NAG-1/MIC-1 in human lung carcinoma cells by retinoid-related molecules and assessment of its role in apoptosis. Cancer biology & therapy. 2006;5(5):518-22.
21. Hübner R-H, Gitter W, Eddine El Mokhtari N, Mathiak M, Both M, Bolte H, et al. Standardized quantification of pulmonary fibrosis in histological samples. BioTechniques. 2008;44(4):507-17.
22. Oruqaj G, Karnati S, Vijayan V, Kotarkonda LK, Boateng E, Zhang W, et al. Compromised peroxisomes in idiopathic pulmonary fibrosis, a vicious cycle inducing a higher fibrotic response via TGF-beta signaling. Proc Natl Acad Sci U S A. 2015;112(16):E2048-57.
23. Chou TC. Drug combination studies and their synergy quantification using the Chou-Talalay method. Cancer research. 2010;70(2):440-6.
24. Richeldi L, Davies HR, Ferrara G, Franco F. Corticosteroids for idiopathic pulmonary fibrosis. The Cochrane database of systematic reviews. 2003(3):CD002880.

25. Douglas WW, Ryu JH, Swensen SJ, Offord KP, Schroeder DR, Caron GM, et al. Colchicine versus prednisone in the treatment of idiopathic pulmonary fibrosis. A randomized prospective study. Members of the Lung Study Group. Am J Respir Crit Care Med. 1998;158(1):220-5.
26. Raghu G, Depaso WJ, Cain K, Hammar SP, Wetzel CE, Dreis DF, et al. Azathioprine Combined with Prednisone in the Treatment of Idiopathic Pulmonary Fibrosis - a Prospective Double-Blind, Randomized, Placebo-Controlled Clinical-Trial. Am Rev Respir Dis. 1991;144(2):291-6.
27. King TE, Albera C, Bradford WZ, Costabel U, Hormel P, Lancaster L, et al. Effect of interferon gamma-1β on survival in patients with idiopathic pulmonary fibrosis (INSPIRE): a multicentre, randomised, placebo-controlled trial. Lancet. 2009;374(9685):222-8.
28. Kubo H, Nakayama K, Yanai M, Suzuki T, Yamaya M, Watanabe M, et al. Anticoagulant therapy for idiopathic pulmonary fibrosis. Chest. 2005;128(3):1475-82.
29. Meuten T, Hickey A, Franklin K, Grossi B, Tobias J, Newman DR, et al. WNT7B in fibroblastic foci of idiopathic pulmonary fibrosis. Respir Res. 2012;13:62.
30. Roth GJ, Heckel A, Colbatzky F, Handschuh S, Kley J, Lehmann-Lintz T, et al. Design, Synthesis, and Evaluation of Indolinones as Triple Angiokinase Inhibitors and the Discovery of a Highly Specific 6-Methoxycarbonyl-Substituted Indolinone (BIBF 1120). J Med Chem. 2009;52(14):4466-80.

31. Taniguchi H, Ebina M, Kondoh Y, Ogura T, Azuma A, Suga M, et al. Pirfenidone in idiopathic pulmonary fibrosis. Eur Respir J. 2010;35(4):821-9.

32. Richeldi L, du Bois RM. Pirfenidone in idiopathic pulmonary fibrosis: the CAPACITY program. Expert review of respiratory medicine. 2011;5(4):473-81.

33. Yamaguchi Y, Takihara T, Chambers RA, Veraldi KL, Larregina AT, Feghali-Bostwick CA. A Peptide Derived from Endostatin Ameliorates Organ Fibrosis. Sci Transl Med. 2012;4(136).

34. Moeller A, Ask K, Warburton D, Gauldie J, Kolb M. The bleomycin animal model: a useful tool to investigate treatment options for idiopathic pulmonary fibrosis? The international journal of biochemistry & cell biology. 2008;40(3):362-82.

35. Sunaga H, Matsui H, Ueno M, Maeno T, Iso T, Syamsunarno MR, et al. Deranged fatty acid composition causes pulmonary fibrosis in Elovl6-deficient mice. Nature communications. 2013;4:2563.

36. Chaudhary NI, Schnapp A, Park JE. Pharmacologic differentiation of inflammation and fibrosis in the rat bleomycin model. Am J Resp Crit Care. 2006;173(7):769-76.

37. Sokol JP, Schiemann WP. Cystatin C antagonizes transforming growth factor beta signaling in normal and cancer cells. Molecular cancer research : MCR. 2004;2(3):183-95.

38. An H, Kim NJ, Jung JW, Jang H, Park JW, Suh YG. Design, synthesis and insight into the structure-activity relationship of 1,3-disubstituted

indazoles as novel HIF-1 inhibitors. Bioorg Med Chem Lett. 2011;21(21):6297-300.

39. Tsui KH, Hsu SY, Chung LC, Lin YH, Feng TH, Lee TY, et al. Growth differentiation factor-15: a p53- and demethylation-upregulating gene represses cell proliferation, invasion, and tumorigenesis in bladder carcinoma cells. Scientific reports. 2015;5:12870.
40. Ishige T, Nishimura M, Satoh M, Fujimoto M, Fukuyo M, Semba T, et al. Combined Secretomics and Transcriptomics Revealed Cancer-Derived GDF15 is Involved in Diffuse-Type Gastric Cancer Progression and Fibroblast Activation. Scientific reports. 2016;6:21681.
41. Seifert R, Wenzel-Seifert K, Gether U, Kobilka BK. Functional differences between full and partial agonists: Evidence for ligand-specific receptor conformations. J Pharmacol Exp Ther. 2001;297(3):1218-26.
42. Go AS, Chertow GM, Fan D, McCulloch CE, Hsu CY. Chronic kidney disease and the risks of death, cardiovascular events, and hospitalization. N Engl J Med. 2004;351(13):1296-305.
43. Snyder JJ, Foley RN, Collins AJ. Prevalence of CKD in the United States: a sensitivity analysis using the National Health and Nutrition Examination Survey (NHANES) 1999-2004. Am J Kidney Dis. 2009;53(2):218-28.
44. Liu Y. Cellular and molecular mechanisms of renal fibrosis. Nat Rev Nephrol. 2011;7(12):684-96.
45. Liu Y. Renal fibrosis: new insights into the pathogenesis and therapeutics. Kidney Int. 2006;69 (2):213-7.

46. Duffield JS. Cellular and molecular mechanisms in kidney fibrosis. J Clin Invest. 2014;124(6):2299-306.

47. Eddy AA. Molecular basis of renal fibrosis. Pediatr Nephrol. 2000;15(3-4):290-301.

48. Strutz F, Zeisberg M. Renal fibroblasts and myofibroblasts in chronic kidney disease. J Am Soc Nephrol. 2006;17(11):2992-8.

49. Breyer MD, Susztak K. The next generation of therapeutics for chronic kidney disease. Nat Rev Drug Discov. 2016;15(8):568-88.

50. Zeisberg M, Neilson EG. Mechanisms of tubulointerstitial fibrosis. J Am Soc Nephrol. 2010; 21(11):1819-34.

51. Zhang Y, Kong J, Deb DK, Chang A, Li YC. Vitamin D receptor attenuates renal fibrosis by suppressing the renin-angiotensin system. J Am Soc Nephrol. 2010;21(6):966-73.

52. Gu X, Mallipattu SK, Guo Y, Revelo MP, Pace J, Miller T, et al. The loss of Kruppel-like factor 15 in Foxd1(+) stromal cells exacerbates kidney fibrosis. Kidney Int. 2017;92(5):1178-93.

53. Grimwood L, Masterson R. Propagation and culture of renal fibroblasts. Methods Mol Biol. 2009;466:25-37.

54. Meng XM, Chung AC, Lan HY. Role of the TGF-beta/BMP-7/Smad pathways in renal diseases. Clin Sci (Lond). 2013;124(4):243-54.

55. Bretones G, Delgado MD, Leon J. Myc and cell cycle control. Biochim Biophys Acta. 2015;1849(5):506-16.

56. Shen Y, Miao N, Wang B, Xu J, Gan X, Xu D, et al. c-Myc promotes renal fibrosis by inducing integrin alphav-mediated transforming growth factor-beta signaling. Kidney Int. 2017;92(4):888-99.

57. Webster AC, Nagler EV, Morton RL, et al. Chronic Kidney Disease. Lancet 2017;389(10075):1238-52. doi: 10.1016/S0140-6736(16)32064-5

58. Yorgin PD, Krasher J, Al-Uzri AY. Pulse methylprednisolone treatment of idiopathic steroid-resistant nephrotic syndrome. Pediatr Nephrol 2001;16(3):245-50.

59. Cattran DC, Rao P. Long-term outcome in children and adults with classic focal segmental glomerulosclerosis. Am J Kidney Dis 1998;32(1):72-9.

60. Schnaper HW. Renal fibrosis. Methods Mol Med 2005;117:45-68. doi: 10.1385/1-59259-940-0:045

61. Rossing K, Jacobsen P, Pietraszek L, et al. Renoprotective effects of adding angiotensin II receptor blocker to maximal recommended doses of ACE inhibitor in diabetic nephropathy: a randomized double-blind crossover trial. Diabetes Care 2003;26(8):2268-74.

62. Trachtman H, Fervenza FC, Gipson DS, Heering P, Jayne DR, Peters H, et al. A phase 1, single-dose study of fresolimumab, an anti-TGF-beta antibody, in treatment-resistant primary focal segmental glomerulosclerosis. Kidney Int. 2011;79(11):1236-43.

63. Cho ME, Kopp JB. Pirfenidone: an anti-fibrotic therapy for progressive kidney disease. *Expert Opin Investig Drugs* 2010;19(2):275-83. doi: 10.1517/13543780903501539

64. Klinkhammer BM, Goldschmeding R, Floege J, et al. Treatment of Renal Fibrosis-Turning Challenges into Opportunities. Adv Chronic Kidney Dis 2017;24(2):117-29. doi: 10.1053/j.ackd.2016.11.002

65. Hesketh EE, Vernon MA, Ding P, et al. A murine model of irreversible and reversible unilateral ureteric obstruction. J Vis Exp 2014(94) doi: 10.3791/52559

66. Vaughan ED, Jr., Marion D, Poppas DP, et al. Pathophysiology of unilateral ureteral obstruction: studies from Charlottesville to New York. J Urol 2004;172(6 Pt 2):2563-9.

67. Chevalier RL, Forbes MS, Thornhill BA. Ureteral obstruction as a model of renal interstitial fibrosis and obstructive nephropathy. Kidney Int 2009;75(11):1145-52. doi: 10.1038/ki.2009.86

68. Sharma K, Ix JH, Mathew AV, Cho M, Pflueger A, Dunn SR, et al. Pirfenidone for diabetic nephropathy. J Am Soc Nephrol. 2011;22(6):1144-51.

69. Akagi Y, Isaka Y, Arai M, Kaneko T, Takenaka M, Moriyama T, et al. Inhibition of TGF-beta 1 expression by antisense oligonucleotides suppressed extracellular matrix accumulation in experimental glomerulonephritis. Kidney Int. 1996;50(1):148-55.

70. Schnaper HW, Hayashida T, Hubchak SC, Poncelet AC. TGF-beta signal transduction and mesangial cell fibrogenesis. Am J Physiol Renal Physiol. 2003;284(2):F243-52.

71. Albertoni M, Shaw PH, Nozaki M, Godard S, Tenan M, Hamou MF, et al. Anoxia induces macrophage inhibitory cytokine-1 (MIC-1) in

glioblastoma cells independently of p53 and HIF-1. Oncogene. 2002;21(27):4212-9.

국문 초록

Fibrosis는 다양한 조직에서 발생하는 비정상적인 상처치료 과정에 의해 유발되는 만성적인 질병이다. 상처회복 과정은 크게 세 단계로 진행 되는

데 이는 크게 (1) 염증반응 (2) 세포 증식 (3) 손상부위의 재건과 흉터 형성 과정을 거쳐 종결된다. 이러한 조직 재생 과정 동안, epithelial cell과 fibroblast의 상호작용은 세포증식 손상부위의 재건 단계에서 점진적으로 조절된다. 세포증식단계에서 과활성화 된 fibroblast는 정상적인 조직의 재구성과 흉터 형성을 위한 extracellular matirix를 구성하는 다양한 물질들을 생산하는 중요한 자원으로 기능을 한다. 정상적인 상처 재생 과정이 종결된 후 활성화된 fibroblast는 세포사멸 과정을 거치면서 제거되고 이 자리를 정상 epithelial cell이 채워야 하는데, 이 때 myofibroblast가 제대로 제거되지 않는 경우 정상적인 epithelial cell이 상처부위를 메꿀 수 없게 되고 조직에 경화가 진행되면서 fibrosis를 일으키게 된다.

본 연구에서 우리는 epithelial layer에서 분비되는 물질이 myofibroblasat의 사멸을 촉진하는 것을 밝히고 이로 인해 세포의 분화가 멈추는 것을 in vitro 실험으로 확인하였다. 이와 함께 epithelial cell이 분비한 cytokine인 cystatin C (CST3) 와 GDF15 보충해주는 경우, 다양한 조직에서의 fibrotic disease의 진행을 막는 치료전략이 될 수 있음을 증명하였다. 이러한 cytokine의 발굴을 위해 proteome profiler array system을 이용하였고 여기서 발굴된 CST3와 GDF15 재조합 단백질이 fibroblast의 분화와 성장을 억제할 수 있음을 확인하였고, 다양한 기관에서 분리한 primary fibroblast에서 두 cytokine이 세포 사멸을 일으키고 ECM 생산을 억제하는 기능을 하는 것을 밝혔다. 또한, in vivo model에서 CST3와 GDF15 재조합 단백질의 fibrotic disease치료효과를 확인하기 위해 bleomycin induced lung fibrosis model과 ureteral obstruction-induced fibrosis model을 이용하였다. 이와 함께, ILD human lung tissue

에서 CST3와 GDF15의 발현이 감소되어 있음을 확인하였다. 이러한 fibroblast의 성장과 분화 억제는 TGF-β receptor 를 antagonizationg하면서 SMAD2/3 signaling cascade를 막음으로 이루어 지는 것을 확인하였고, 또한 N-Myc의 활성을 저해하는 기능을 하는 것을 확인하였다.

이상의 결과들은 정상 epithelial cell이 분비하는 CST3와 GDF15 cytokine에 의해 epithelial-fibroblast 의 tissue homeostasis가 정밀하게 조절될 수 있음을 제안하고 특히 myofibroblast의 과성장, 과분화를 억제하는 기능을 할 수 있음을 밝히고 있다. 이로 인해, CST3와 GDF15 cytokine는 fibrosis progression을 억제하는 새로운 치료제로서 가능성을 가지고 있음을 확인할 수 있다.

주요어 : Epithelium, Fibroblast, 폐 섬유화, 신장 섬유화, cystatin C, growth differentiation factor 15

학 번 : 2013-31175